MODELLING OF NARMADA RIVER BASIN USING GWAVA

INTERNATIONAL COLLABORATIVE PROJECT WITH UK CENTRE FOR ECOLOGY & HYDROLOGY

FINAL REPORT

NATIONAL INSTITUTE OF HYDROLOGY, ROORKEE, INDIA
UK CENTRE FOR ECOLOGY AND HYDROLOGY, WALLINGFORD, UK

June, 2021

Preface

The water resources management in highly regulated large river basins has become much more challenging due to the unprecedented pressure on the water resources as a result of the ever-increasing demands of a growing population. A rapidly burgeoning population generates higher water demands for food production, energy production, drinking water, health and sanitation. Climate change is expected to further aggravate the water stress by intensification and altering the hydrological cycle possibly leading to increased frequency of extreme events including floods and droughts. In addition to this, the large scale land degradation and deforestation also affects water availability. The adoption of high yielding water intensive crops creates further stress on the surface and groundwater systems. The consequences of these changes that are quite visible now, and may translate into the issues related to water security in many large river basins of the world.

Climate change impacts on water availability is an active area of research today, as investigation and understanding of the future water availability will provide vital information in the hands of the decision makers in planning the future water resources development and management accordingly. Hydrological models are used to derive the future water availability by driving these models with climate projections for multiple future scenarios. The hydrological impacts of the basin interventions like dams, afforestation/deforestation and changing cropping pattern can also be assessed using hydrological models. However, the accurate simulation of the water cycle in highly regulated basins faces challenges in reliably incorporating the effects of water resources management.

This study is the result of the international collaboration between National Institute of Hydrology, Roorkee and UK Centre for Ecology and Hydrology, Wallingford wherein the focus of the study was to simulate the runoff in the Narmada basin using large scale hydrological model with very few parameters and thereafter evaluate the impacts of climate change and other anthropogenic interventions on the future water availability. In the first phase of the study, Global Water Availability (GWAVA) model and MIKE-SHE model has been applied to the Upper Narmada basin to evaluate the impacts of climate change on the hydrology. After understanding the strengths and limitations of GWAVA, the model was refined as GWAVA 5.1 with improvements in the reservoir operation routine and groundwater routine and extended to cover the complete Narmada basin. The comprehensive assessments of the impacts of climate change, afforestation, population growth, upcoming projects, change in cropping pattern have been carried out and presented. The study has been carried out by Dr. T. Thomas, Scientist-E & PI; Dr. Manish Nema, Scientist-D; Dr. P. K. Mishra, Sc-C; Dr. P. K. Agarwal, Scientist-B; Dr. Sanjay K. Jain, Scientist-G and Dr. Sharad K. Jain, Ex-Director from National Institute of Hydrology, India; Mr. Nathan Rickards, Hydrologic Modeller; Ms. Alexandria Kaelin, Hydrologist; Ms. Robyn Horan, Hydrologist; Ms. Helen Houghton Carr, Senior Hydrologist & Project Manager; Prof. Harry Dixon, Group leader, WRS; Dr. Gwyn Rees, Science Area Head, WR; and Prof. Alan Jenkins, Director of Science from UK Centre for Ecology and Hydrology, UK; and Prof. Julian R. Thompson, Professor; and Ms. Amanda J. Robinson, Research Scholar from University College of London, UK under the able guidance of Dr. A. K. Lohani, Scientist-G & Coordinator, RC Bhopal.

(J. V. Tyagi)
Director

CONTENTS

LIST OF FIGURES

LIST OF TABLES

Abstract

Management of water resources has always been a challenging task owing to the complexities and uncertainties involved in the hydrologic processes. Water resources management is a matter of concern to everyone considering the increased variability in climate with associated uncertainties. The impacts of various anthropogenic influences including climate change on water resources can be understood in detail by hydrologic modelling. However, hydrological modelling is a very complex proposition due to the inter-linkages between the various processes in the hydrological cycle, many of which are non-linear processes. The modelling exercise become much more complex in highly regulated river basins as the management of the reservoirs has a vital influence on the flows in the river, downstream of these structures. Many a times, there is no definite reservoir operation policy and most of the time it is rather difficult to acquire the inflow and reservoir release data from the project authorities.

A number of large scale hydrological models are available for simulation of the runoff, sediment and water quality in river basins. But many of these models are data intensive and comprise of large number of model parameters. Therefore a large scale hydrological model with few parameters would be ideal for solving complex hydrological processes for simulation of runoff in large river basins. The model should be able to incorporate the land use, soil properties, crops, dams and lakes etc., to ably represent the real world scenario in the basin. In the backdrop of these considerations, GWAVA, a semi-distributed grid based model was used to simulate the hydrology in the highly regulated Narmada river basin in Central India. GWAVA along with a MIKE-SHE, a complex and distributed hydrological model was used to model the daily runoff in Upper Narmada basin, and thereafter the assessment of the impact of climate change on water resources was carried out by driving these tested modes with the future climate simulations from 17 Global Climate Models (GCMs) that participated in the Coupled Model Intercomparison Project 5 (CMIP5) for one Representative Concentration Pathway (RCP) viz., RCP4.5 scenario.

The second phase of the project saw the study area being extended to cover the complete Narmada basin after understanding the inherent strength and limitations of GWAVA. The model was refined with improvements in the reservoir operation routine and groundwater routine and named as GWAVA 5.1. The multisite calibration was performed at 13 gauging sites located both in the headwater catchments and in the main river channel of Narmada River. The results of the model were encouraging, with improvements in stream flow simulations, particularly the low flows. The model was then driven by bias-corrected daily future climate data of 13 GCM of CMIP6 for two Shared Socioeconomic Pathways (SSP) scenarios viz., SSP245 and SSP585. Scenario analysis was

carried out to evaluate the impacts of changes in cropping pattern from soyabean to paddy in kharrif season, afforestation in 400 m buffer strip along the river, population growth scenario, livestock growth scenario, upcoming water resouces projects, and climate change under SSP245 and SSP585. Assessment of the changes in the mean flows, high flows and low flows have been carried out by comparing these variables during two future time horizons viz., 2050s (2036-2065) and 2080s (2066-2095) as compared to the baseline (1981-2010). The results of the study indicate that the GWAVA 5.1 is able to simulate the runoff in the Narmada river basin with a fair degree of accuracy. Therefore the model can be used to assess the impacts of various alternate scenarios including climate change on the future water resources in the basin. The projected runoff derived by forcing the GWAVA 5.1 with bias-corrected future climate data indicates that the mean flows are projected to increase in both future time periods, in the headwater catchments and also in the main river. The highest increase in mean flow is projected during the 2080s under SSP585 scenario. The high flows are expected to increase in future whereas the low flows are projected to decrease both in the headwater catchments and in the main river channel. Therefore the water resources management and development plans have to be formulated in the light of these projected changes keeping in mind the series of uncertainties involved in the modelling and impact assessment study.

1.0 Introduction

The management of water resources across the world is becoming an increasingly challenging task, owing to the impending threats of climate change, rapid urbanisation, growing population, and unsustainable exploitation. Humans have been increasingly altering the hydrological cycle through the construction of reservoirs, change in land use, water abstraction and urbanisation (Döll, et al., 2016). In few places is the impact of climate change and human intervention on water resources more prominent than in India (Madhusoodhanan et al., 2016; Mall et al., 2006; Gosain et al., 2006). Many of India's major rivers are impounded along their course for multifarious purposes (Gupta et al., 2005). The semi-arid and arid regions of the country are facing multiple challenges of water scarcity and deteriorating water quality. The National Water Policy of India (GoI, 2012) recognises the need for a national perspective on the development and management of water resources in the context of a changing climate and anthropogenic influences, in order to conserve the already scarce water resources in an integrated and environmentally sound way. Ensuring the food security of a burgeoning population will further increase water requirements from systems that are already under stress due to the conflicting demands of multiple users, including domestic, agricultural, energy generation, industrial and environmental (Madhusoodhanan et al., 2016; Rijsberman, 2006). An accurate large-scale quantification of freshwater flows and storage is important to support the development water management and governance in the near and far future (Vorosmarty, et al., 2015).

Future climate change will likely lead to increases in average temperatures across south-east Asia over the next century, along with changes in rainfall distribution, magnitude and intensity (Mishra et al., 2017; IPPC, 2013). Mukherjee et al. (2018) showed that the intensity of extreme rainfall events in India has increased over recent decades. Episodes of intense precipitation are expected to become more commonplace, with more overall rainfall being produced for any given storm. The year-to-year variability of the monsoon ultimately shapes the extremity of hydrological events, from severe droughts through to devastating floods. This has a direct effect on water storage and utilisation (Mall et al., 2006; SMHI, 2020) at present, around 45% of the average annual precipitation in India reaches the sea as runoff (Mall et al., 2006; Immerzeel et al., 2010], whilst drought events become ever more prevalent [SMHI, 2020; Udmale et al., 2014].

Future water availability will be affected not only by climate change, but also by growing demands across user sectors. The domestic, agricultural and industrial sectors are projected to increase water use over the next half century [Asokan & Dutta, 2008]. Water demand is growing fast due to rapid population growth and economic activity, and is not being matched by water supply [Saleth, 2011]. If such trends continue, many regions of India will face critical levels of

water scarcity during the dry season exacerbated by climate change, causing conflicts amongst sectors and regions, and affecting food supply and livelihoods (Madhusoodhanan et al., 2016; Mall et al., 2006; Asokan & Dutta, 2008; Pathak et al., 2014). The sustainable management of water resources across India, and the means to achieve this, is imperative going forward (Simonovic, 2012) water availability and appropriate allocation are therefore likely to become an even more prominent issue in the near future (Loch et al., 2020; Delorit et al., 2017).

Hydrological modelling is a key tool for improving our understanding of water resources and assessing the potential impacts of a variety of scenario types upon water resources, from climate (Thompson et al., 2013; 2014a; Ho et al., 2015) and land cover change (Kalantari et al., 2014; Wijesekara et al., 2014), to irrigation and dam regulation scenarios (Ahrends et al., 2008; Singh et al., 2011; Räsänen *et al.*, 2012). It therefore has an important role to play in catchment management and planning (Loucks and van Beek, 2005; McCartney and Acreman, 2009). However, uncertainties are inevitably introduced into all hydrological scenario impact assessments (Refsgaard and Henriksen, 2004; Gosling et al., 2011), and it is important that the resultant uncertainty in the modelling results is recognised and taken into account.

Large-scale hydrological modelling estimates water fluxes, such as evapotranspiration, river discharge and groundwater recharge, and water storage, such as soil water, groundwater and reservoirs (Döll, et al., 2016) at a basin or continental scale. Large-scale hydrological models are increasingly used for the simulation of water availability and extreme events, including droughts and floods (Schumacher et al., 2018; Prudhomme et al., 2011; Kauffeldt et al., 2016). This facilitates scenario-based analysis, wherein the impacts of climate change, land use change and water resource development activities can be comprehensively evaluated for the formulation of appropriate adaptation and mitigation strategies (Pappenberger et al., 2011; Alfieri et al., 2013; Van Loon et al., 2012; Lindstrom et al., 2012). The need for robust, coherent river basin management plans has thus become a driving force behind the use and development of large-scale hydrological models in understanding how basin hydrology will be affected by naturally and human-induced changes, and the influence of inter-sectoral resource linkages on water availability (Madhusoodhanan et al., 2016; Vicente-Serrano et al., 2017; Anis et al., 2017; Johnston et al., 2014).

Large-scale hydrological modelling does, however, involve many challenges [Kauffeldt et al., 2016; Muller et al., 2014; Beven et al., 2012; Guo et al., 2006; Van Huijgevoort et al., 2011; Wetterhall et al., 2013). The high spatial variability of input data such as land use, soil properties and topography across large catchments, the uncertainties in driving climate data, along with the

difficulties of capturing micro-watershed scale hydrological processes and the ever-growing number of anthropogenic interventions incorporated at different periods in many river basins, directly affect the hydrological regime. This can make the accurate representation of river basins extremely difficult. For example, global runoff estimations can differ by as much as 70% between studies for individual continents (De Couet & Maurer, 2009). Due to the highly influenced nature of many of India's major river basins, including the presence of dams and water abstractions, the modelling of Indian water resources becomes extremely challenging (Wada et al., 2013). The acquisition of reliable, relevant data poses a major challenge, where information on river flow and interventions is often not widely available. In light of this, a more holistic methodology and long-term assessment are needed for water resources management across many Indian catchments (Kumar et al., 2005). Large-scale model application in India ideally needs to incorporate anthropogenic basin interventions, such as water resource development projects, and account for population growth and demand from other water users (Anand et al., 2018), including industry and irrigated agriculture.

A better representation of groundwater processes need to be included into large-scale hydrological models to improve simulations and the understanding of feedbacks between the human and natural systems (Scheidegger, et al., 2021). Groundwater accounts for approximately a third of total water withdrawals globally and an estimated two billion people rely on groundwater as their primary source of water. Additionally, more than half of the irrigation water globally is abstracted from groundwater sources (Famiglietti, 2014). Most of the available models allow for the groundwater to be recharged through rainfall, wetlands and reservoirs and abstracted to meet demand.

Reservoir operations have a considerable impact on natural discharge regime of rivers. The available storage and volume and timing of reservoir releases pose a significant challenge to hydrological modelling at a basin and continental scale (Zhao, et al., 2016). Reservoir operational data are rarely freely available therefore hydrological model include various schemes to estimate reservoir storage and releases. GWAVA (Meigh, et al., 1999) models regulated reservoir release using a fill and spill routine utilising mean inflow, reservoir capacity and two outflow parameters. It is important to select a model that is able to accurately simulate low flows, particularly in basins where the main source of baseflow generation depends on groundwater storage and also able to incorporate the reservoirs and the reservoir operation.

This International Collaborative Project involved collaboration between National Institute of Hydrology (NIH), Roorkee, India; UK Centre of Ecology and Hydrology (CEH), Wallingford,

United Kingdom and University College of London (UCL), London, United Kingdom, with the aim of supporting the improvement of water-related science in India. This study has been carried out in two phases. In the Phase I, the Global Water Availability Assessment (GWAVA) model and the MIKE-SHE model has been applied to the Upper Narmada basin (upto Hoshangabad) whereas in the Phase II, the GWAVA model has been applied to the full Narmada basin. During Phase II of the study, improvements have been effected to the reservoir operation module and new module on groundwater interaction has been added, which has improved the results of the model simulations particularly during the lean flow periods. The objectives of the study are (1) to test the suitability of a large-scale grid-based water resources model in replicating the hydrology of the heavily impacted Upper Narmada, and (2) to assess the impacts of future climate change on the hydrological regime and future water resources of the basin.

2.0 The Study Area

The Narmada basin was selected as a suitable catchment for the application of hydrological modelling and analysis of future scenarios to understand the impact of climate change on water resources in the basin. The basin has a population of over 16 million (Government of India Ministry of Water Resources, 2014) and a drainage area of 98,796 km^2 (India-WRIS, 2015). The Narmada river basin is a highly regulated system, traversing the states of Chhattisgarh, Madhya Pradesh, Maharashtra and Gujarat, supporting a population of over 16 million people [GoI, 2012]. The main river reach, the Narmada river, is the largest west-flowing river in India, with a drainage area of 98,796 km^2 (GoI, 2012; GoI, 2014). The majority of the basin sits between 300 and 500 m in elevation, with extremes in the steep hills of the upper tributaries of the Maikala to the east, reaching 1317 m in elevation, through to the west coast where the river drains into the Arabian sea through the Gulf of Khambhat (Gupta et al., 2017). The Narmada basin is subject to a tropical monsoon climate, with the south-west monsoon between July and September the major controlling factor of river discharge. The monsoon supplies over 75% of the basin's annual precipitation, with a rainfall gradient of 650 mm per annum to more than 1400 mm per annum in the upper regions. This climate also leads to two distinct growing seasons, the Kharif (monsoon season) and the Rabi (non-monsoon season). Average temperatures range from 18°C to 32°C in January and May, respectively (GoI, 2014).

The Narmada is an example of a river basin facing numerous managerial challenges with sectoral competition for water. Over half of the catchment is used for agricultural production, with the majority of this designated as irrigation command area. In particular, there are multiple ongoing and planned dams and irrigation development projects for the basin (Government of India Ministry of Water Resources, 2014). There are over 4000 water-related interventions in operation across the basin, with more than 250 dams (Gupta & Chakrapani, 2005). The dams vary in purpose and size, from supplying water for irrigation through to the generation of hydropower and supply for consumptive and domestic use. Previous studies have applied models for the establishment of hydrological parameters for the Narmada basin for stream flow simulation, and for the assessment of the impacts of climate change on river basin hydrology (Gosain et al., 2006; Jain et al., 1992; Khare et al., 2017; Raje at al., 2014). However, the influence of anthropogenic modifications present in the basin is often under-represented or excluded entirely, therefore providing little information on plausible future states of water resources for water practitioners and stakeholders (Gosain et al., 2006).

The Phase I of the study models the water resources of the Upper Narmada basin, from the most eastern extent of the basin to the downstream gauging station at Hoshangabad, draining 44,548 km^2 (Figure 2.1). The index map of complete Narmada basin is given in Figure 2.2. Major dams, abstractions, irrigation practices and corresponding canal networks are included to gain an improved representation of the impact of future climate change on water resources in the Upper Narmada basin.

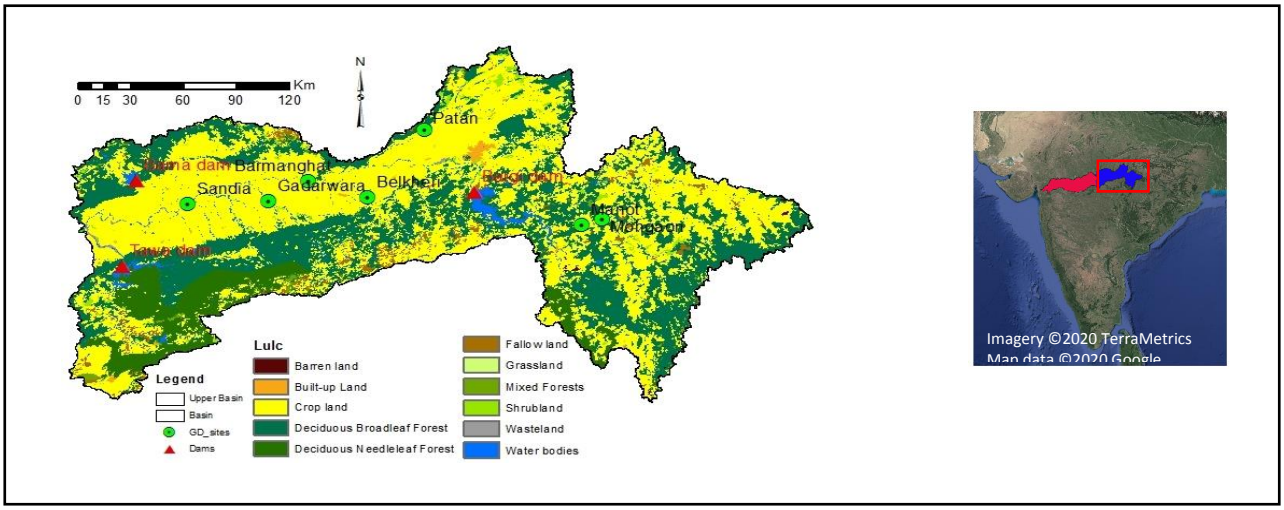

Figure 2.1: Index map of Upper Narmada basin

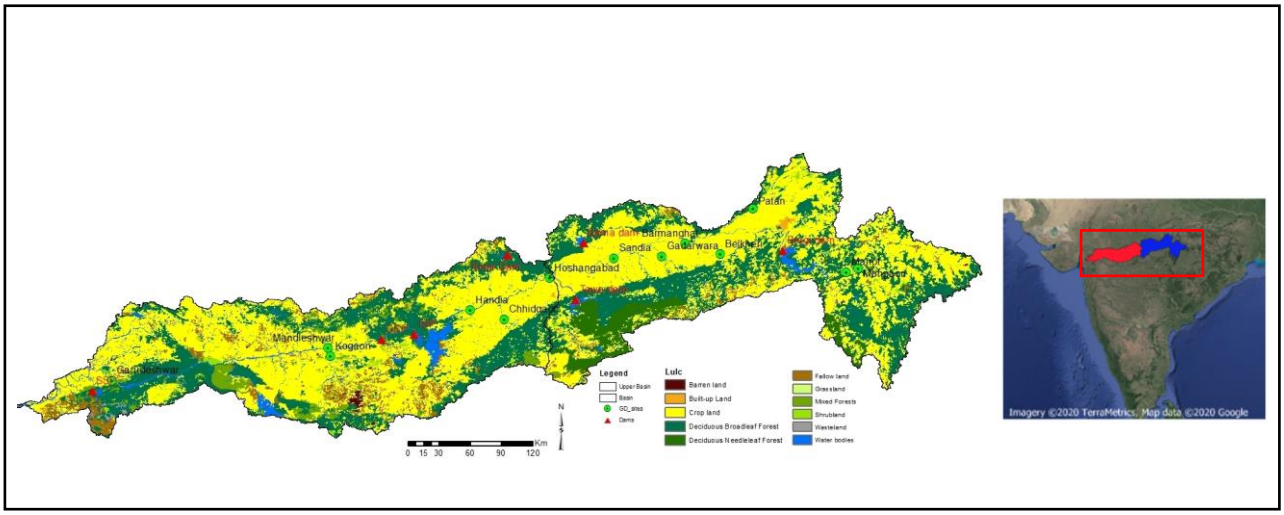

Figure 2.2: Index map of complete Narmada basin

3.0 Methodology

During the Phase I of the study, hydrological models of the Upper Narmada were developed using two different model codes viz., MIKE SHE and GWAVA. The brief about these models is given in Section 3.1 and Section 3.2 respsectively.

3.1 GWAVA Model

The UK Centre for Ecology & Hydrology (UKCEH) and the British Geological Survey (BGS) first developed the Global Water AVailability Assessment model (GWAVA) in the late 1990s. The model provides a methodology for the assessment of water resources in relation to water demand for application at the global scale. The key objective of the model was to develop a method that had a more realistic representation of the world than previous assessments achieved. GWAVA can be used for water resource assessments at a basin, regional, or global scale. It accounts for natural hydrological processes, such as river routing, lakes, wetlands and glaciers, as well as human influences, including reservoirs, transfers, and sectoral water demands. The main output of GWAVA is the comparison of water availability and demand at the grid cell level at a daily or monthly time step, thus enabling the user to evaluate the variability and complexity of the water resources situation.

GWAVA has been developed to be usable in data-sparse regions, so can be applied worldwide, and auto-calibrates to just four parameters which helps avoid overfitting. It can be run with current and future scenarios, facilitating the assessment of impacts of future changes, such as global warming, demographic changes, increased water demands and policy changes on global water distributions. The major advantage of GWAVA is that it combines natural hydrology with human influences for integrated water resources assessments, is adaptable to represent current and future scenarios to explore the impacts of future climate, socio-economic pathways and management options, has flexible spatial and temporal resolution, and an auto-calibration routine is available. The semi-distributed conceptual model can be run on a monthly or daily temporal resolution and on a regular size grid (50 km x 50 km, 0.5^{o} x 0.5^{o}). However, the grid size can be varied based on the resolution of the available input data (rainfall, land use, soil etc.). GWAVA is a tool that provides policy makers and others with valuable information to make better informed resource allocation decisions.

The hydrological processes accounted for within each grid cell in a sequential order include a) representation of water losses through evapotranspiration (ET); b) calculation of effective rainfall; c) representation of snowmelt and ice melt; d) modelling of direct runoff from each grid cell using Probability Distributed Model (PDM; Moore, 2007) based on the local vegetation, soil

types and climate characteristics; e) estimation of groundwater recharge; f) estimation of surface runoff by routing the direct runoff through the surface storage; g) routing of groundwater recharge through the subsurface storage to provide the baseflow; h) routing of groundwater recharge through the subsurface storage to provide the baseflow; i) estimation of water abstractions based on population density, urbanisation, livestock, industry, irrigation, crops, return flows, and groundwater to surface water use ratios; and j) adjustment of the modelled runoff to account for water consumption and return flows.

GWAVA simulates the local runoff from each grid cell using a lumped conceptual PDM (Moore, 1985). The PDM represents the spatial variations in soil moisture by means of a probability distribution (Moore, 2007). The PDM requires a limited set of parameters. The GWAVA model configuration is given in Figure 3.1.

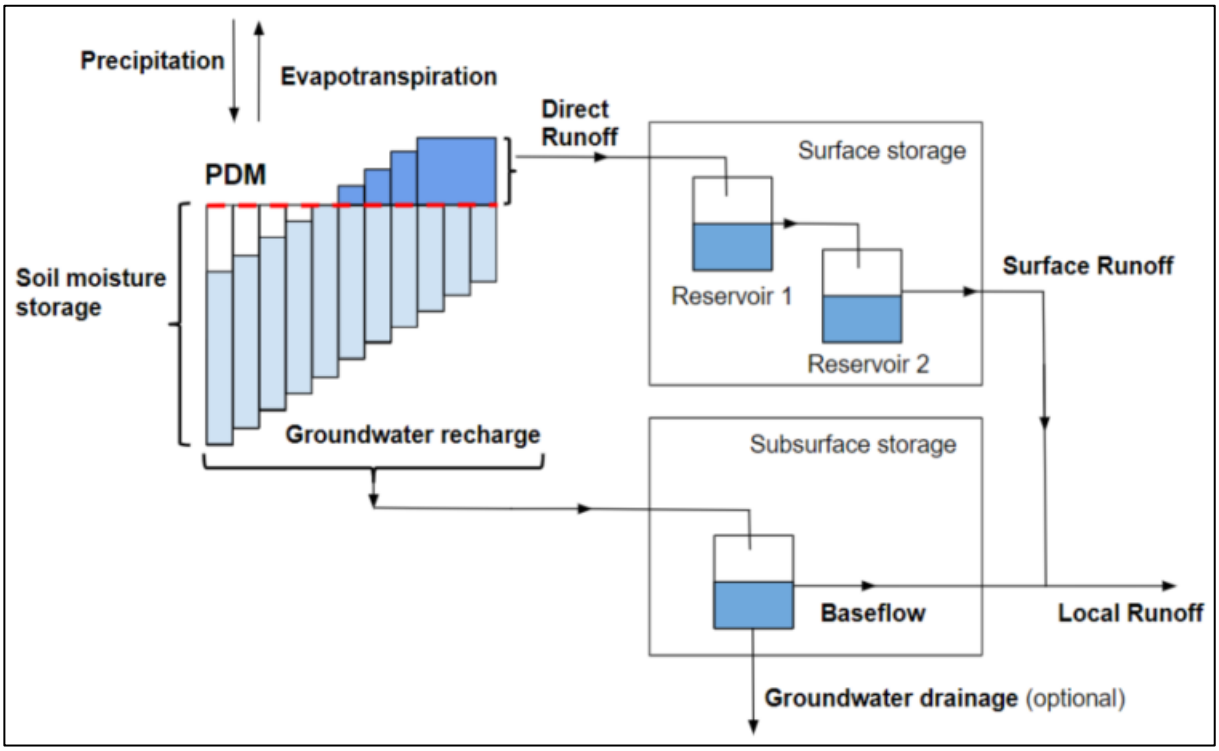

Figure 3.1: Schematic of the PDM based rainfall-runoff model

The model configuration has the following three components viz., i) Probability-distributed soil moisture storage component based on a Pareto distribution of soil moisture storage capacity over the grid cell. It represents the generation of direct runoff and groundwater recharge; ii) Surface storage component which transforms direct runoff to surface runoff by routing the direct runoff through two cascading linear reservoirs. The surface storage is a ‘fast response system’ and represents channel flow and other fast translation flow paths; and iii) Groundwater storage component which receives groundwater recharge from the soil moisture storage and also provides

baseflow by routing the recharge through a non-linear reservoir. The subsurface storage is a 'slow response system' representing groundwater and other slow flow paths.

The flow direction determines in which direction, water flows out of the grid cell. The flow direction is defined based on the code given in Figure 3.2. There are four land use types in GWAVA viz., trees, grass (crop), bush/shrubs, and bare soil. The user can define the proportion between the four land use types for each grid cell. Furthermore, GWAVA has seven soil classes viz., sand, sandy loam, silt loam, clay loam, clay, lithosol and organic. The user can assign a single soil type to each grid cell. The code values for the soil classes are given in Table 3.1.

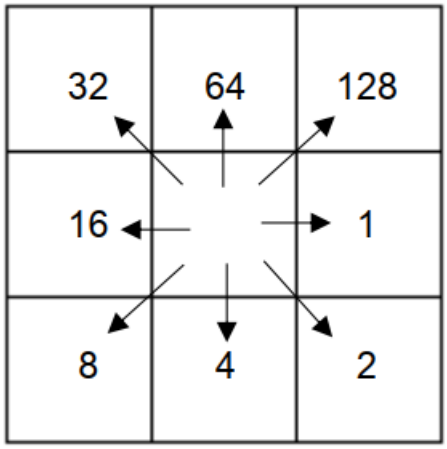

Figure 3.2: GWAVA flow-direction codes

Table 3.1: GWAVA soil codes

S. No	Soil class description	Soil code
1.	Sand	1
2.	Sandy loam	2
3.	Silt loam	3
4.	Clay loam	4
5.	Clay	5
6.	Lithosol	6
7.	Organic	7
8.	Cell completely covered by water (lake/wetland)	99

The soil moisture characteristics (Brouwer et al., 1985) of each soil type / land use combination are defined by means of wilting points (WP), field capacities (FC), and saturation capacities (SatCap). During rainfall/irrigation, the soil pores fill with water. When all pores are filled with water, the soil is saturated (SatCap). After a rainfall event or irrigation, some of the

water within the pores will drain. Field capacity (FC) is reached when air and water fills the larger pores (also referred to as macro-pores) while the smaller pores are still full of water. The soil moisture conditions are then ideal for crop growth. In the absence of rainfall or irrigation, the soil gradually dries out as the water is taken up by the plants or evaporated from the soil. As the soil dries up, the water is less easily extractable. Therefore, water uptake from the plants is more difficult. At a certain stage, the plant can no longer take up sufficient water to meet its need and wilts, before dying. Although the soil still contains some water, the plants cannot extract it; the soil water content at this stage is referred to as permanent wilting point (WP). The total amount of water available to plants is the difference between FC and permanent WP, and depends on the soil texture. The water amount above field capacity drains away too rapidly below the root zone for the plant to use it.

Soil moisture and runoff in GWAVA are calculated using the probability distributed model (PDM) (Moore, 1985). In this model, the variable depth and absorption capacity of the soil is characterised by a Pareto probability density function which defines a set of soil stores, as depicted in Figure 3.3a. The model calculates the direct runoff and soil moisture separately for each land use type in a grid cell, this is then summed to obtain the total direct runoff and soil moisture for each grid cell. For a given land use type in a given cell, the largest soil store depth is the maximum storage capacity (*Cmax*, mm). The average depth of water that can be held in storage is the saturation capacity (*SatCap*, mm). At *t=0*, the soil stores are empty, and fill up during rainfall events. When effective rainfall (Peff, (mm), exceeds the remaining storage capacity, the soil stores spill over and so generate runoff. The shallowest stores fill first and start generating runoff earlier than deeper stores. Therefore, different storage depths produce differing amounts of direct runoff (Figure 3.3b).

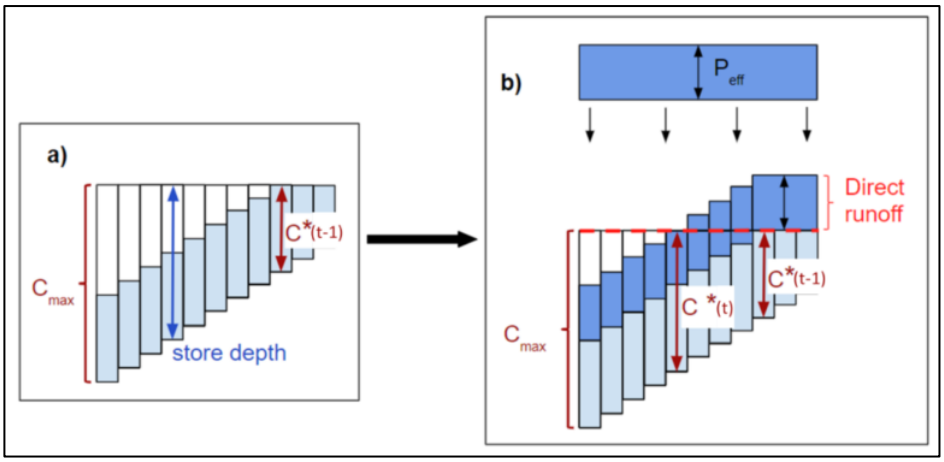

Figure 3.3: Schematic of the Probability distributed model (PDM)

a) Storage units sorted according to store depth. Cmax is the store with the largest depth. C*(t-1) is the store depth below which all stores are full at the end of the previous time step.

b) Illustrates the generation of direct runoff. Peff is the effective rainfall and C*(t) is the store depth below which all stores are full at the end of the current time step.

The amount of generated runoff depends on the critical capacity below which all soil stores are full (C_*, mm). If the critical store is greater than the maximum depth (for a given land use in a given cell), then the whole section becomes saturated and overspills. The soil moisture for the current time step is then equal to the saturation capacity. If the critical store is less than the maximum depth (for a given land use in a given cell), then only a fraction of the land surface will become saturated. In this case, the model calculates direct runoff using the exponent of the Pareto distribution (b). This parameter controls the spatial variability of the soil store capacity, and can either be user-defined or calibrated. Finally, the total direct runoff generated within a grid cell is the sum of all land use types within a grid cell. The model calculates groundwater recharge per time step by assuming that all water above field capacity (FC, mm) drains in one day to groundwater. It calculates the recharge separately for each land use type within a grid cell. The model updates the soil water storage of each land use type needs to account for loss due to groundwater recharge. Finally, the model calculates the total groundwater recharge for the grid cell by summing the recharge for all land use types within the grid cell.

The direct runoff is routed through a combination of conceptual storage units to represent the behaviour of surface and sub-surface flows. The surface storage consists of two cascading linear reservoirs (Reservoir 1, and then Reservoir 2), through which the direct runoff is routed (Figure 3.3). The reservoirs are not land use dependant; there is a single set of cascading reservoirs in each grid cell. These two reservoirs are empty at the start of the simulation. There is a routing parameter (S_{rout}), which is the same for both reservoirs and is user defined. The higher the value of S_{rout}, the shorter the time-delay. To optimise the model outputs, the user can calibrate S_{rout}. The groundwater recharge (GW, mm) is routed through a single subsurface storage (GW_{stor}, mm), Figure 3.3. As for the routing of direct runoff, the subsurface storage parameters are independent of land use, so there is only one subsurface storage per grid cell. This storage is initialised with 50 mm of water.

Baseflow is capped at the total groundwater storage. The user needs to define the baseflow routing parameters $Grout$ and bf_{power}, and can calibrate these for optimal results. Smaller values of the routing parameter $Grout$ and bf_{power}, means higher time-delay. Within the routing of the groundwater recharge, additional groundwater drainage can be applied. This functionality is most

relevant in arid areas, where rivers often dry up seasonally. It is important to note that groundwater drainage (GW_{drain}, mm) is considered as a simple loss and thus is not stored between time steps. After routing the baseflow and calculating the groundwater drainage, the model updates the groundwater storage (GW_{stor}, mm). The model adds up the simulated surface runoff and baseflow of a grid cell to obtain the local runoff per time step (in Mm^3) leaving the grid cell.

After estimating the local runoff for each grid cell for all time steps, the flows are routed between the grid cells and summed to derive the total flow for each grid cell (Meigh et al., 1999). The model implements two routing schemes as follows. a) In the simple accumulation routing, the river flows move without time delay through the river network. This method is preferable if the grid cells are relatively small and no time delay is expected (i.e., the runoff generated in the headwaters reaches the catchment outlet within the same time step); b) The Muskingum method was originally developed to route the flows through natural and man-made channels. The Muskingum routing is turned off if there are grid cells where the following is not valid as given by 2⁄3 days < k < 2 days. Values of k below 2⁄3 days would be likely for relatively small grid cell sizes (< 0.5 × 0.5°).

When using the simple accumulation routing, the model adds the total upstream grid cell flows to the local flows of the grid cell to generate the total runoff. Within the Muskingum method, the time step is always daily even when the model runs at a monthly resolution. However, it is advised not to use Muskingum routing for monthly runs (as the method used to disaggregate from monthly to daily can give unrealistic results). The Muskingum method requires the three parameters c_0, c_1 and c_2, which is calculated for each grid cell. The parameter k_j corresponds to the time delay in a grid cell (in days) and is user defined. The Muskingum method also considers water loss during the transmission (e.g. drainage into groundwater). This is achieved by means of a proportional loss factor (p_{loss}). Finally, the model adds the routed upstream flows to the local flow to get the total flow for a particular cell.

Lakes/reservoirs and wetlands are structurally different from river channels. Therefore, flows are routed differently through these specific water bodies. Lakes/reservoirs and wetlands are characterised by their shape, storage capacity, initial storage and surface area at full capacity. The user needs to define these characteristics as inputs. Within the GWAVA model, lakes/reservoirs and wetlands be allocated as one of two possible shapes, i.e., rectangular or V-shaped. Several categories of lake/reservoir and wetlands are available, depending on their nature and presence of an outlet release (Table 3.2). The model then calculates the surface area depending on the type of designated structure. In some cases, the water body can cover more than one grid cell. In this case, the model treats grid cells which do not contain the outlet as normal (e.g. same as a cell without a lake) when calculating local runoff. The exception is that the model calculates the local runoff only

for the proportion of the grid cell covered by the land surface. The model applies the routing equations for lake/reservoir and wetlands only to the grid cells containing the outlet. This includes the total area and storage of the water body (Meigh et al., 1999). The routing method applied to these lake/reservoirs and wetlands depend on the type of lake selected lake category.

Table 3.2: GWAVA lake category

S. No	Description of water body	Lake category
1.	No lake, reservoir or wetland	0
2.	There is a lake/reservoir but the outlet is not in this grid cell	1
3.	Outlet of a natural lake	2
4.	Outlet of a regulated reservoir	3
5.	Outlet of a reservoir with direct abstraction (water supply, etc.)	4
6.	There is a wetland but the outlet is not in this grid cell	5
7.	Outlet of a wetland	6
8.	Outlet of a special lake	7

The GWAVA model can account for water demands for various sectors, namely domestic, industry, irrigation and livestock. For a given grid cell, the model calculates the water demand after being generated by the probability distributed model (PDM), and the flows routed through any storage structures. The computation of the subtraction of water demands from the flow follows a 4-stepprocedure, i) estimation of the dynamic water demands (industrial and irrigation) per time step and their return flows (in Mm^3 day^{-1}); ii) Estimation of the static water demands (urban, rural and livestock) per time step and their return flows (in Mm^3 day^{-1}); iii) Splitting of the total water demand (static + dynamic) into groundwater and surface water consumption; and iv) Adjustment of the river flow by subtracting the surface water consumption and adding return flow. Within GWAVA, static water demands refer to all urban, livestock and rural water demands that are constant over time. Dynamic water demands are time dependent and include industrial demand, as well as seasonal water use for crop irrigation.

The model calculates the water demand for irrigation based on crop area (ha), crop type, planting month of crop and the potential evaporation for the grid cell. GWAVA can incorporate up to eight different crop types within a grid cell. The model calculates the required amount of irrigation water needed by each crop type based upon its monthly water demand, taking into account irrigation efficiency, minus the proportion of rainfall taken up by the crop (i.e. effective precipitation). The model calculates the monthly water use/consumption per crop based upon a reference potential evapotranspiration from crop. The crop area (A) indicates the total irrigated area for the considered crop in each cell in hectares. The crop code as given in Table 3.3 defines the type

of crop and the crop code. Accordingly the set of crop factors is provided in GWAVA. The *crop factor* for a given crop is usually determined experimentally. The *crop factor* values represent the integrated effects of changes in leaf area, plant height, crop characteristics, irrigation method, rate of crop development, crop planting date, degree of canopy cover, canopy resistance, soil and climate conditions, and management practices. Each crop will have a set of specific crop factors and will predict different water use for different crops for different growth stages.

Table 3.3: GWAVA crop codes

S. No	Crop type	Crop code
1.	Wheat/barely	1
2.	Rice	2
3.	Peanuts	3
4.	Cotton	4
5.	Millet	5
6.	Maize	6
7.	Sugarcane	7
8.	Citrus	8
9.	Vegetables	9
10.	Short crop	10
11.	Fodder	11
12.	Horticultural fruits	12
13.	Sorghum	13
14.	Bananas	14
15.	Tea / Coffee	15

The user needs to define the proportional split of the demand that is met from surface water and groundwater. The user can specify a unique value for each sectoral demand (i.e. rural, urban, irrigation and industrial which the model will apply across the whole spatial domain. Alternatively, the user can set this proportion to vary spatially per cell, but in this case the model will apply the same value for all sectors. GWAVA allows the user to specify how much groundwater is available annually. The model then calculates the groundwater consumption as the difference between the total water demand and the surface water consumption. If the groundwater consumption exceeds the groundwater availability, the model will adjust the surface water consumption to include the proportion of the groundwater demand that cannot be met by available groundwater.

Return flows are defined as abstracted water that returns to surface flow after use. GWAVA calculates return flows separately for urban, rural and industrial demands. It calculates urban return flow as a proportion of the urban water consumption which is user defined. Rural return flow is

calculated as a proportion of the rural population water demand, plus livestock water demand. Actual industrial demands vary with time, but the model keeps the proportion of return flow constant. The model subtracts the water consumption and then adds the return flows to the total surface flow. The model assumes zero return flows for water used for crop irrigation. When providing water demand data for the various sectors, it is important to consider the impact abstractions may have on surface water flows within the model. Excessive abstractions may result in zero flow within a cell. Water transfers are possible to and from grid cells within the model, allowing for the representation of features such as canals and pipelines. GWAVA applies water transfers before accounting for water demands for urban and rural populations, livestock and industries; any water transfer in to, or out of, a cell will therefore directly affect water availability to meet water requirements. Note that transfers are not allowed to move from a downstream cell to an upstream cell within the model domain.

The GWAVA software comprises three modules, i) Pre-processor, ii) Core Engine and iii) Post-processor. The Pre-processor module converts user-generated input files (.csv) into binary files (.dat). GWAVA adopts this approach to reduce model runtime. In addition to converting the files, this step also checks the data for atypical or unusual values and provides a basic quality control of the input data. The Core Engine is the main module of the model. The pre-processed files are read in, and the GWAVA model generates runoff for each grid cell in the model domain. An initialisation file (.csv) allows the user to define the set-up of the model run(s). This can be done in either a normal or calibration mode. The Post-processor module is designed to interpret the data that the core engine produces. It has the option of creating output in various formats, as required by the user. The ‘Parameter file’, ‘Demands file’ and ‘Climate file’ are mandatory data input and must be pre-processed. The pre-processing of the remaining files is optional, and only needs to be done should these input data be required. The details of the mandatory and optional GWAVA input files are given in Table 3.4.

Table 3.4: GWAVA input files

S. No.	Input file	Pre-processor option number
Mandatory inputs		
1.	Parameter	1
2.	Demands	2
3.	Climate	3
Optional inputs		
4.	Sub catchments	4
5.	Mountains	5
6.	Glaciers	6
7.	Extra demands	7
8.	Groundwater availability	8

3.2 MIKE-SHE model

The MIKE SHE (Refsgaard and Storm 1995) modelling system is based on the model SHE (Syste`me Hydrologique Europe´en) (Abbott et al. 1986a, b). MIKE SHE is an advanced, flexible framework for hydrologic modelling. It includes a full suite of pre- and post-processing tools, plus a flexible mix of advanced and simple solution techniques for each of the hydrologic processes. Each of these processes can be represented at different levels of spatial distribution and complexity, according to the goals of the modelling study, the availability of field data and the modeller's choices (Butts et al. 2004). Figure 3.4 shows the hydrologic processes simulated by MIKE SHE. It contains procedures that can be applied in basic studies including the model structure and internal evaluation model (Butts et al. 2004; Christiansen et al. 2004). MIKE SHE is applicable at spatial scales ranging from a single soil profile, for evaluating crop water requirements, to large regions including several river catchments (Andersen et al., 2001).

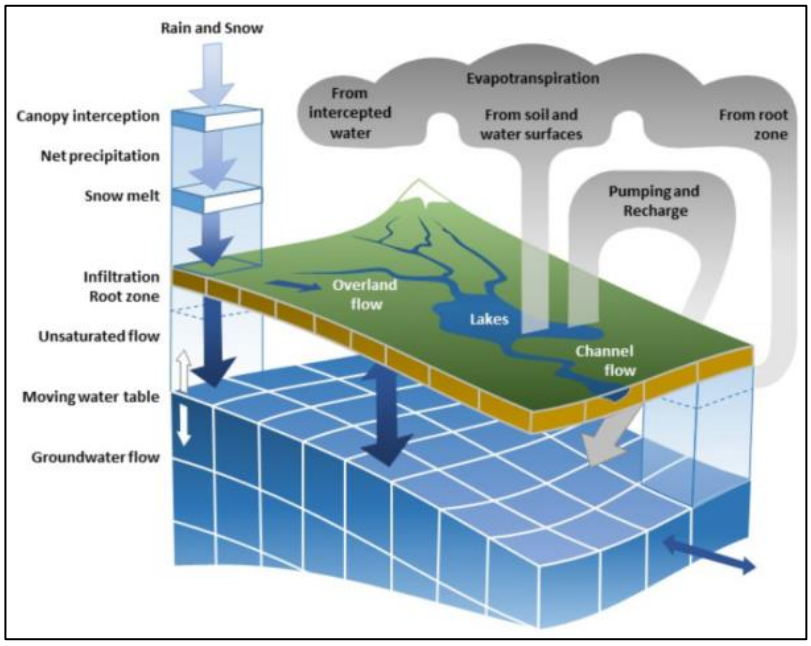

Figure 3.4: Hydrologic processes simulated by MIKE SHE

(Source: MIKE SHE Manual)

MIKE SHE, in its original formulation, could be characterized as a deterministic, physics-based, distributed model that solves the partial differential equations describing mass flow and momentum transfer. MIKE SHE is a comprehensive modelling system, capable of simulating the major processes of the land phase of the hydrological cycle (Graham and Butts, 2005). It was developed as a fully integrated alternative to the more traditional lumped, conceptual rainfall-runoff models. MIKE SHE can use fully distributed conceptual approaches to model the watershed processes. For advanced applications, MIKE SHE can simulate all the processes using physics-

based methods. Alternatively, MIKE SHE can combine conceptual and physics based methods-based on data availability and project needs. The flexibility in MIKE SHE's process-based framework allows each process to be solved at its own relevant spatial and temporal scale. However, it has high calculation accuracy and strict requirements on data accuracy.

MIKE SHE model divides the watershed into a unit grid horizontally for discrete calculation of complex terrain. Relationship of grid codes is established by solving the continuity equation and the motion equation. In the vertical direction, a soil column is formed on each cell, and the difference in soil properties is indicated by different horizontal layers on the soil column. MIKE SHE model is computations are accomplished by three modules viz., water body motion module (WM), water quality module (WQ) and water balance tool, in which the water body motion module simulates the water body migration process through different calculation sub-modules, including snow melting module (SM), Overland Flow Module (OL), Rivers and Lakes Module (OC), Evapotranspiration Module (ET), Unsaturated Flow Module (UZ), and Saturated Flow Module (SZ). The relationship between each sub-module and the calculation method involved in each sub-module are shown in Figure 3.5. The input data requirements for MIKE SHE model is given in Table 3.5.

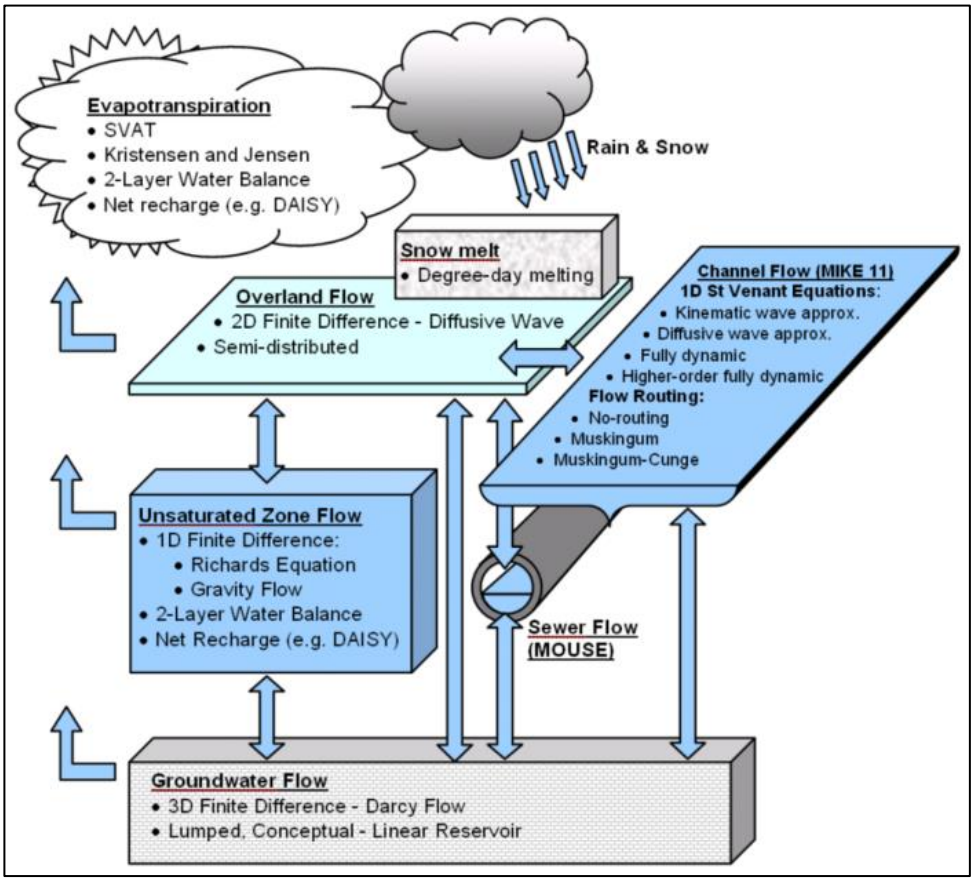

Figure 3.5: Schematic view of the processes in MIKE SHE

Table 3.5: Input data requirement for MIKE SHE

S. No	Input data	Data type
1.	Model extent	typically as polygon
2.	Topography	as point or gridded data
3.	Precipitation	as rain gauge station data
4.	*Additional basic data*	*Based on hydrologic processes included*
4a.	Reference evapotranspiration	as station data or calculated from meteorological data
4b.	Air Temperature	for calculating snowmelt (station data)
4c.	Solar Radiation	for calculating snowmelt (station data)
4d.	Sub-catchment delineation	for runoff distribution
4e.	River morphology (geometry + cross-sections)	for river flow and water level calculations
4f.	Land use distribution	for vegetation and paved runoff calculations
4g.	Soil distribution	for distributing infiltration and calculating runoff
4h.	Subsurface geology	for calculating groundwater flow
4i.	Species to be simulated	For water quality
4j.	Source locations	For water quality

The model operates at a daily time step which aims towards the assessment of the surface runoff. The MIKE SHE model parameters have physical meaning and can theoretically be measured in the field. However, there is always a range in which each parameter value can be varied. The basic model parameter list is given in Table 3.6. The parameters in these equations can be obtained from measurements and used in the model. The calibration of the model includes the choice of the parameters that play a key role in the natural process of converting rainfall into runoff. During the calibration, importance has been given towards the best representation of total water balance, to make possible the successful calibration of all the available observed hydrographs. The main objective of calibration is to reproduce the observed runoff data by calculating realistic values for actual evapotranspiration and other water balance parameters. The calibration procedure had as its objective function of minimising the errors between the observed and simulates runoff for the correct estimation of surface runoff.

Table 3.6: Basic MIKE SHE model parameters

S. No	Process	Main calibration parameters	Other parameters
1.	Unsaturated flow (finite difference)	Saturated hydraulic conductivity	Soil water contents at saturation, field capacity, and wilting point, Soil function parameters
2.	Unsaturated flow (2-layer method)	Saturated hydraulic conductivity	Soil water contents at satu ration, field capacity, and wilting point Capillary thickness
3.	Actual evapotranspiration	Leaf Area Index Root depth	Canopy Interception FAO Crop coefficient Kristensen and Jensen ET parameters
4.	Groundwater flow (finite difference)	Hydraulic conductivity Specific yield Specific storage	Hydraulic conductivity Specific yield Specific storage
5.	Groundwater flow (linear reservoir)	Reservoir time constants Reservoir volumes (specific yield, depths)	Inter-basin transfers (dead zone storage)
6.	Water quality	Porosity Soil bulk density Dispersivities Sorption and degradation rate constants	Source strength

The need for fully integrated surface and groundwater models, like MIKE SHE, has been highlighted in many research studies. MIKE SHE has been used to analyse river basin management and planning; water supply design, management and optimisation; irrigation and drainage; soil and water management; surface water impact from groundwater withdrawal; conjunctive use of surface and groundwater; wetland management and restoration; ecological evaluations; groundwater management; environmental impact assessments; aquifer vulnerability mapping; contaminant transport modelling; surface and groundwater quality remediation; flood plain studies; impacts of land use and climate change; and impact of agriculture.

MIKE SHE has been extensively used to study the hydrological responses in land use/land cover, changes, climate and climate variability (Graham and Butts 2005; Zhang et al. 2008), irrigation operations (Jayatilaka et al. 1998; Singh et al. 1999), hydrological manipulations of the flora of wetlands (Thompson et al. 2004), forest management and forest fires and the impact assessment (Lu 2006; McMichael and Hope 2007) and the sustainable management of groundwater

(Demetriou and Punthakey 1999). Other areas of study for the MIKE SHE include analysing the sensitivity and spatial scale effects (Xevi et al. 1997; V'azquez et al. 2002; V'azquez and Feyen 2007), the parameterization of the model calibration and verification (Refsgaard 1997; Andersen et al. 2001; Henriksen et al. 2003; Madsen 2003) and evaluation methods of potential evapotranspiration (V'azquez and Feyen 2003).

4.0 Model Application

The Phase I of the hydrological modelling efforts focuses on the hydrological modelling of stream flows in the Upper Narmada Basin up to Hoshangabad, which lies within the States of Madhya Pradesh and Chhattisgarh only. The hydrological models of the Upper Narmada basin were developed using two different model codes viz., GWAVA and MIKE SHE. The development of these models is discussed in following sections given below.

4.1 Hydrological modelling of Upper Narmada Basin using GWAVA

The model provides a comparison of water availability and demand at the scale of the grid cell for the comprehensive assessment of the spatial and temporal variability of the water resources scenario over a basin. The model is capable of carrying out the combined assessment of both surface water and groundwater and also has the capability to assess the future water resources under the impacts of climate change and land use changes. The model is a FORTRAN90 program and runs on a PC under Windows XP or later, in a MS-DOS box. The simplified conceptual structure of the PDM based rainfall-runoff model is given in Figure 4.1. The model was initially developed and applied on a grid with a resolution of 0.5^{o} latitude x 0.5^{o} longitude, but it can also be applied for fine resolutions.

The choice of grid size is a compromise between the need to represent the spatial variability and the availability of suitable data. For this study, the Upper Narmada Basin was divided into 318 grid cells of 0.125° × 0.125° (approximately 13 km × 13 km). This resolution was chosen largely as a consequence of data availability and suitability for the analysis of regional water resource assessment. The data requirement for the GWAVA model application includes Drainage map and basin boundary, Digital Elevation Model (DEM), Land use/Land cover (LULC) map, Soil map, Reservoir command area maps, Crop type map in command areas, Population and Livestock maps. Also the data pertaining to climate including the daily temperature, precipitation and Potential Evapotranspiration (PET), reservoir area-elevation-capacity, average water consumption rate for human and livestock population, industrial demands, irrigation demands, inter-basin water transfers etc. are required. Based on these data requirements and the objectives of the modelling exercise, few input files need to be prepared in the format desired by the pre-processor of the GWAVA model. Two major types of input files include, i) compulsory input files viz., physical parameter file, general water demands file and the climate data and ii) optional input files viz., sub-catchment calibration file, mountain region information, glacier information, groundwater information, daily water demands, water transfers and climate scenarios. Table 4.1 shows data sources used.

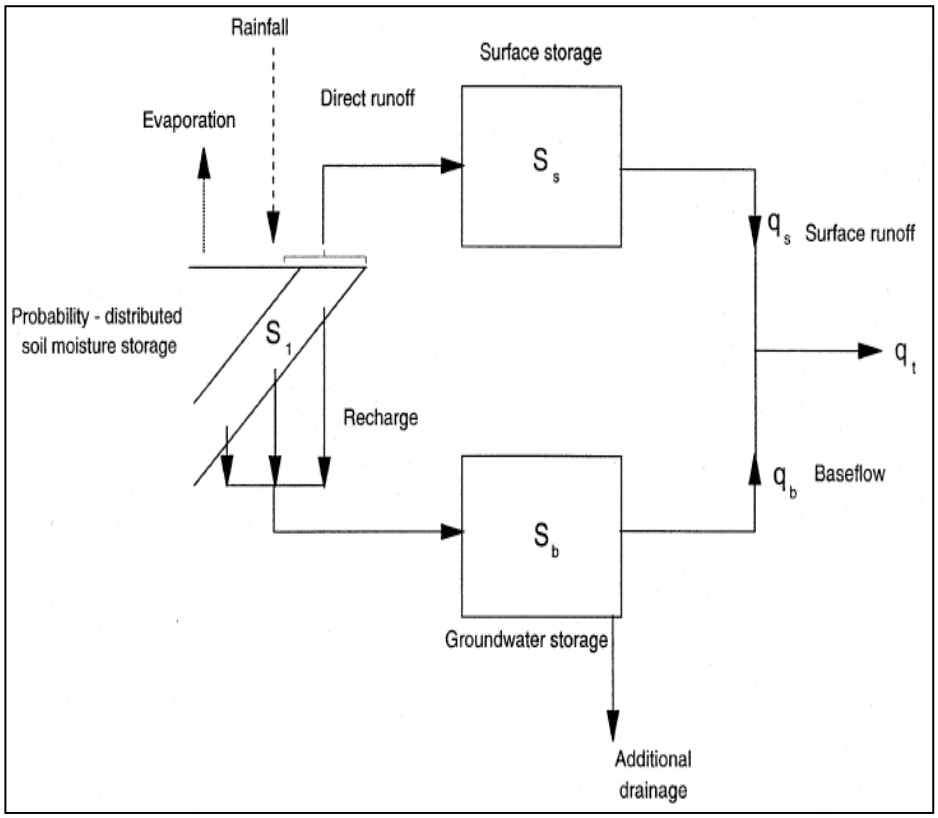

Figure 4.1. Conceptual structure of the PDM based GWAVA Rainfall-Runoff model (Moore, 2007)

Table 4.1: Data sources used for GWAVA model configuration

Model Component	Key Inputs	Data Sources/Derivation
Topography	Topography	Extracted from SRTM (Shuttle Radar Topography Mission) 90 m resolution DEM (Digital Elevation Model) [49].
Land use/vegetation	Land use distribution	USGS LULC map [50]. Reclassified to six land cover types: Forest, Shrub, Water bodies, Wetlands, Bare soil and Grass/cropland.
Soil	Soil classes	The spatial distribution of six soil classes was specified using a 1 km × 1 km grid based on a georectified and digitised soil map [51].
River discharge	Discharge time series	India-WRIS (Water Resources Information System) [52].
Catchment meteorology Precipitation and evapotranspiration modules.	Precipitation and Temperature	0.25° × 0.25° gridded daily precipitation obtained from the IMD (India Meteorological Department) / NCC (National Climate Centre) High Spatial Resolution (0.25° × 0.25°) Long Period (1901–2013) Daily Gridded Rainfall Data Set Over India [53].
Artificial influences	Reservoir and lake	Relevant information obtained from

	abstractions/operations, water body dimensions	literature [38,54,55].
	Population and Domestic consumption	Indian Population Census [56,57].
	Irrigated crops	Relevant information obtained from literature [58–60].
	Water transfers	Relevant information obtained from literature and field surveys [55,61].
	Cattle, sheep and goat populations	Indian Livestock Census [62].

The physical parameter file contains the information pertaining to area of grid cell; flow direction in the grid cell; soil class; land cover comprising of four types viz., percentages of tree cover, shrub cover, grass (crop) cover and bare soil cover; grid coordinates; routing parameter; percentage of lake, wetland and lake characteristics like surface area capacity, shape parameter, outflow constant and value of the outflow power. The soil class is used to determine the major parameters of the model which is based on the dominant soil texture in each grid cell. As per the requirements of the GWAVA model the soil map has been reclassified into seven major classes viz., sand, sandy loam, silt loam, clay loam, clay, lithosol and organic. If a complete grid cell is covered by lake or wetland, a value of 99 has been assigned. The soil map of the Narmada basin in Madhya Pradesh is given in Figure 4.2.

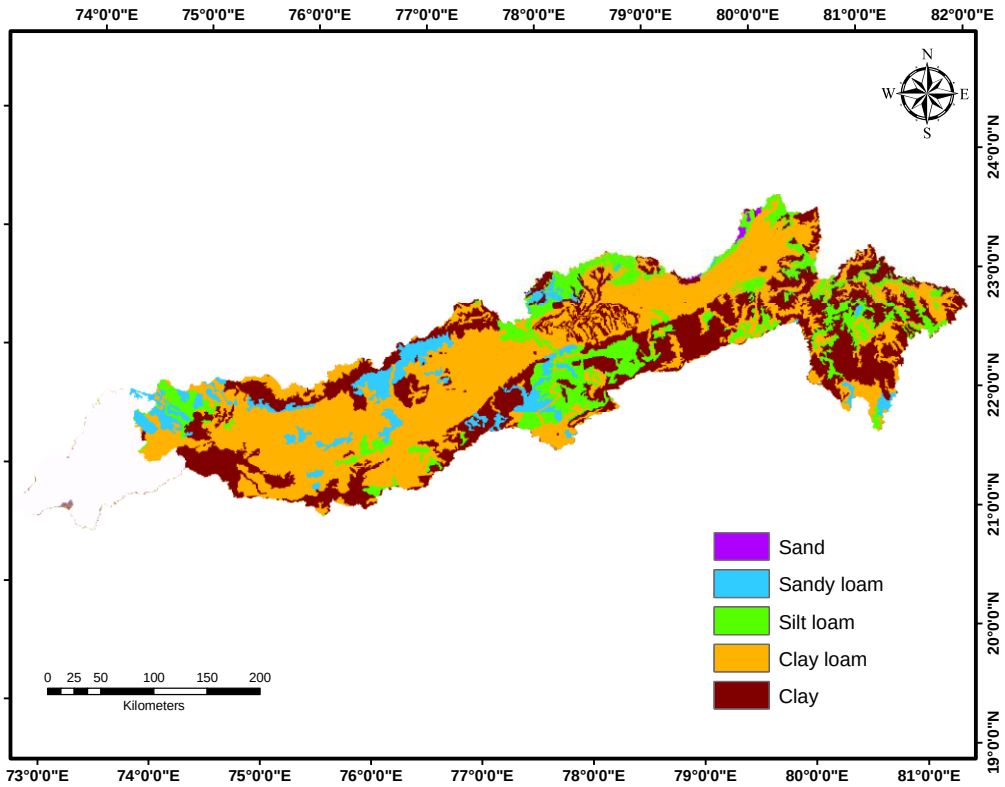

Figure 4.2: Soil map of Narmada basin in Madhya Pradesh

The area under various soil classes is given in Table 4.2. The LULC map of the study area has been reclassified accordingly into four major classes and is given in Figure 4.3. The area under the various LULC classes is given in Table 4.3. The model also has a parameter to account for the transmission losses in flows between the cells and a value in the range of 0 to 0.999 can be assigned. The model uses the Muskingum method of routing the flows between the cells and has two parameters 'x' and 'k'. The parameter 'x' is fixed at 0.5 whereas the parameter 'k' which represents the time delay in days can be assigned values in the range of 0 to 50. The 90 meter resolution SRTM (Shuttle Radar Topography Mission) Digital Elevation Model (DEM) data has been resampled at the desired resolution of GWAVA model at 0.125^{o} latitude x 0.125^{o} longitude. The flow direction map has been prepared from the processed DEM and is given in Figure 4.4. The physical parameter file for Narmada basin has been prepared based on information extracted from these GIS shape files and other parameter values were assigned suited to the study area.

Table 4.2: Area under various soil classes

Soil type	Area (km^2)	Area (%)
Sand	25333	28.4
Sandy loam	5650	6.3
Silt loam	13486	15.1
Clay loam	182	0.2
Clay	44469	49.9

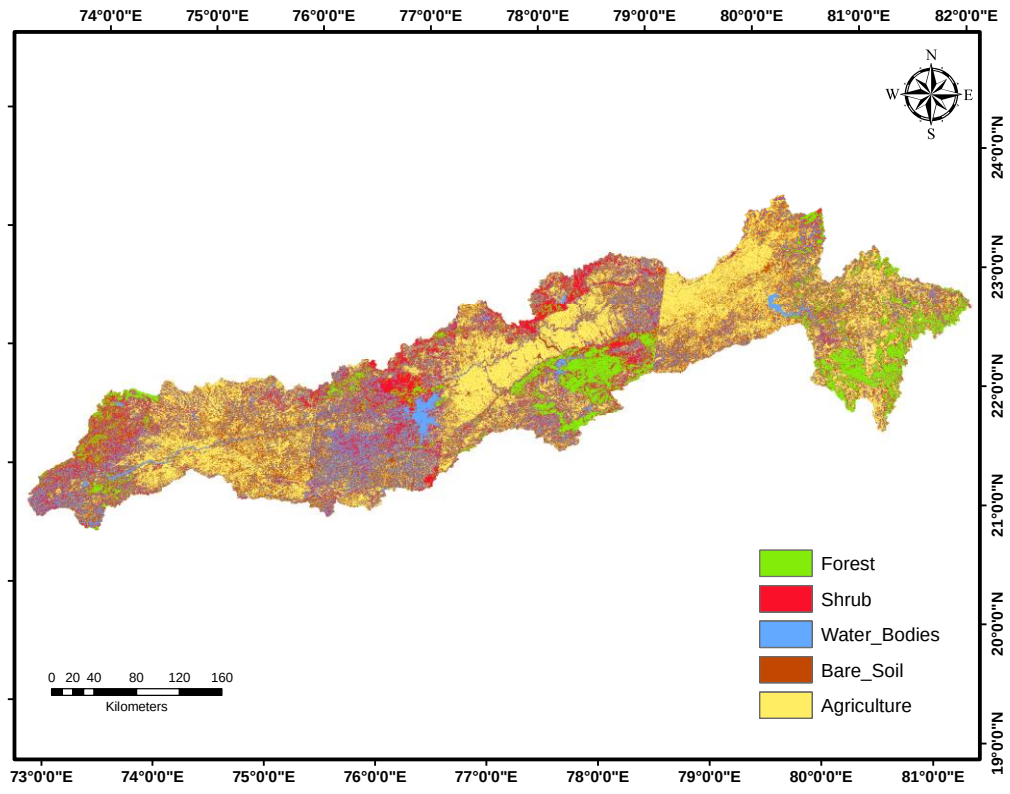

Figure 4.3: Land use land cover map of the Narmada basin

Table 4.3: Area under various LULC classes

LULC classes	Area (km^2)	Area (%)
Forest	20551	21.5
Shrub	22643	23.7
Water bodies	1523	1.6
Bare soil	3008	3.1
Agriculture	47802	50.0

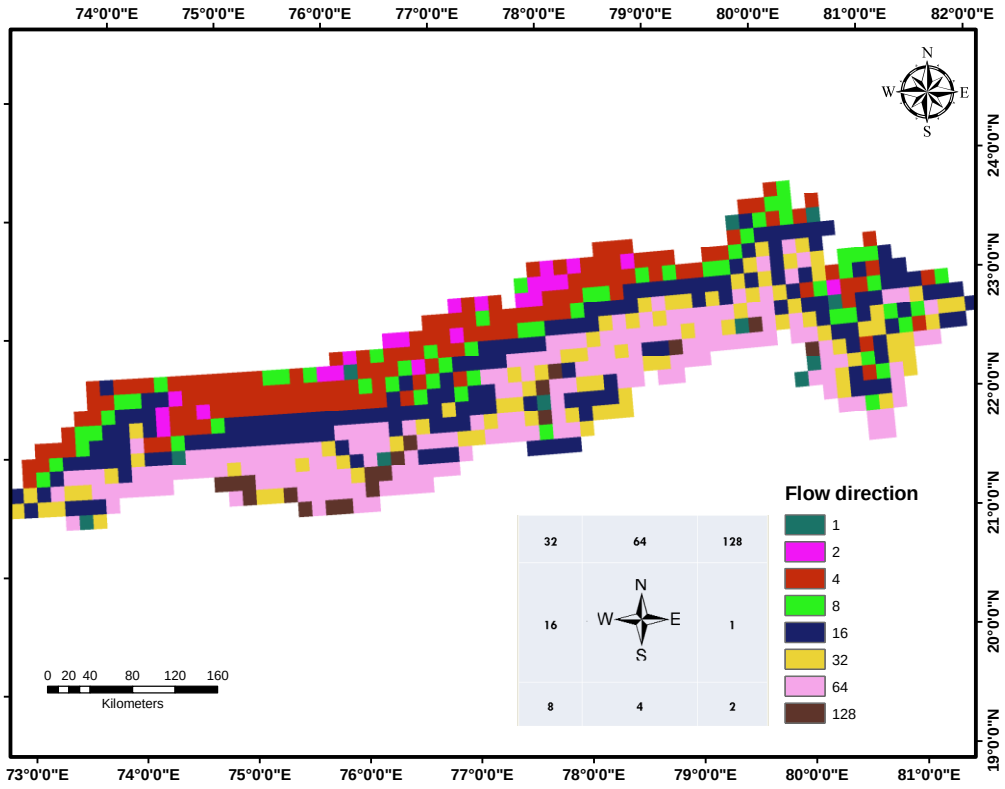

Figure 4.4: Flow direction map up to Hoshangabad of the Narmada basin

The water demand file contains the grid cell information pertaining to total population, urban population, cattle population, population of sheep and goats, urban water demand rate, rural water demand rate and industrial water demands in the appropriate units recognised by the model. Presently, GWAVA reads industrial demands but does not use them anywhere. Rural and urban domestic water use in GWAVA is determined based on the human population per grid cell and per capita water demand. Estimates of return flows and, where relevant, network losses, are included to provide gross amount of water abstracted, i.e., consumptive use. Domestic water demands are assumed to be constant throughout the year. For this study, the Indian population census (GoI, Indian Population Census, 2011) provided information at the taluk level (i.e., an administrative division), which were then classified as urban or rural based upon their locality to major cities and towns. Additional agricultural water demands arise from livestock watering, estimated by the number of cattle, sheep, pigs and small ruminants and a per head water requirement. Livestock

water demands are assumed to be constant throughout the year. Information on these requirements in the Upper Narmada basin were gathered from the Indian Livestock Census [GoI, Indian Livestock Census, 2007], with consumption applied via estimates from the Food and Agricultural Organization (FAO, 2020).

Crop water demands in GWAVA are modelled using the FAO crop water requirement model (Doorenbos & Pruitt, 1977), based on established crop coefficients that vary throughout the growing season (Alen et al., 1998). Irrigation efficiencies are included to provide an estimate of the gross amounts of water abstracted. For this study, surface irrigation methodologies were assumed via the use of canals and their offtakes. The information pertaining to crop type, crop area, planting month etc., is also given in the general water demands file. However the model has the capability of including only eight types of crops for any grid cell. The crop water demands are calculated based on the crop details and PET for the grid cell. Thereafter the crop water demands of all the crops are summed up for each cell. The water demand file has also been prepared based on the information extracted from the GIS shape files and general information pertaining to the crop characteristics in the study area. In the Upper Narmada, the two main command areas are those supplied by the Bargi and Barna reservoirs, covering an area of 1570 km^2 and 579 km^2, respectively. The command area for the Tawa is located downstream of the Upper Narmada basin; therefore, any water allocation from this reservoir was treated as a water transfer to outside of the model domain. The Rabi and Kharif growing seasons were represented on an annual basis with crop rotation.

The climate data file to be used in the GWAVA model can be basically of two types, i) monthly climate normal and anomalies and ii) daily climate. The daily climate data essentially needs to be in the binary format whereas the monthly climate data can be either in ASCII or binary format. The high resolution gridded precipitation data set prepared by India Meteorological Department (IMD) of 0.25^o latitude x 0.25^o longitude has been used to extract the precipitation over the Narmada basin. Similarly the gridded temperature data of IMD at a resolution of 1^o latitude x 1^o longitude has been used to extract the temperature over Narmada basin. The PET has been computed using the Hargreaves method. Thereafter the daily climate data file has been prepared in the binary format.

The Narmada basin up to its confluence with the Arabian sea comprises of 661 grid cells of 0.125^o latitude x 0.125^o longitude resolution. All the mandatory as well as the optional input files have been prepared at this resolution by resampling the original datasets. Even though the input data has been prepared for the complete basin, the modelling exercise has been initially be limited to Upper Narmada Basin up to Hoshangabad. The Upper Narmada Basin comprises of three major

dams viz., Bargi multipurpose dam, Tawa dam and Barna dam. Also many more major, medium and minor projects are being planned in Upper Narmada Basin. For the model application in the Upper Narmada, reservoir operations were based on releases disaggregated in to seasonal regimes, including those releases via irrigation canals to command areas. Reservoir operations were included for the major Tawa, Bargi and Barna dams (Figure 2.1), and simplified to enable their inclusion in the model configuration. Detailed water transfers out of the basin were also incorporated, including those running from the Bargi Dam to the adjacent Ganga basin. Table 4.4 gives the details of the three reservoirs included in the model.

Table 4.4: Reservoirs included in the Upper Narmada application

Dam	River	Year of completion	Gross storage capacity (MCM)
Bargi	Narmada	1988	3924.8
Barna	Barna	1978	539
Tawa	Tawa	1978	2312

The model application for this study is primarily concerned with assessing the impact of climate change on surface water availability. Groundwater reserves are drawn upon to meet grid cell demands based on a ratio split between surface water and groundwater withdrawals. Multi-site model calibration was conducted at a daily time step using an automatic calibration routine, based on Nelder and Mead, (1965). Calibration was undertaken against mean daily flow data for eight gauging stations in the Upper Narmada basin (Figure 4.5 and Table 4.5), obtained from India-WRIS (GoI, India-WRIS). The selection of these stations was based upon the completeness of their records and their location within the basin. A general overview of the modelling approach used in this study is displayed in Figure 4.6.

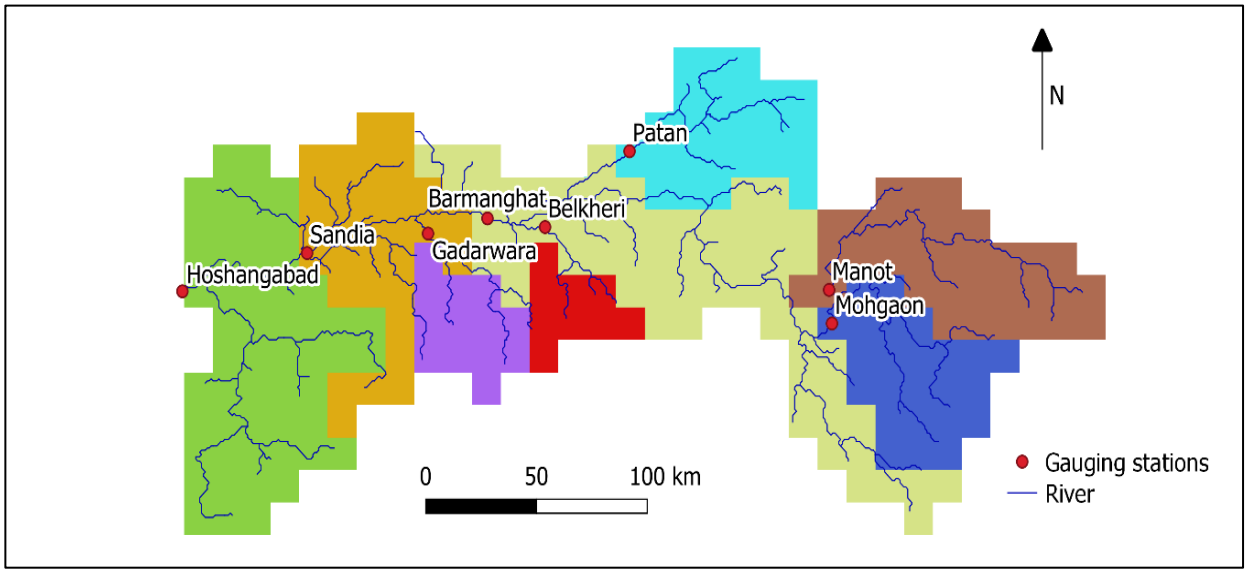

Figure 4.5**:** Drainage area for each of the eight river gauges used for the study (Note that Barmanghat, Sandia and Hoshangabad all gauge the main stem of the Narmada river)

Table 4.5: Information on the gauged sub-catchments used for this study

Gauge	River reach	Catchment area (km^2)
Manot	Narmada	4467
Mohgaon	Burhner	4090
Patan	Hiren	4795
Belkheri	Sher	1508
Barmanghat	Narmada	26453
Gadarwara	Shakkar	2270
Sandia	Narmada	33954
Hoshangabad	Narmada	44548

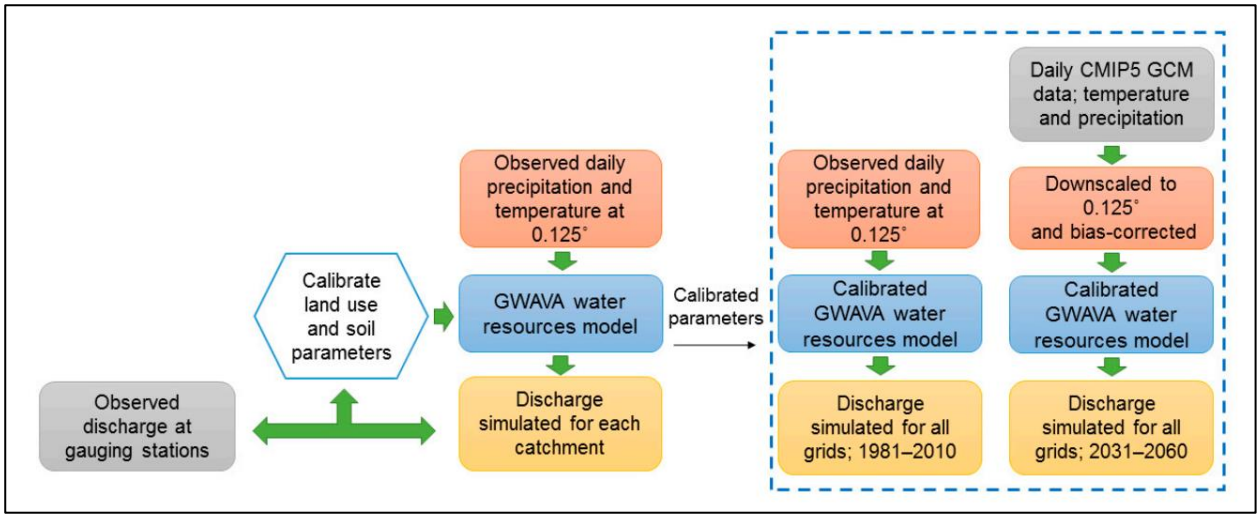

Figure 4.6: Methodology used for assessing the impact of climate change in Upper Narmada

4.1.1 GWAVA calibration and validation

GWAVA model has to option to be run in normal mode or in calibration mode. For running the model is calibration mode, the optional sub-catchment calibration file is to be created to allow the use of calibrated parameters in the sub-catchments desired by the user. Critical model parameters include PDM parameter of power law probability distribution (b) which describes the spatial variations in soil moisture storage capacity, Surface runoff routing parameter (S_{rout}), Groundwater routing parameter (G_{rout}), Multiplier to adjust rooting depths (fact), snowmelt factor, threshold temperature for snowmelt, threshold temperature defining whether precipitation falls as rain or snow, baseflow recession equation power for glacier cells and base flow recession equation power for non-glacier cells needs to be given for the various sub-catchments in the sub-catchment calibration parameter file. The likely ranges of the major parameters are given in Table 4.6.

Table 4.6: Likely range of the few parameters

Parameter	Upper bound	Expected value	Lower bound
b	4	1	0.25
fact	4	1	0.25
S_{rout}	1[2]	-	0
G_{rout}	100		

[1]: A negative value of G_{rout} is allowed. However, this means that there is no routing delay, i.e. all water that drains from the soil store becomes baseflow immediately without being temporarily stored in the groundwater store.
[2]: S_{rout} values above 1 are allowed, however then surface routing is modelled as if S_{rout} is 1.

The high resolution gridded rainfall and temperature data of (India Meteorological Department (IMD)/National Climate Centre (NCC) have been used for the model calibration and validation (Pai et al., 2014; Rajeevan et al., 2006). The potential evapotranspiration (PET) was calculated from using the FAO56 Hargreaves methodology (Allen et al., 1998). The calibration and validation was selected considering only years following the construction of all three dams, to gain a better understanding of their impact on the hydrology in the Upper Narmada, and to represent their influence on the key hydrological processes within the basin. After the automatic calibration, model parameters were fine-tuned through comparison of the modelled and observed hydrographs. The model output was aggregated to a monthly time step and the performance evaluation carried out using statistical measures, including Nash-Sutcliffe coefficient (NSE), Pearson correlation coefficient (r) and percentage deviation in simulated mean flow from the observed mean flow (Dv) (Henriksen et al., 2003).

4.2 Hydrological modelling of Upper Narmada Basin using MIKE-SHE

MIKE SHE has a modular structure and although it was originally designed as physically-based model code, many of the modules now offer a range of process descriptions, some of which are conceptual and semi-distributed. These are particularly applicable for large basins such as the Narmada where the focus is the simulation of river flow and where detailed data, such as hydrogeological characterisation, required for more physically-based approaches, are seldom available (Andersen *et al.*, 2001; Stisen *et al.*, 2008; Refsgaard *et al.*, 2010). Table 4.7 summarises the components of the MIKE SHE model of the Upper Narmada and the data employed within them. The model domain was specified using a shape file based upon the catchment shape file for the whole of the Narmada basin. Watershed delineation was undertaken using topographic data (see below) and this shape file within ArcSWAT (Winchell *et al.*, 2013) to define the catchment extent of the Upper Narmada Basin to just downstream of Hoshangabad discharge station. This provided a catchment area of 44,725 km^2. The model grid size was set to 2 km × 2 km in order to retain a balance between representing catchment characteristics and efficient computation time (Vázquez *et*

Table 4.7: Summary of key data (and data processing) required for each component of the coupled MIKE SHE/MIKE 11 model of the Upper Narmada

Model component	Key inputs/ data required	Initial data format	Processing undertaken externally to MIKE Zero*	Processing undertaken in MIKE Zero
Model domain	Catchment extent – the basin area upstream of Hoshangabad	ESRI polygon shapefile	In ArcGIS: Converted to a different coordinate system (Projected coordinate system WGS 1984 UTM Zone 44N). Edited the edge to prevent gridding errors in MIKE SHE.	N/A
Topography	Topography	ESRI grid raster file with a resolution of 0.0008333° × 0.0008333°. Data source: SRTM (Shuttle Radar Topography Mission)	In ArcGIS: Converted to UTM 44N coordinate system and to a spatial resolution of 1 km × 1 km to match the initial model grid. Final model grid size: 2 km × 2 km.	Converted to MIKE Zero's dfs2 grid file format.
Land use/ vegetation	Land use distribution	Imagine image raster file. There are five land use classes: Forest, Shrub, Water bodies, Bare soil and Agriculture.	In ArcGIS: Converted to UTM 44N coordinate system and to a spatial resolution of 1 km × 1 km. Buffer generated around available data.	Converted to MIKE Zero's dfs2 grid file format.
	Leaf Area Indexes	N/A	Values for the different land cover classes are based on those used in similar work undertaken by UCL (Thompson *et al.*, 2013; Thompson *et al.*, 2014).	
	Root depths	N/A	As above.	
Overland flow: modelled using the 2D finite-difference method	Manning's M for overland flow resistance	N/A	Manning's M values distributed according to land use/ land cover, using a dfs2 grid file based on the land use dfs2 file. Values for the different land cover classes based on Vieux (2004).	
Unsaturated zone: modelled using the two-layer water balance method	Soil classes	ArcGIS polygon shapefile and rasters that provide soil class data for the majority (~80%) of the basin.	In ArcGIS: Converted to UTM 44N coordinate system and to a spatial resolution of 1 km × 1 km. Buffer generated.	Converted to MIKE Zero's dfs2 grid file format.
Saturated zone: modelled using the conceptual, linear reservoir method	Spatial distribution of ground-water sub-catchments, interflow reservoirs and baseflow reservoirs	NIH consulted with on the number and location of gauging stations to be employed during model calibration.	Polygon shapefile has been generated in ArcGIS. The basin was divided into five groundwater sub-catchments based on topography and the locations of the five calibration gauging stations.	N/A
Catchment meteorology: Precipitation and evapo-	Spatial distribution of precipitation	N/A	Polygon shapefile of 0.25° × 0.25° grid squares covering the basin extent, generated in ArcGIS.	N/A

transpiration modules.	Precipitation	0.25° × 0.25° gridded daily precipitation for India for the period 1901–2013. Data for each year is in a different file, in a gridded binary format.	Data first converted to ASCII file format using C script provided with data. Data then processed in Matlab into the necessary format for input to MIKE Zero.	Data converted into MIKE Zero's dfs0 time series file format.
	Spatial dist. of PET	N/A	Generated 1° × 1° polygon shapefile.	N/A
	Potential evapotrans-piration	Gridded (1° × 1°) temperature data received from NIH for the calculation of PET.	PET data calculated in Matlab – for the cells covering the basin down to Hoshangabad only.	Data converted into MIKE's dfs0 time series file format.
MIKE 11 one-dimensional hydraulic model for simulating channel flow (using Kinematic routing)	Plan of the main river channels	An ESRI polyline shapefile. This dense river network is divided into seven stream orders.	In ArcGIS: Different stream orders extracted to separate shapefiles. New field generated: length of each branch.	River network digitised in MIKE Zero / MIKE 11.
	Synthetic cross-sections	N/A	Synthetic cross-sections generated in Excel.	Data input to MIKE 11 model.
	Manning's n for bed resistance	N/A	Representative value based on the literature (Chow, 1959) and previous modelling experience.	
N/A	River discharge time series for model calibration/ validation.	Data for the calibration/validation period of 2002–2013 received for five gauging stations.	Data for the five stations have been processed in Excel and Matlab into the necessary format for input to MIKE Zero.	Data converted into MIKE Zero's dfs0 time series file format.

al., 2002; Thompson *et al.*, 2013). Consequently, although most spatial inputs to the model, such as topography and land cover, have a resolution of 1 km × 1 km, during model runs, all input data are automatically resampled to the 2 km × 2 km model grid. Topography was specified using SRTM (Shuttle Radar Topography Mission) based data (Figure 4.7) (available from the USGS EarthExplorer: http://earthexplorer.usgs.gov/).

The spatial distribution of five different land cover classes within the basin was extracted using remote sensing (Figure 4.8). The Leaf Area Index (LAI) values for the different land cover classes were based on a combination of those used in the Mekong MIKE SHE model and values from Jain et al., (1992), a study that modelled the Kolar sub-catchment of the Narmada basin. The Root Depth (RD) values for the different land cover classes were based on those used in the Mekong MIKE SHE model (Table 4.8). The overland flow in the Upper Narmada model is calculated using a finite-difference approach to solve the two-dimensional Saint–Venant equations (Graham and Butts, 2005). The land cover data were employed to spatially distribute Manning's M (the inverse of Manning's n) values for overland flow resistance (Table 4.8), with values based on Vieux (2004).

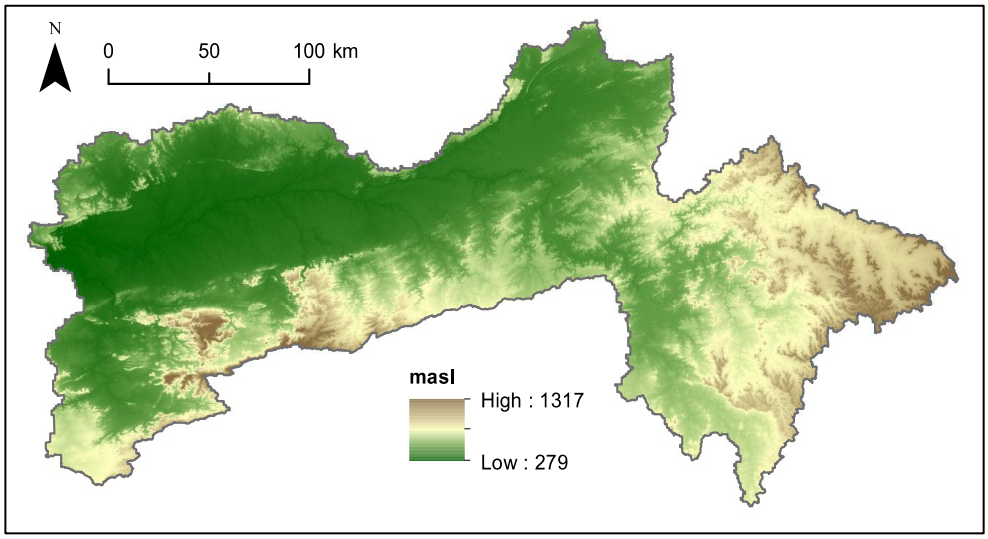

Figure 4.7: Topographic data for the Upper Narmada Basin

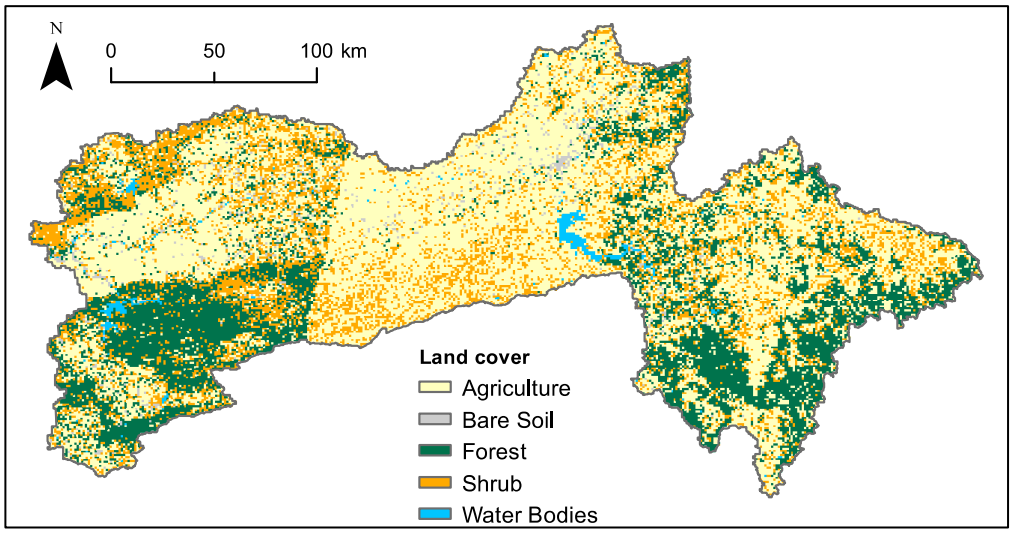

Figure 4.8: Land cover classes within the Upper Narmada Basin

Table 4.8: Summary of land cover classes and related parameters

Code	Land cover	Root depth (mm)[1]	LAI[2]	Manning's M[3]
2	Forest	900	1.0–6.0	10
3	Shrub	500	2.6–3.8	8
4	Water bodies	0	0	25
5	Bare soil	10	0	50
6	Agriculture	500	0.3–6.9	29

[1] Based on the MIKE SHE model of the Narmada.
[2] Based on the MIKE SHE model of the Narmada and Jain *et al.* (1992).
[3] Based on Vieux (2004).

Following initial calibration attempts that revealed overestimation of discharge at downstream discharge stations (Barmanghat and Hoshangabad), irrigation was included within the

model over two command areas: Bargi (1570 km^2) and Barna (579 km^2). The locations of the command areas (Figure 4.9) were based on a map from Government of India Ministry of Water Resources (2014) that was georectified and digitised in ArcGIS. Data on the location of the culturable command area (land actually irrigated) within the gross command area (the overall region containing irrigated land) were not available. However, the acreages of the command areas included in the MIKE SHE model were made to match those reported on the India-WRIS (Water Resources Information System) website (India-WRIS, 2013a, b) and in Government of India Ministry of Water Resources (2014). Irrigation water for the Bargi and Barna command area was specified as being abstracted from the river sections at the locations of Bargi Dam and Barna Dam, respectively. During model calibration, an evapotranspiration crop coefficient (Kc) of 1.2 was added over the command areas for the months of May–September. This means that the input PET over these areas is multiplied by 1.2 in these months. Crop coefficients are commonly employed to adjust potential evapotranspiration estimates specifically for cropland, and a Kc of 1.2 is within the range of normal Kc values according to Allen *et al.* (1998).

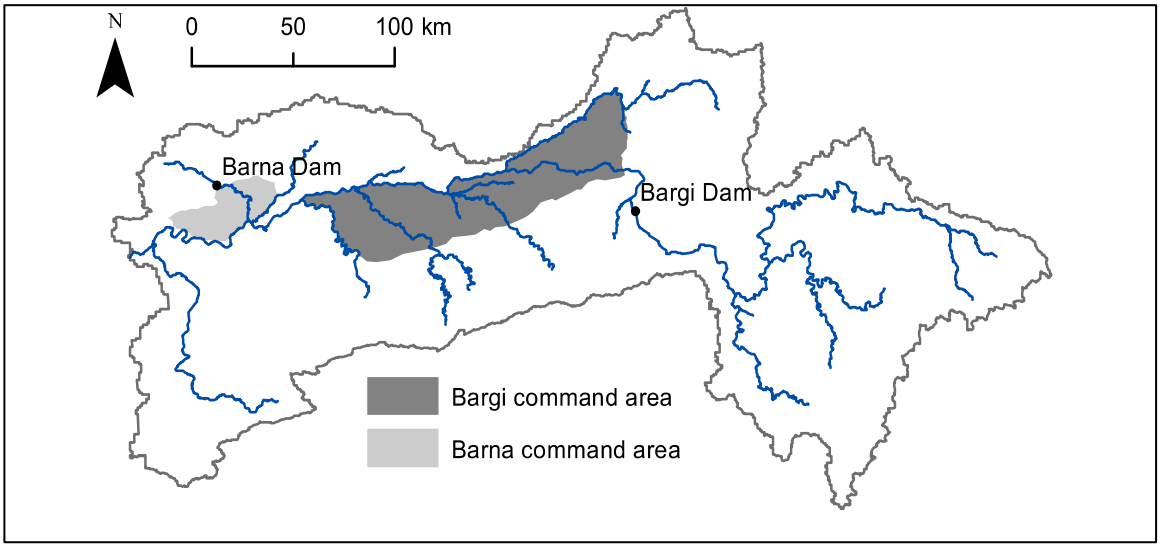

Figure 4.9: Gross command areas and associated dams included in MIKE-SHE

The two-layer water balance method was employed for the unsaturated zone. For this module, the spatial distribution of soil classes was specified using a 1 km × 1 km grid based on a geo-rectified and digitised version of a soil map that was used. Soils were aggregated into six classes (Figure 4.10) and the required hydraulic parameters for each soil class were taken from the literature as given in Table 4.9. For modelling the saturated zone, the conceptual, semi-distributed, linear reservoir method was selected. Advantages of this method include lower data requirements and reduced computation time compared to physically based solutions (Andersen *et al.*, 2001; Stisen *et al.*, 2008; Thompson *et al.*, 2013; 2014a; 2014b). Using the approach employed for the

Mekong (Thompson *et al.*, 2013), the Upper Narmada was divided into five sub-catchments (Figure 4.11 & Figure 4.12) based upon topography and the location of the discharge gauging stations for which data for model calibration/validation were available. Within each sub-catchment, the saturated zone is represented by a shallow interflow reservoir, and two baseflow reservoirs to simulate faster and slower baseflow storage. Exchanges between reservoirs, and ultimately the MIKE 11 hydraulic model, are controlled by time constants (DHI-WE, 2009). The two time constants (interflow and percolation) for each interflow reservoir and the baseflow time constant for each baseflow reservoir were varied during model calibration.

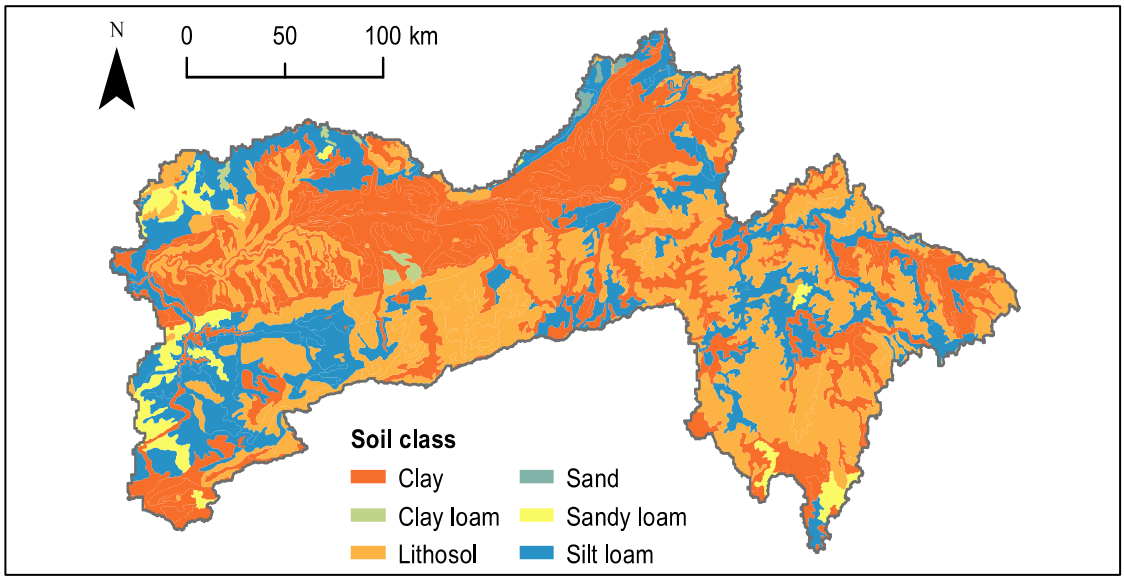

Figure 4.10: Soil class distribution within the Upper Narmada Basin

Table 4.9: Soil classes and associated parameter values

Soil_ code	Soil_class	Water content at saturation*	Water content at field capacity+	Water content at wilting point+	Saturated hydraulic conductivity (m/s)
1.	Sand	0.40	0.14	0.04	0.00018
2.	Sandy loam	0.43	0.26	0.09	3.5e-005
3.	Silt loam	0.49	0.34	0.16	7.2e-006
4.	Clay loam	0.47	0.34	0.18	2.5e-006
5.	Clay	0.48	0.42	0.25	1.3e-006
6.	Lithosol	0.45	0.30	0.13	7e-006

* from Clapp and Hornberger (1978) + from Norman and Dixon (1995)

The daily gridded precipitation data for the Upper Narmada were derived from the IMD (India Meteorological Department) / NCC (National Climate Centre) High Spatial Resolution (0.25° × 0.25°) Long Period (1901–2013) Daily Gridded Rainfall Data Set Over India (Pai et al.,

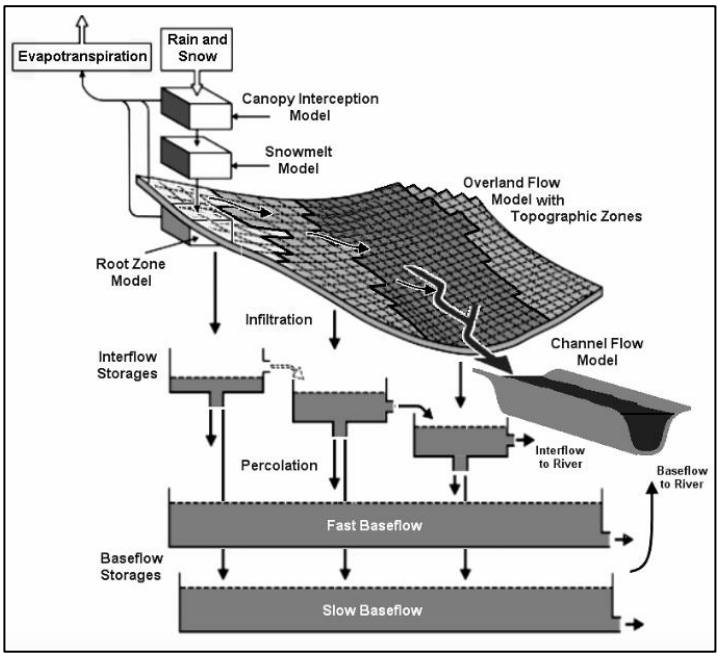

Figure 4.11: Conceptual structure of the sub-catchment based linear reservoir saturated zone module. Source: Graham and Butts (2005).

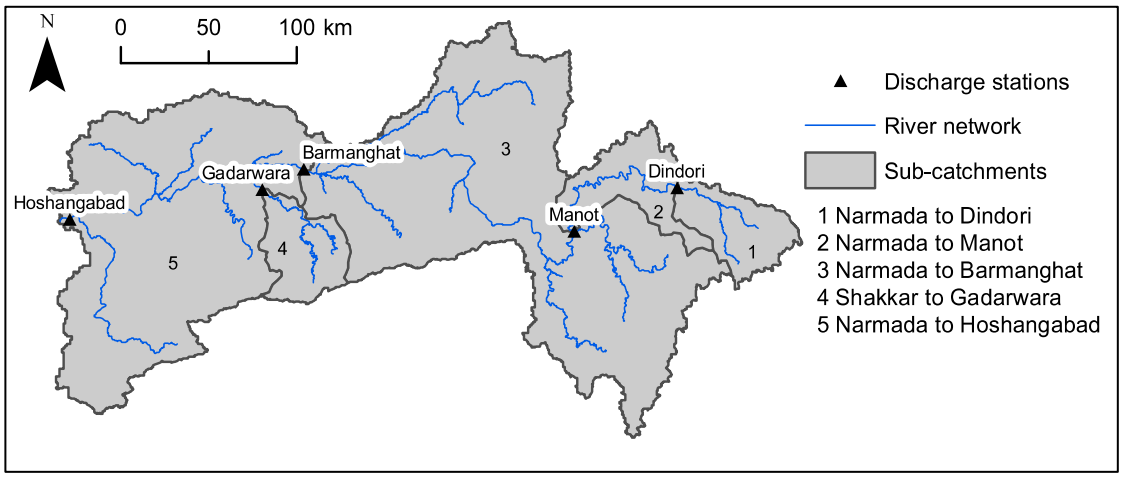

Figure 4.12: Sub-catchment distribution and river discharge gauging station locations

2014), obtained from the IMD. During model calibration, a precipitation lapse rate was introduced over the spatial extent of sub-catchments 1, 2 and 4, which are upstream sub-catchments located at higher elevations. The three lapse rates were then subject to calibration. For the calculation of daily gridded potential evapotranspiration (PET), IMD/NCC high resolution (1° × 1°) gridded daily temperature data (Srivastava et al., 2009) were used. PET was calculated using the Hargreaves method, as this method is recommended by the FAO for use in situations where there are insufficient data to calculate Penman-Monetith (Allen et al., 1998). Parameters for the equation were based upon those obtained from ECALTOOL, a computer program that provides calibrated values for the CH and EH parameters of the Hargreaves equation (Patel et al., 2014). The

parameters vary through the year, with the values for some months subjected to further calibration independent of the ECALTOOL. The spatial distributions of precipitation and PET inputs are shown in Figure 4.13.

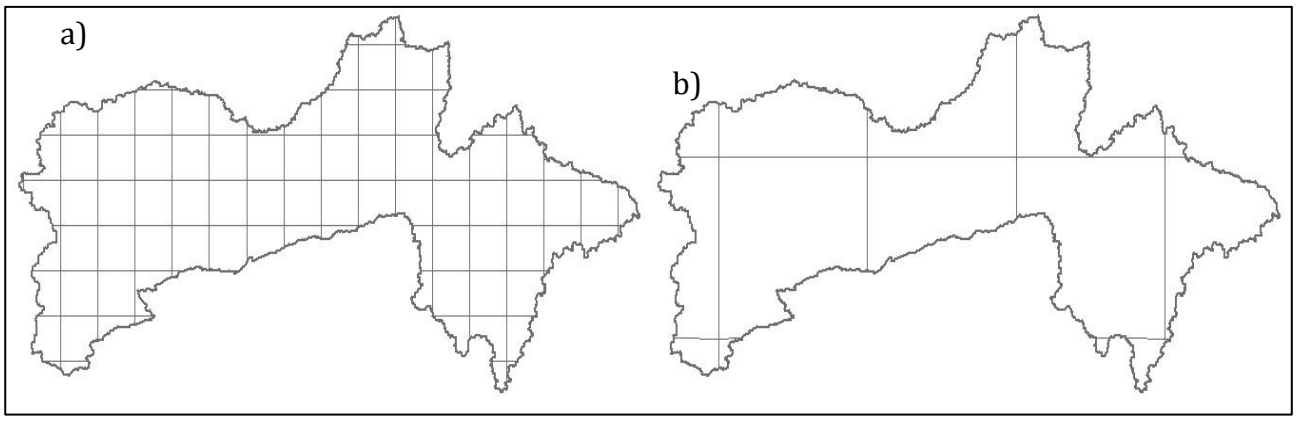

Figure 4.13: Spatial distribution of a) precipitation inputs and b) PET inputs.

For the simulation of channel flow, MIKE SHE is dynamically coupled to MIKE 11 (Havnø *et al.*, 1995), a one-dimensional hydraulic model. A plan of the main river network was digitised in MIKE 11. For the generation of synthetic cross-sections, channel width measurements were taken from satellite imagery in Google Earth. A generalised cross-section profile and a relationship between channel width and maximum channel depth were based on limited data available from NIH (a single cross-section for the river channel at Hoshangabad discharge station) and the literature (Rajaguru *et al.*, 1995; Payasi, 2015). Cross-sections were specified as depths relative to the bank, with bank elevations taken from the SRTM DEM (digital elevation model). The Kinematic routing method was employed.

4.2.1 MIKE-SHE calibration and validation

The model calibration was undertaken against discharge records from five gauging stations for the period 2002–2008. The calibration parameters were the time constants of the saturated zone's interflow and baseflow linear reservoirs and the precipitation lapse rates over selected sub-catchments. As described above, irrigation command areas were added to the model in the early stages of calibration and a Kc of 1.2 was added over these areas for the months of May–September. Model performance at each discharge station was evaluated both qualitatively, through visual comparison of graphs of observed and simulated discharge, and quantitatively, using model performance statistics. The indicators used were the Nash–Sutcliffe coefficient (NSE; Nash and Sutcliffe, 1970), the Pearson correlation coefficient (r) and the percentage deviation in simulated mean flow from the observed mean flow (Dv) (Henriksen et al., 2003). NSE can vary between -1 and 1, whilst r can vary between 0 and 1; in both cases, the closer the value to 1, the better the

model performance according to that criteria. In the case of Dv, the closer the value to 0, the better. Model performance according to the NSE and Dv values was classified using the scheme of Henriksen et al. (2008). Model validation was subsequently undertaken for the period 2009 to May 2013 using the same stations and performance statistics.

5.0 Results and Discussions

5.1 GWAVA Application in Upper Narmada Basin

5.1.1 Calibration and Validation

The model performance statistics for the calibration (1990-2000) and validation (2001-2010) are given in Table 5.1.

Table 5.1: Model performance statistics during calibration and validation

Station	Period		Dv	NSE	r
Manot	Cal: 1990–2000		5.72	0.95	0.97
	Val: 2001–2010		2.30	0.96	0.98
Mohgaon	Cal: 1990–1996		−0.55	0.87	0.88
	Val: 2001–2010		−6.7	0.90	0.95
Patan	Cal: 1990–2000		16.93	0.92	0.97
	Val: 2001–2010		17.8	0.90	0.97
Belkheri	Cal: 1990–2000		11.07	0.87	0.94
	Val: 2001–2010		5.2	0.80	0.89
Barmanghat	Cal: 1992–2000		0.25	0.90	0.94
	Val: 2001–2010		−6.2	0.90	0.95
Gadarwara	Cal: 1990–2000		8.60	0.92	0.96
	Val: 2001–2010		−5.4	0.64	0.80
Sandia	Cal: 1990–2000		6.73	0.92	0.96
	Val: 2001–2010		2.5	0.87	0.93
Hoshangabad	Cal: 1990–2000		1.16	0.93	0.97
	Val: 2001–2010		−2.1	0.89	0.95
Performance indicator	Excellent	Very good	Fair	Poor	Very poor
Dv	<5%	5–10%	10–20%	20–40%	>40%
NSE	>0.85	0.65–0.85	0.50–0.65	0.20–0.50	<0.20

The model generally performs well during calibration and validation periods in reproducing monthly river discharges at all the eight gauging stations. The NSE values range from 0.64 to 0.96, except for the validation period at Gadarwara categorised to fall in “very good” to “excellent”, class with ‘r’ values ranging from 0.88-0.98. Dv again falls in “very good” to “excellent” class for both calibration and validation at six gauging sites. However, Patan and Belkheri, both overestimate total flows, indicating that the overall processes present in these catchments might not be well represented as compared to other gauging sites. This overestimation of the total flows is seen, at

few other gauges also, but it is to a lesser extent. The possible reason may be attributed to the large number of small-scale watershed interventions in the form of check dams, stop dams, field bunds and farm ponds present throughout the basin, which are not possible be represented in the model set-up, largely due to a lack of data being available for these features. Such structures are likely to attenuate flow and reduce quick flow response, promoting groundwater recharge and therefore slower flow pathways. These small structures also lead to greater rates of actual evapotranspiration (AET) resulting in the higher quantum of water losses from the system. Despite this, the annual hydrological regime is well represented by the model, with the timing and magnitude of flow for the south-west monsoon being captured reasonably well at all sites for both the calibration and validation periods, as can be observed in Figure 5.1 and Figure 5.2.

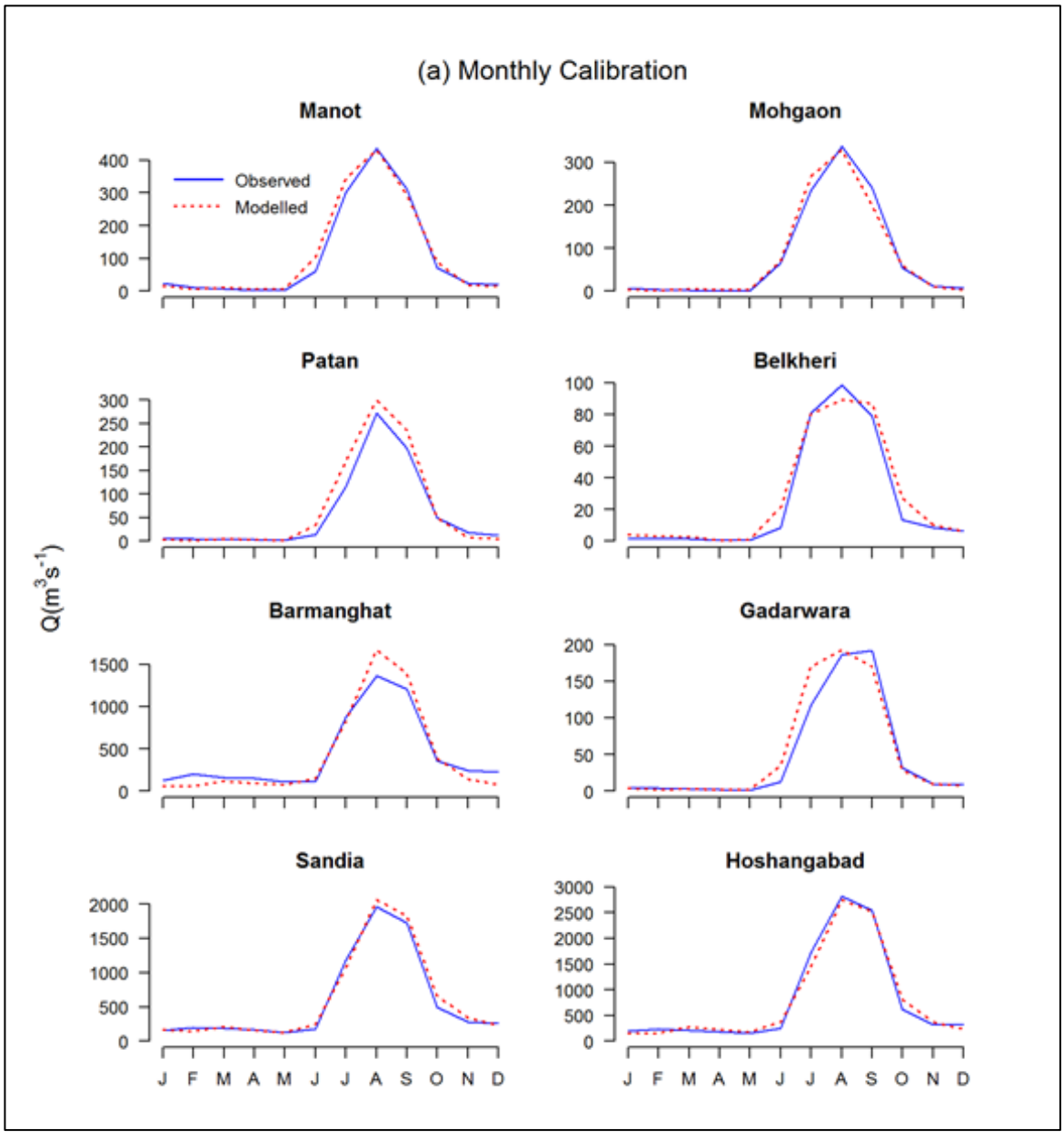

Figure 5.1: Average monthly observed and modelled output at the eight gauging sites during validation

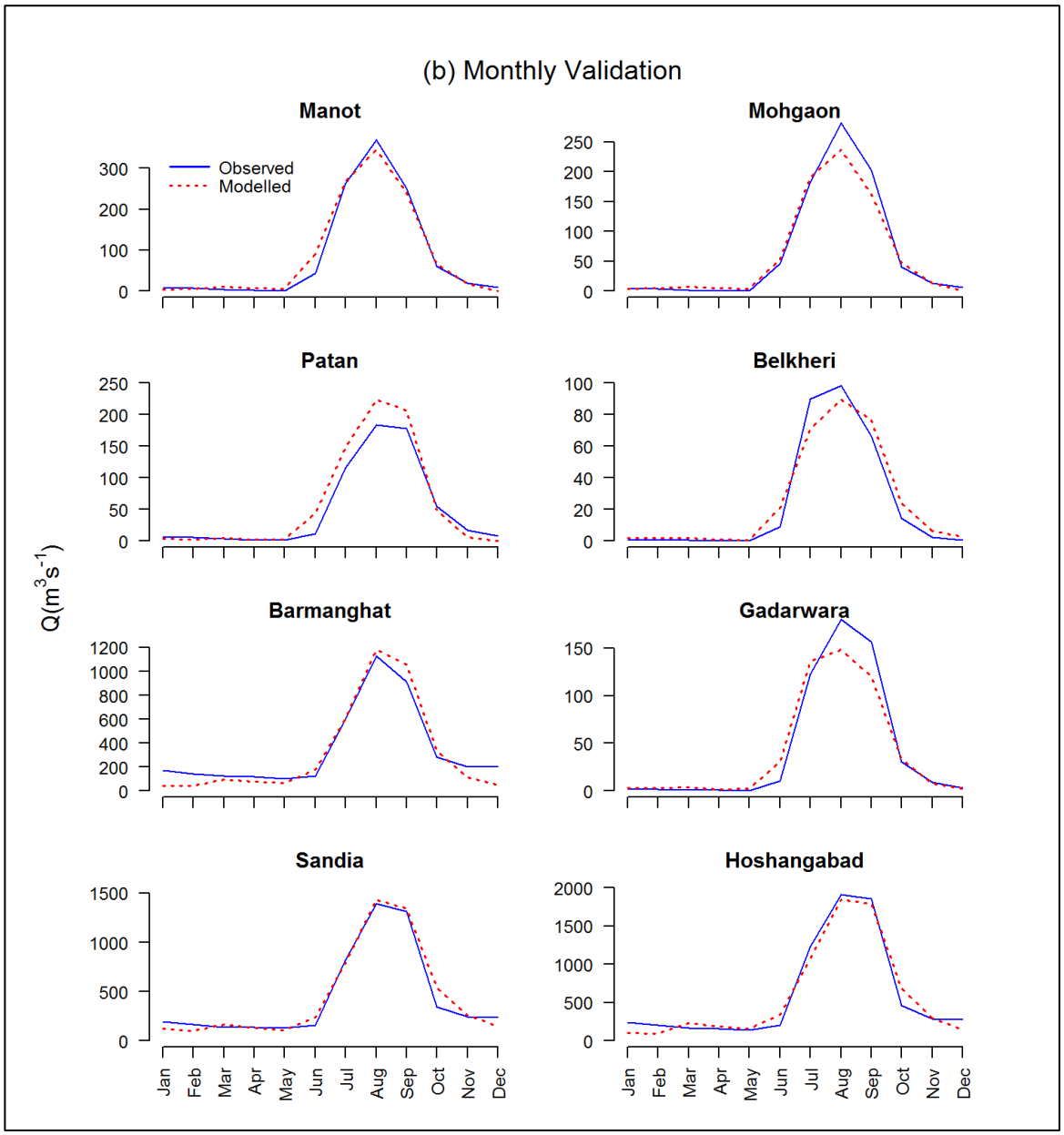

Figure 5.2: Average monthly observed and modelled output at the eight gauging sites during validation

The performance evaluation statistics flow suggest a good fit of the simulated flows to the observed flows, especially when taking in to account the relatively coarse temporal and spatial resolution being used and the extent of modification along the river reaches of river Narmada. Therefore, the application GWAVA model to the Upper Narmada is found to be satisfactory and may be considered as suitable for exploring the future impacts of climate change on the water resources of the basin using the calibrated parameters.

5.1.2 Climate Change Impact Assessment

The calibrated GWAVA model was forced with gridded IMD climate data to obtain simulated discharge for a 30-year baseline period, i.e. for the period 1981–2010. GWAVA was

forced with GCMs included in CMIP5 for a future period of 2031–2060, under a RCP 4.5 scenario (Representative Concentration Pathway that can produce 4.5 W m^{-2} radiative forcing by the end of 21st Century) for obtaining the projected river flow in future. Table 5.2 provides the details of the GCMs used in this study. The CMIP5 GCM data were downscaled and bias corrected to a spatial resolution of 0.25◦ × 0.25◦ using the Bias-Correction Spatial Disaggregation (BCSD) method (Rahman et al., 2020). An additional stage of bias correction was subsequently undertaken, where the GCM bias for the historical period was assessed in relation to the IMD/NCC data, and this information used to correct the future GCM projections. The final GCMs chosen for the study are exemplars from the CMIP5 database, providing different representations of global climate features (Thompson et al., 2017).

Table 5.2: Details of Global Circulation Models (GCMs) used in the study

Model Name	Institution
ACCESS1-0	Commonwealth Scientific and Industrial Research Organisation (CSIRO) and Bureau of Meteorology (BOM), Australia
bcc-csm1-1	Beijing Climate Center, China Meteorological Administration
BNU-ESM	College of Global Change and Earth System Science, Beijing Normal University
CanESM2	Canadian Centre for Climate Modelling and Analysis
CCSM4	National Center for Atmospheric Research
CESM1-BGC	Community Earth System Model Contributors
CNRM-CM5	Centre National de Recherches Météorologiques/Centre Européen de Recherche et de Formation Avancée en Calcul Scientifique
CSIRO-Mk3.6.0	Commonwealth Scientific & Industrial Research Organisation in collaboration with the Queensland Climate Change Centre of Excellence
GFDL-CM3	NOAA Geophysical Fluid Dynamics Laboratory
GFDL-ESM2M	
IPSL-CM5A-LR	Institut Pierre-Simon Laplace
IPSL-CM5A MR	
MIROC5	Atmosphere and Ocean Research Institute (The University of Tokyo), National Institute for Environmental Studies, and Japan Agency for Marine-Earth Science and Technology
MIROC-ESM	
MIROC-ESM-CHEM	
MPI-ESM-LR	Max-Planck-Institut für Meteorologie (Max Planck Institute for Meteorology)

The projected changes in future climate for the period 2031–2060 were assessed relative to the baseline period of 1981–2010. The projected mean annual precipitation is increasing across all GCMs show an increase at all grids by 2060, with a median increase of between 13.7% at

Barmanghat and 18.1% at Hoshangabad (Figure 5.3a). There is considerable variation in mean annual precipitation between the GCMs, with IPSL-CM5A-LR predicting increases of over 40% at Sandia, Gadarwara and Hoshangabad. Also, the Interquartile Range (IQR) is relatively small, varying between 13% at Hoshangabad and 16.6% at Patan. Only three out of seventeen models across all sites show a decrease in annual precipitation, these being at Belkheri, Gadarwara and Patan. Figure 5.3b shows the majority of GCMs projecting an increase in precipitation. The baseline median of the annual mean rainfall of 1136.61 mm is exceeded by all models, the largest increase being projected by the IPSL-CM5A-LR model at 1560.54 mm (+37%). Inter-annual variation is relatively large and is also projected to increase for all the GCMs when compared to the baseline IQR of 242.19 mm. The IPSL models again show the largest variation in mean annual precipitation, with IQR values of 872.75 mm (260.3%) for IPSL-CM5A-LR and 902.56 mm (272.6%) for IPSL-CM5A-MR.

Changes in PET within the basin are less pronounced, although the annual mean across all GCMs increases at all eight sites (Figure 5.3c). Median values range from a +2.5% increase at Patan, through to a +4.6% increase at Manot. The spread in mean annual values across all sites is relatively small, with the largest IQR being displayed at Belkheri. Total PET variation between years within models is more pronounced (Figure 5.3d). The median baseline PET from 1981–2010 of 1758.63 mm is exceeded by all of the GCM models, the most substantial increase displayed by the CanESM2 model with a median of 1879.39 mm (+6%). The variation between GCMs is less marked for future precipitation, with the lowest median value of 1805.37 mm being projected by the CNRM-CM5 model. The IQR between models is also less pronounced, ranging from 40.06 mm for the CCSM4, through to 122.45 mm for the IPSL-ESM2-MR model, compared to a baseline IQR of 73.29 mm; −45% and +67% change, respectively. Despite considerable variation between individual GCMs for both future precipitation and PET, the direction of change remains consistent throughout for the majority of years from 2031–2060, with projected increases in both precipitation and PET at all eight gauging sites.

All projected changes in flow under the RCP 4.5 scenario are assessed relative to the baseline period of 1981-2010. Figure 5.4 displays simulated river regimes of mean monthly discharge at the eight gauging stations for each of the seventeen GCMs, along with those for the baseline period and ensemble mean. It is during the months of the prevailing south-west monsoon where the greatest changes can be seen between baseline and future scenario flows, as there is little change during the dry season low flows. All stations display the largest difference between baseline and ensemble mean in August, for example, with the flow at Hoshangabad and Manot increasing by

1143 m^3s^{-1} and 166 m^3s^{-1}, respectively. The timing of the monsoon closely follows that of the baseline period across all sites, but intensifies earlier in June before reaching its peak in August,

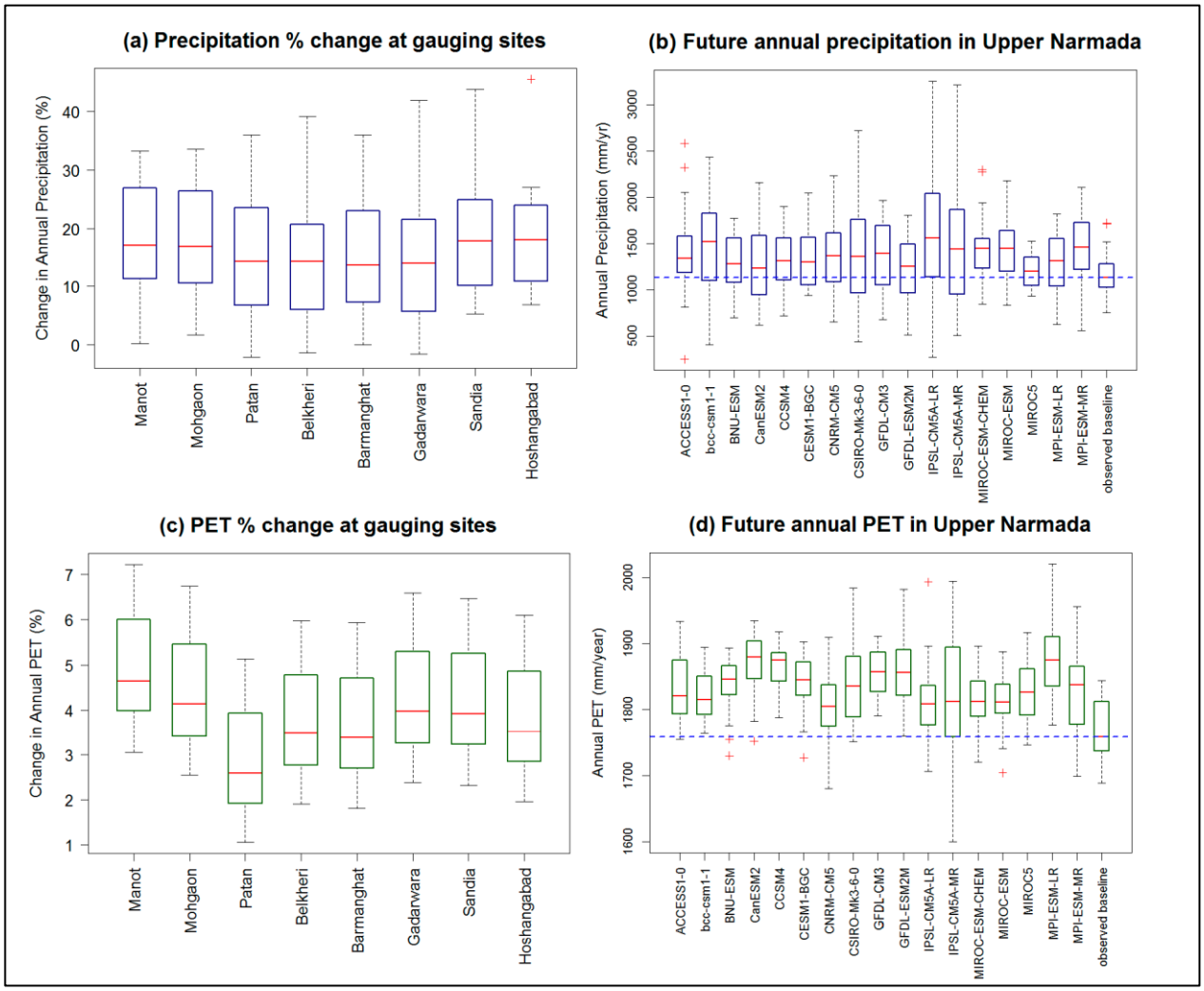

Figure 5.3 (a): Percentage change in total mean precipitation at each gauging site between baseline and future period; (b) Annual precipitation in the Upper Narmada for each GCM; (c) Percentage change in total mean Potential Evapotranspiration (PET) at each gauging site between baseline and future period; (d) Annual PET in the Upper Narmada for each GCM. Values more than 1.5 times the interquartile range below the 25th quartile or above the 75th quartile are plotted as outliers (+).

with the recession of flows hereon through to the start of October. The increase in flows during the monsoon is substantial for a number of the individual GCM runs, with MIROC-ESM1 projecting a 101.3% increase in flow in August at Hoshangabad, and MIROC-ESM-CHEM an increase of 68.1%. MIROC5 projects a less extreme change in stream flow, predicting lower peaks in August than that of the baseline period.

Figure 5.5 shows how flows across the whole basin are projected to change based on the annual mean output from GWAVA for the CMIP5 ensemble. Changes in flow generally follow the

same trend as that seen at the eight gauging stations in Figure 5.4, with increases displayed in the majority of river reaches across the basin. The ensemble mean flow are projected to increase by up to +49% for tributaries to the north of the Bargi command area, with an average increase of 25%

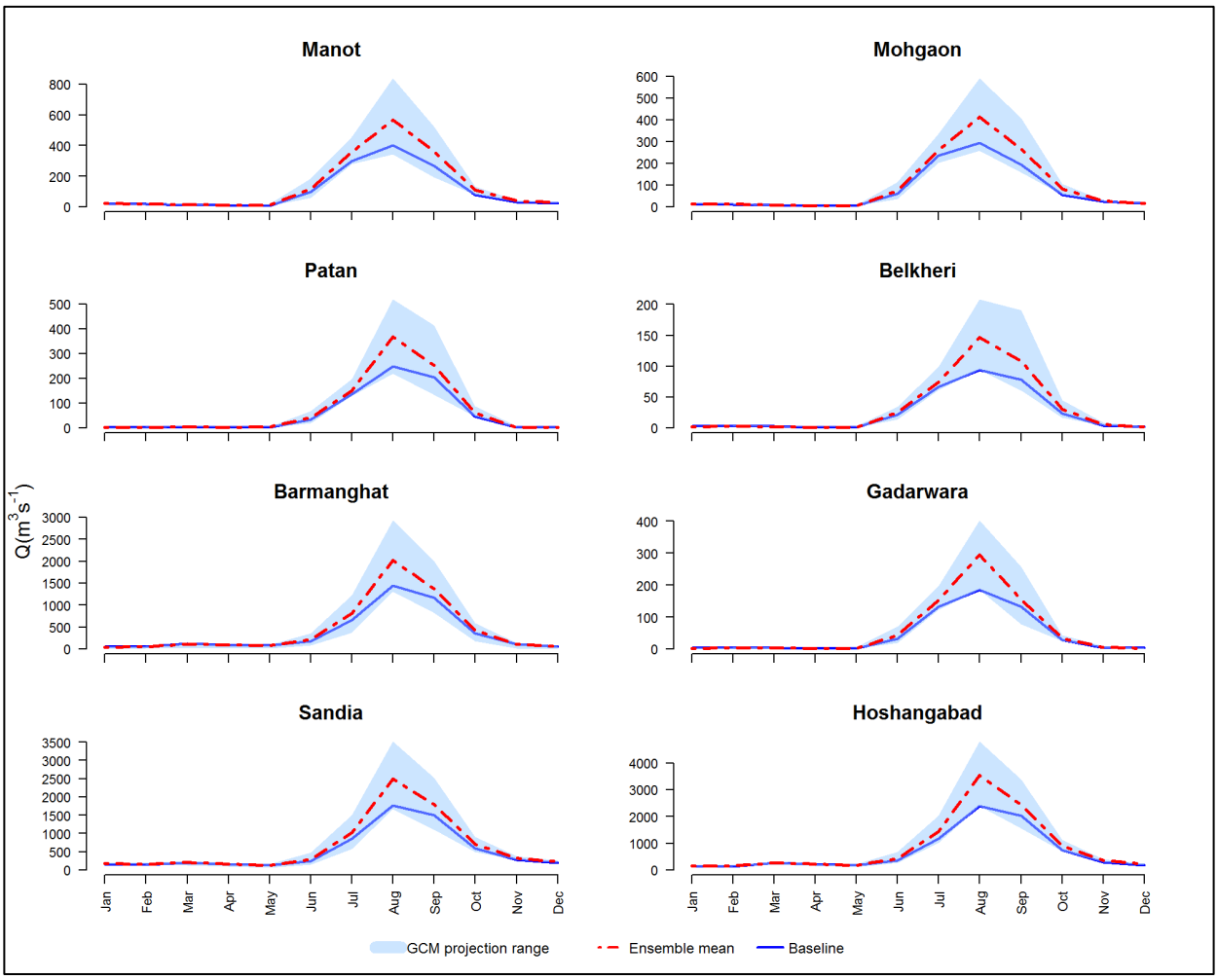

Figure 5.4: Mean monthly flow from seventeen CMIP5 GCM models with ensemble mean (2031–2060) and baseline (1981–2010)

across all river cells. Changes in mean flow also show an increase across all gauging stations, the highest being 183.2 m^3s^{-1} at Hoshangabad, representing a +27.1% increase from the baseline flow. As would be expected, the smaller tributary catchments of Manot (1), Mohgaon (2), Patan (3), Belkheri (4) and Gadarwara (6) show the smallest increase in absolute flow.

Flows at the 10% exceedance level (Q10) represent high flows during the monsoon season, and again show an increase for most of the basin, largely driven by the rise in monsoon rainfall. This increase in high flows is particularly prevalent in the smaller tributaries in the west of the basin, with increases of up to 58%. An average rise of 21% at Q10 is seen across the basin. Increases in Q10 flow are also seen at each of the gauging stations, with fifteen of the seventeen GCMs displaying amplified Q10 flows from the baseline across all sites. Flows at Sandia and Hoshangabad display the largest absolute increases from the baseline, with mean values of 150.3

m^3s^{-1} and 196.8 m^3s^{-1}, respectively. Decreases in mean Q10 flows are also evident within the ensemble runs, with a 46.7% decrease at Barmanghat (5), a 27% decrease at Sandia, and a 21.6% decrease at Hoshangabad, all of which are driven by the same GCM, IPSL-CM5A-MR.

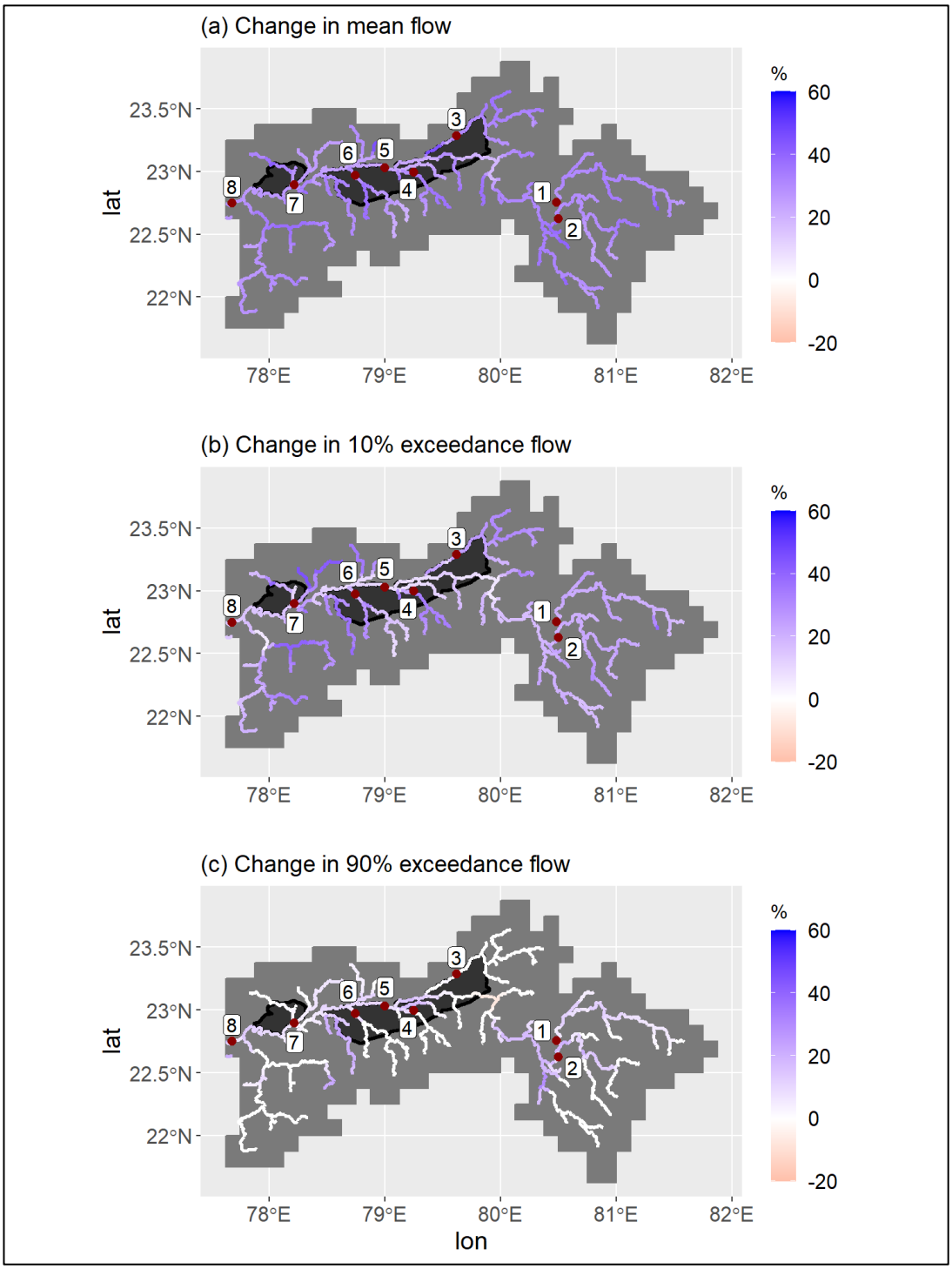

Figure 5.5: Percentage changes in flow between the baseline (1981–2010) and the simulated future period (2031–2060) for the Upper Narmada basin: (a) Change in mean flow (b) Change in 10% exceedance flow (Q10); (c) Change in 90% exceedance flow (Q90). (1) Manot; (2) Mohgaon; (3) Patan; (4) Belkheri; (5) Barmanghat; (6) Gadarwara; (7) Sandia; (8) Hoshangabad. Dark grey depicts the two command areas

Future mean flows at the 90% exceedance level (Q90) display a less significant change from the baseline, with large stretches of the river network showing only small increases in low flows. These increases are evident in 20% of river cells, ranging from 0.5% to 47%. The largest percentage changes are seen in the smaller tributaries of the basin, however, and represent relatively small absolute increases in flow. This results in a 2.5% average increase at Q90 across the basin. Low flows also display slight increases at each of the eight gauging sites, most noticeable again at Hoshangabad, which has an average increase of 22.5 m^3s^{-1}, equating to a +24.2% rise in Q90 flows compared to the baseline period. Q90 flows at Manot, Mohgaon, Patan, Belkheri and Gadarwara show very little change, with Patan and Belkheri displaying no change due to the intermittent nature of the gauged rivers, i.e., Q90 flow values are 0 m^3s^{-1} for baseline and all future ensemble runs.

5.2 MIKE SHE Application in Upper Narmada Basin

Dindori, Manot and Gadarwara are the upstream sub-catchments located at higher elevations and exhibit relatively large ranges in elevation. Therefore, precipitation lapse rates were employed over these sub-catchments as initial model runs consistently underestimated the discharge at these gauging sites. This has been done as the rain gauge networks in mountainous regions often display a bias as stations located at lower elevations may lead to systematic underestimation of precipitation as compare to the actual precipitation at occurring at higher elevation ranges (Frei and Schär, 1998; Frei et al., 2003). Therefore, Immerzeel et al., (2012b) and Wijesekara et al., (2012) have suggested the use of precipitation lapse rates to try and address this issue of underestimation of precipitation. The final lapse rate values are within the range of those previously reported in mountainous regions (Immerzeel et al., 2012a; 2012b). The optimised calibrated parameters are given in Table 5.3.

Table 5.3: Final calibration parameter values

Sub-catchment number	1	2	3	4	5
Sub-catchment name	Dindori	Manot	Barmanghat	Gadarwara	Hoshangabad
Precipitation lapse rate (%/100 m)	6	6		7	
Interflow time constant for interflow reservoir	4	6	14	4	14
Percolation time constant for interflow reservoir	4	14	14	4	14
Time constant for baseflow reservoir 1 (days)	35	35	65	65	65
Time constant for baseflow reservoir 2 (days)	250	200	1500	120	350

The model performance has been evaluated for daily and monthly flows using Nash Sutcliffe Efficiency (NSE) and Difference in Volume (Dv). The performance statistics during the calibration period is given in Table 5.4. As shown, a shorter period of 2001–2006 was employed at Manot, due to shorter data availability. The comparison of the observed and simulated daily flows is given in Figure 5.6a and Figure 5.6b whereas the monthly observed and simulated daily flows is

given in Figure 5.7a and Figure 5.7b. The mean monthly discharges are compared and shown in Figure 5.8. It can be observed that the model is fairly able to represent the annual river regime in the Upper Narmada basin, as is the case for the monthly discharges, with good sequencing of the annual monsoon flood pulse achieved at all discharge stations.

Table 5.4: Model performance statistics for the calibration and validation periods (validation shaded).

Station	Period	Dv		Daily NSE		Daily r	Monthly NSE		Monthly r
Dindori	Cal: 01/02–12/08	-10.22	***	0.40	**	0.64	0.83	****	0.91
	Val: 01/09–05/08	0.73	*****	0.58	***	0.79	0.84	****	0.93
Manot	Cal: 01/02–12/06	-8.98	****	0.53	***	0.73	0.93	*****	0.97
Barmanghat	Cal: 01/02–12/08	3.89	*****	0.60	***	0.80	0.82	****	0.93
	Val: 01/09–05/10, 06/11–05/13	10.39	***	0.64	***	0.82	0.79	****	0.92
Gadarwara	Cal: 01/02–12/08	-6.77	****	0.35	**	0.59	0.64	***	0.80
	Val: 01/09–05/10, 06/12–05/13	-21.14	**	0.76	****	0.89	0.86	*****	0.97
Hoshangabad	Cal: 01/02–12/08	6.66	****	0.63	***	0.82	0.84	****	0.95
	Val: 01/09–05/08	23.16	**	0.66	****	0.84	0.77	****	0.94

Performance indicator	Excellent *****	Very good ****	Fair ***	Poor **	Very poor *
Dv	< 5%	5–10%	10–20%	20–40%	>40%
NSE	>0.85	0.65–0.85	0.50–0.65	0.20–0.50	<0.20

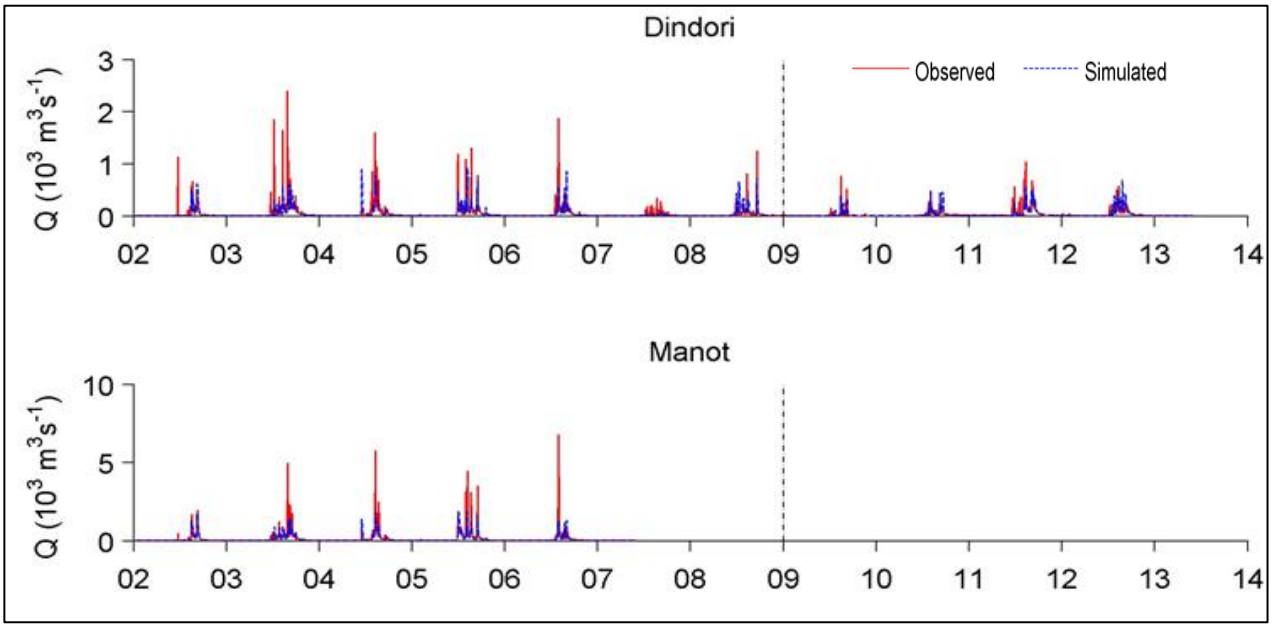

Figure 5.6a: Observed and simulated daily discharge for the calibration and validation periods (separated by dashed line) at Dindori and Manot

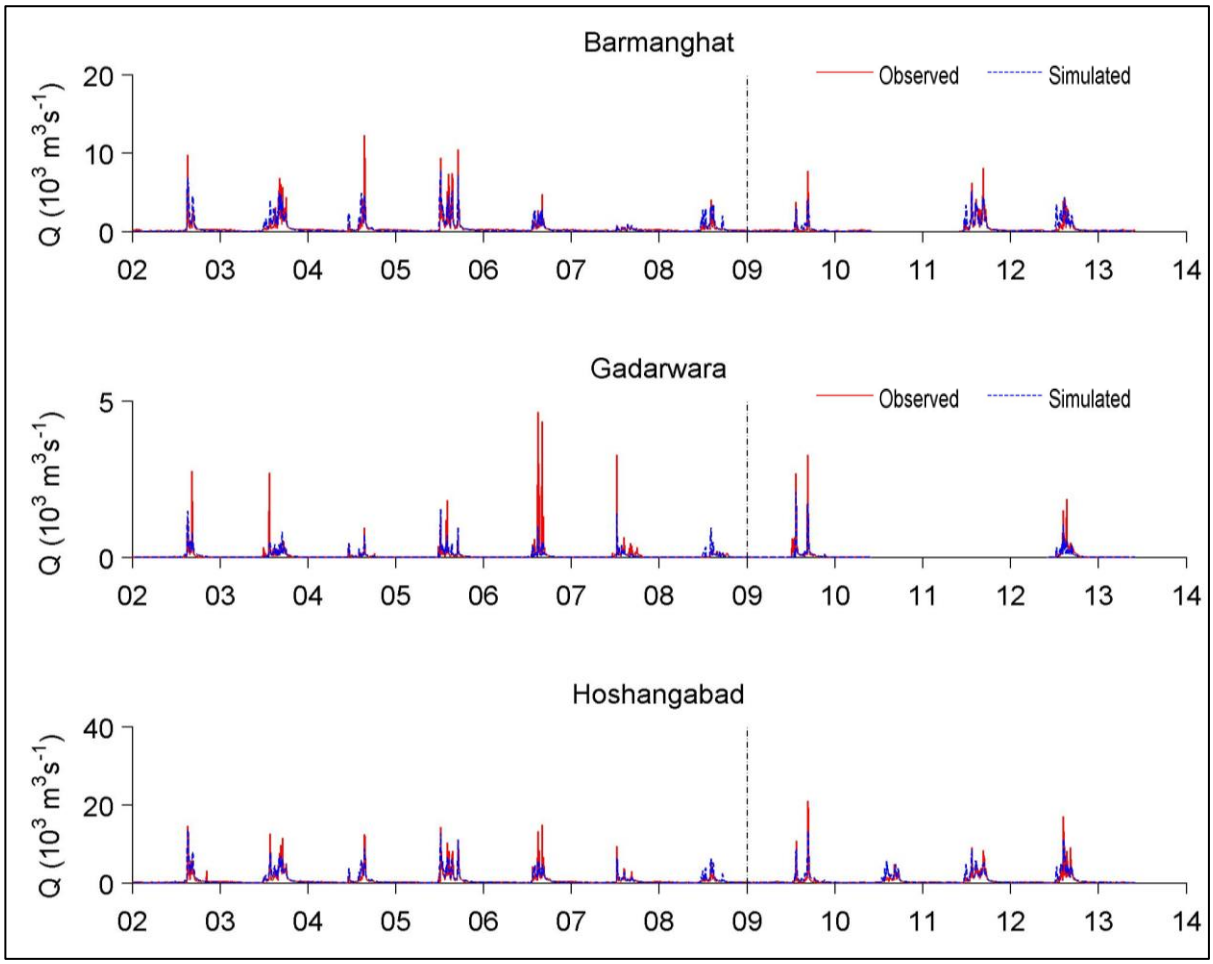

Figure 5.6b: Observed and simulated daily discharge for the calibration and validation periods (separated by dashed line) at Barmanghat, Gadarwara and Hoshangabad

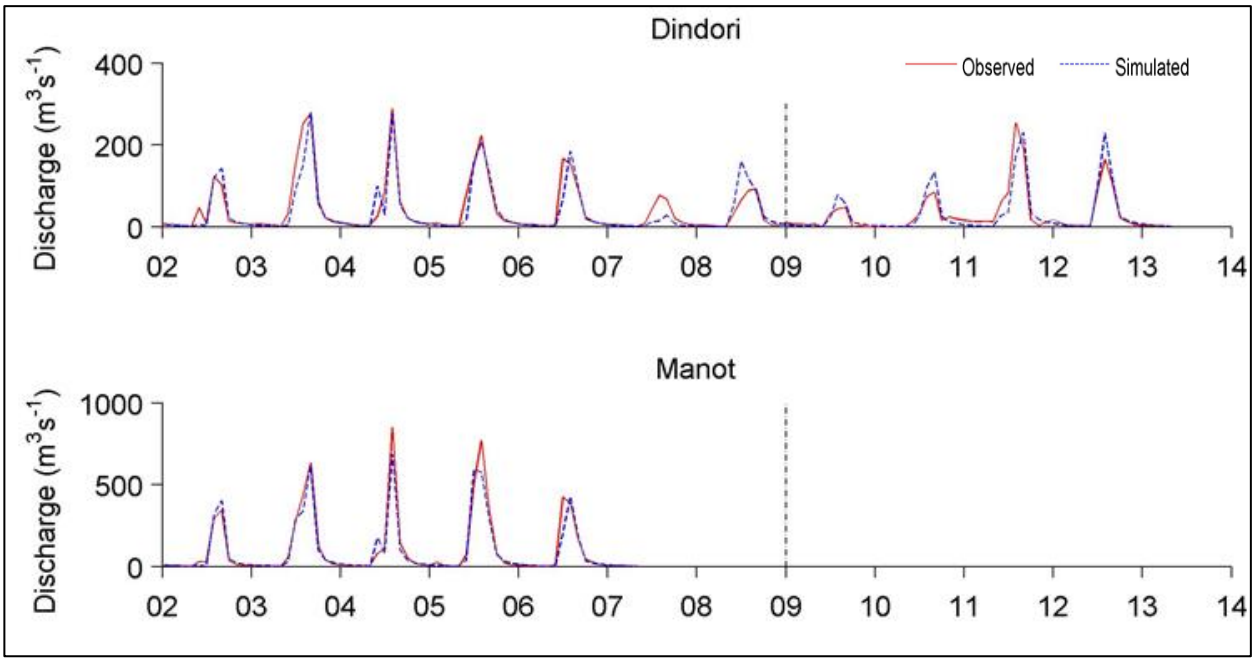

Figure 5.7a: Observed and simulated monthly discharge for the calibration and validation periods (separated by dashed line) at Dindori and Manot

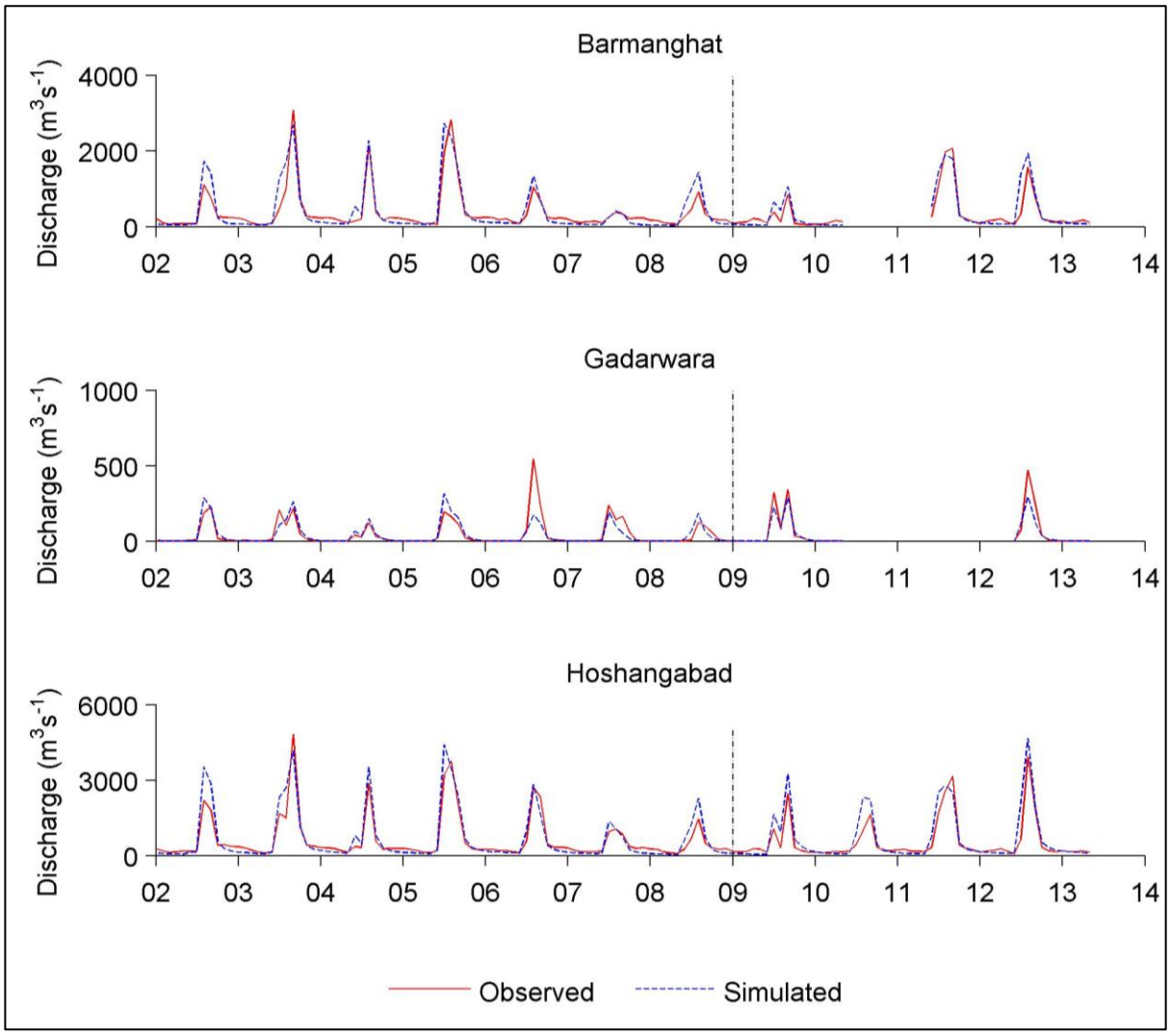

Figure 5.7b: Observed and simulated monthly discharge for the calibration and validation periods (separated by dashed line) at Barmanghat, Gadarwara and Hoshangabad

The mean monthly simulated river regimes at Barmanghat and Hoshangabad are given in Figure 5.8. It can be observed that there is a systematic bias towards in the lean season flows (monthly) are being underestimated whereas the peak flows (monthly) are being overestimated. However, the year-to-year timing and magnitude of the monthly flows are well simulated as can be seen from Figures 5.7a and Figure 5.7b.

The reservoir releases from Bargi, Barna and Tawa Dams in the Upper Narmada Basin may be the reason for the observed lean season flows being higher than the simulated flows. Similarly, observed wet season discharges are lower than the simulated flow due to the storages being held in these dams during the monsoon season.. Future collaborative work, if possible, will seek to explore the potential of including the variability in the reservoir releases from major dams using the range of control structure approaches that are available within MIKE 11 with dam operation being varied to improve model performance in the absence of detailed records of actual operation. Despite these

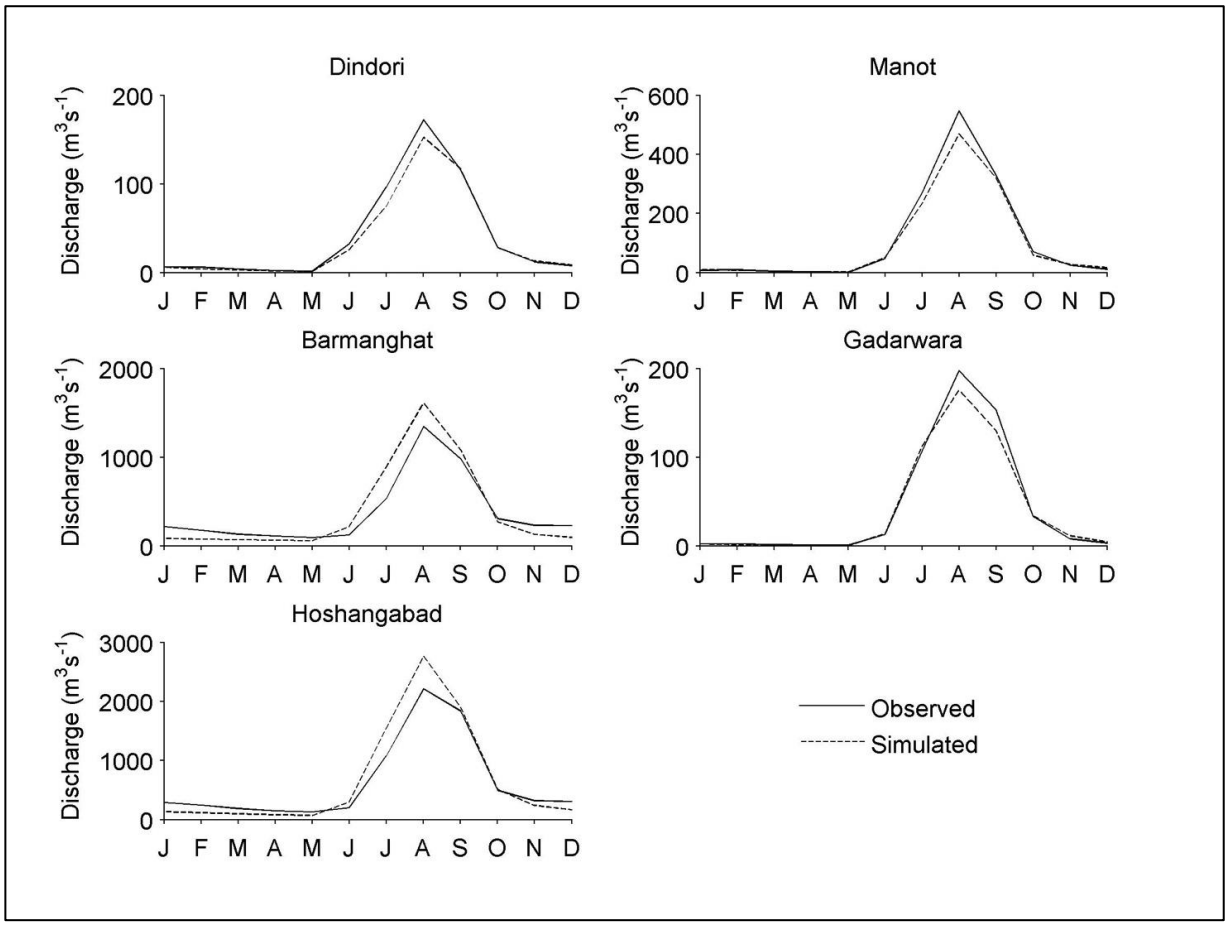

Figure 5.8: Observed and simulated river regimes for the period 2002–2008

issues, mean discharges are well represented by the model, with Dv classed as 'very good' to 'excellent' at all stations (Table 5.4).

As compared to the model performance at a monthly resolution the performance at the daily resolution is relatively lower, as can be visualized from Figure 5.6 and Table 5.4. Using monthly discharges, NSE values for the calibration period falls under the 'fair' to 'excellent' class as and 'r' values of 0.80 and above are achieved. In comparison, at a daily resolution, NSE falls under the 'poor' (four stations) to 'fair' (at Hoshangabad only, the most downstream station) class and 'r' values range between 0.59 and 0.82. This weaker performance at a daily resolution may partly be related to the quality and spatial resolution of the gridded precipitation and PET data.

The model validation was undertaken during the period June 2009 to May 2013. The observed discharge records were limited at Manot with data available for three and a half years at Barmanghat and two and a half years at Gadarwara and demonstrated visually in Figure 5.7 a&b. Similar to the calibration period, good sequencing of annual monsoon flood pulse is achieved at all fours stations during the validation period (Figure 5.7 a&b). Furthermore, daily 'r' is close to 0.8 or

higher and monthly r is over 0.9 at all stations (Table 5.4), representing a strong positive correlation between observed and simulated discharges.

The model performance evaluation metrics at Dindori during the validation period are better than during calibration period. For example, Dv falls in the 'very good' class, rather than 'fair' class (as previously) and daily NSE falls under 'fair' class, instead of 'poor'. An overestimation of mean discharge is seen at Barmanghat during the validation period where the Dv shows an increase. The daily NSE values point toward an improvement in model performance at the daily resolution, while the monthly NSE continues to be classed as "very good". The mean discharge at Gadarwara, shows greater underestimation for the validation period (higher negative Dv), NSE and r indicate an overall improvement in model performance, at daily and monthly resolutions. Lastly, Dv displays an increase for Hoshangabad, leading to its classification falling from 'very good' to 'poor'. Despite this, performance at a daily resolution based on NSE improves at Hoshangabad; from 'fair' to 'very good', and the monthly NSE value also remain under 'very good' class. At Barmanghat and Hoshangabad, the tendency towards overestimation of peak monthly discharges and underestimation of dry season monthly discharges that was exhibited during the calibration period is repeated for the validation period (Figure 5.7). This is, again, likely to be due to the effects of large dams being not properly represented due to lack of detailed reservoirs releases indicating their variability during the wet and dry seasons.

The performance of the model in general can be considered to be satisfactory to allow the application of the model for further investigations, such as climate change scenario simulation (Thompson et al., 2013) and the assessment of the impacts of climate change on environmental flows (Thompson et al., 2014b), particularly as comparisons between baseline and scenario discharges at temporal resolution of monthly or annual. In addition, the potential for including reliable estimates of dam releases and transfers within the model to enhance model performance can be explored later.

5.3 GWAVA Application in complete Narmada Basin

5.3.1 GWAVA Model Enhancements

The representation of groundwater processes and reservoirs in highly regulated river basins in large scale models helps to widen the applicability of these models to large river basins. The inclusion of the detailed groundwater processes in large-scale hydrological models helps to improve the simulations including understanding the feedbacks between the human and natural systems (Clark et al., 2015; Pokhrel et al., 2016; Scheidegger, et al., 2021). Hanasaki et al., (2006) developed an algorithm for the setting of reservoir operating rules within global hydrological

models. This algorithm reflects these parameters and allows for use with currently available global datasets. The reservoir operation scheme fixes reservoir operations to reflect available river discharge data and the reservoir operating rule is set to minimise inter-annual and seasonal stream flow variation for reservoirs, where the primary purpose is water supply and not irrigation, whereas daily release is considered to be proportional to irrigation water requirement downstream for irrigation supply reservoirs.

The GWAVA5.1 hydrological model has been developed to improve reservoir operations and account for groundwater processes. Two additional reservoir release equations and a revised groundwater routine have been included based on Hanasaki and AMBHAS-1D respectively. The revised groundwater routine included in the model improved the stream flow simulation in the headwater catchments by successfully improving the baseflow component representation; whereas the new reservoir routine substantially improved the stream flow simulation in catchments located downstream of major reservoirs, where the stream flow is largely regulated from the upstream reservoir. This routine provides a better representation of the annual volumes and daily outflows and is applicable to different types of operational reservoirs. This research demonstrated that the reliability of stream flow prediction can be improved by adapting appropriate groundwater and reservoir representation within the available existing hydrological model.

The analysis for the complete Narmada Basin incorporated seven major dams viz., Bargi multipurpose dam, Barna dam, Tawa dam, Kolar dam, ISP, OSP and SSP. Many other projects are being planned in Narmada basin, some of which have been considered for the upcoming reservoir scenario under the scenario analysis carried out for impact assessment of anthropogenic influences and climate change on the long-term water resources in the basin. The reservoir operations were considered based on releases for multiple uses, including releases for irrigation in command areas through irrigation canals. Reservoir operations were included and simplified to enable their inclusion in the model configuration which was improved based on the Hanasaki scheme. Detailed water transfers out of the basin were also incorporated, including that from Bargi Dam to the adjacent Ganga basin trough RBC and also included the upcoming reservoirs scenario. Table 5.5 gives the details of the major reservoirs included in the model setup for simulation of daily runoff. The model simulations were carried out based on the model setup and its calibration and validation at the 13 gauging sites located both in headwater catchments and in main river channel (Table 5.6).

5.3.2 Calibration and Validation

The revised GWAVA 5.1 with the improved representation of groundwater and reservoir operation rules has been applied for the complete Narmada basin. The multisite

Table 5.5: Reservoirs included in the complete Narmada application

Dam	River	Year of completion	Gross storage capacity (MCM)
Bargi	Narmada	1988	3924.8
Barna	Barna	1978	539
Tawa	Tawa	1978	2312
Kolar	Kolar	1984	270
ISP	Narmada	2005	12211.45
OSP	Narmada	2008	1500
SSP	Narmada	2017	9500

Table 5.6: Gauging sites used for this study

Gauge	River Reach	Catchment Area (km^2)
Manot	Narmada	4467
Mohgaon	Burhner	4090
Patan	Hiran	4795
Belkheri	Sher	1508
Barmanghat	Narmada	26453
Gadarwara	Shakkar	2270
Sandia	Narmada	33954
Hoshangabad	Narmada	44548
Handia	Narmada	54027
Kogaon	Kundi	3919
Chidgaon	Ganjal	1729
Mandleshwar	Narmada	72809
Garudeshwar	Narmada	87892

calibration approach has been adopted at the 13 gauge-discharge sites located in Narmada basin. The tributaries and headwater catchments have been calibrated in the first step and thereafter the catchments on the main river channel have been calibrated based on the location of the gauging site in the direction of stream flow. In general, the calibration period spanned between 1990 and 2000 for most of the gauging sites except at Mohgaon (1990-1996); Chidgaon (1996-2000); Kogaon (1995-2000); Mandleshwar (1990-1996); and Garudeshwar (1990-1996). Similarly, the validation period spanned between 2001 and 2010 for most of the gauging sites, except Chidgaon (1990-1995); Kogaon (1990-1994); Mandleshwar (2007-2010); Garudeshwar (2007-2010). The comparison of simulated stream flow during calibration and validation periods is given in Figure 5.9 to Figure 5.21.

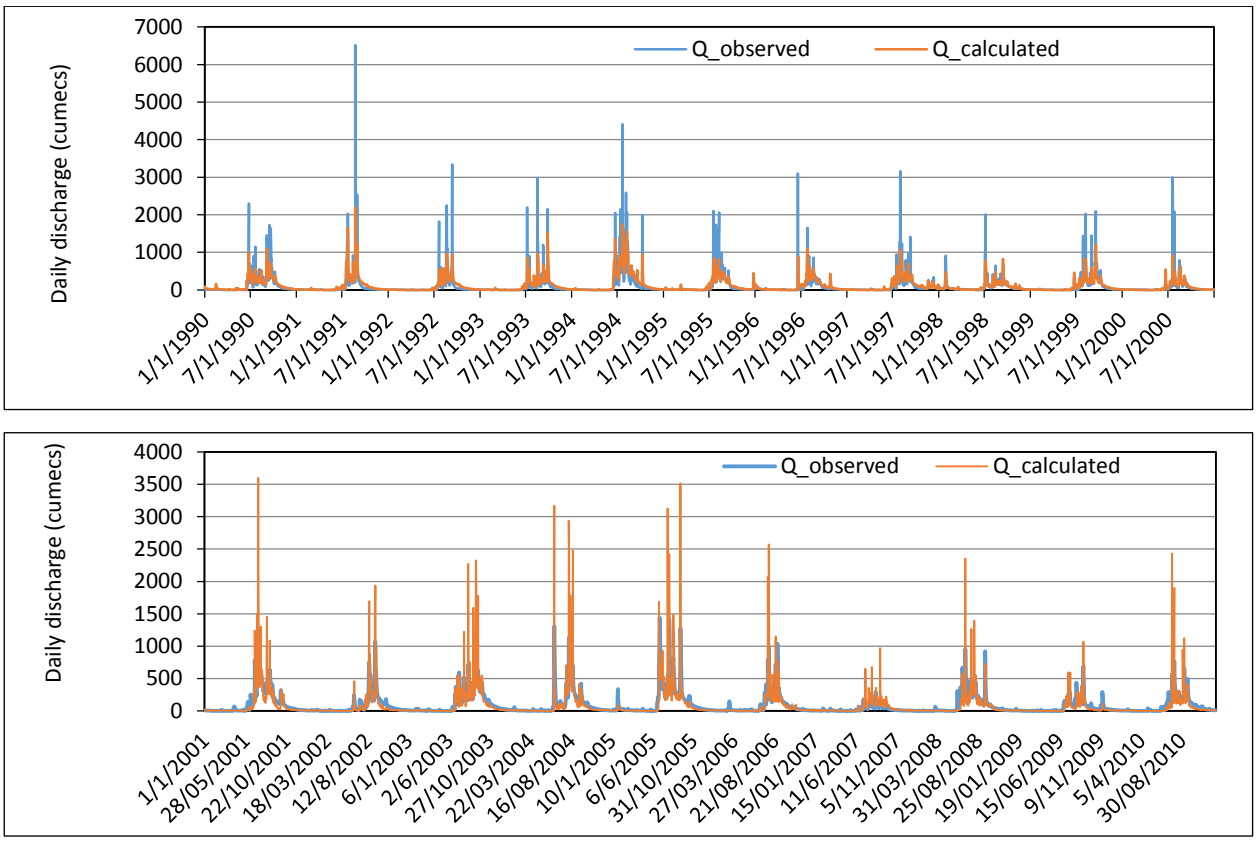

Figure 5.9: Comparison of observed and simulated runoff at Manot a) calibration, b) validation

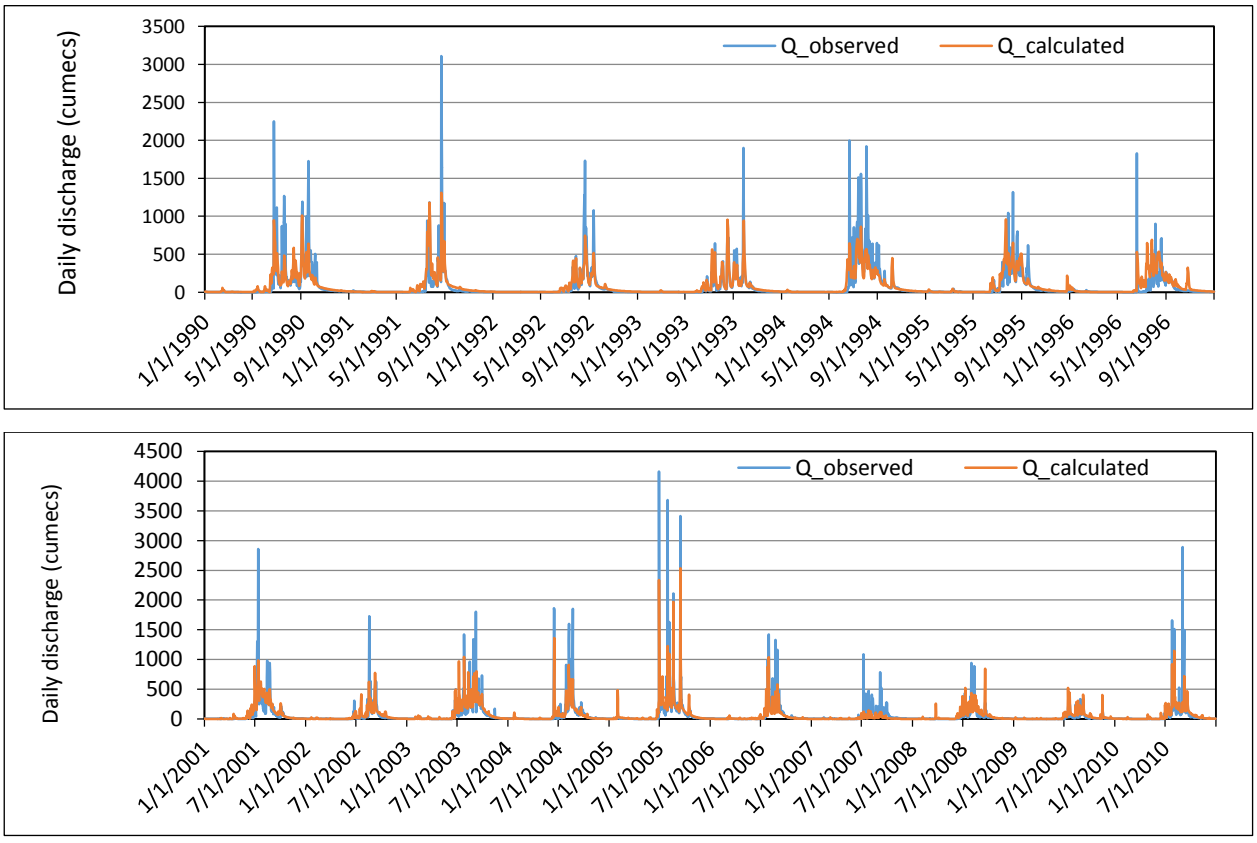

Figure 5.10: Comparison of observed and simulated runoff at Mohgaon a) calibration, b) validation

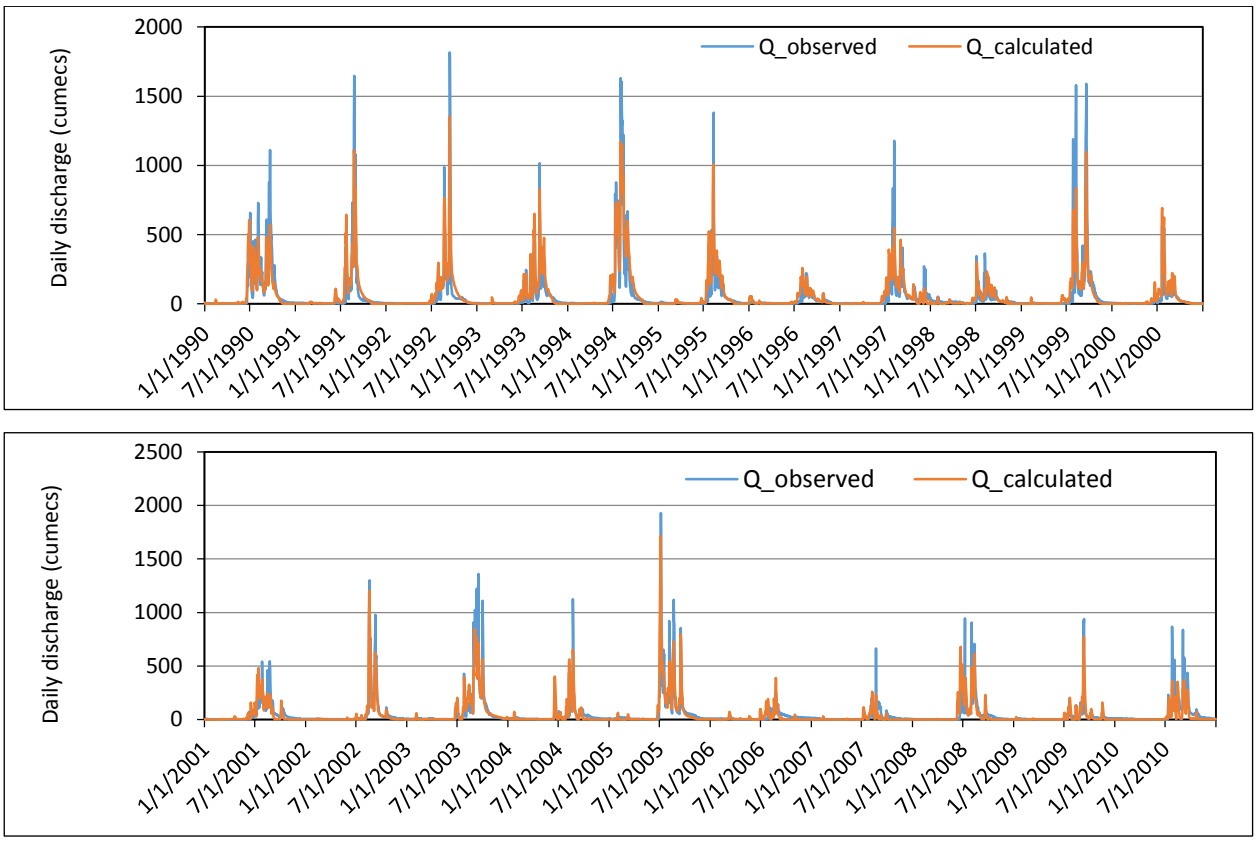

Figure 5.11: Comparison of observed and simulated runoff at Patan a) calibration b) validation

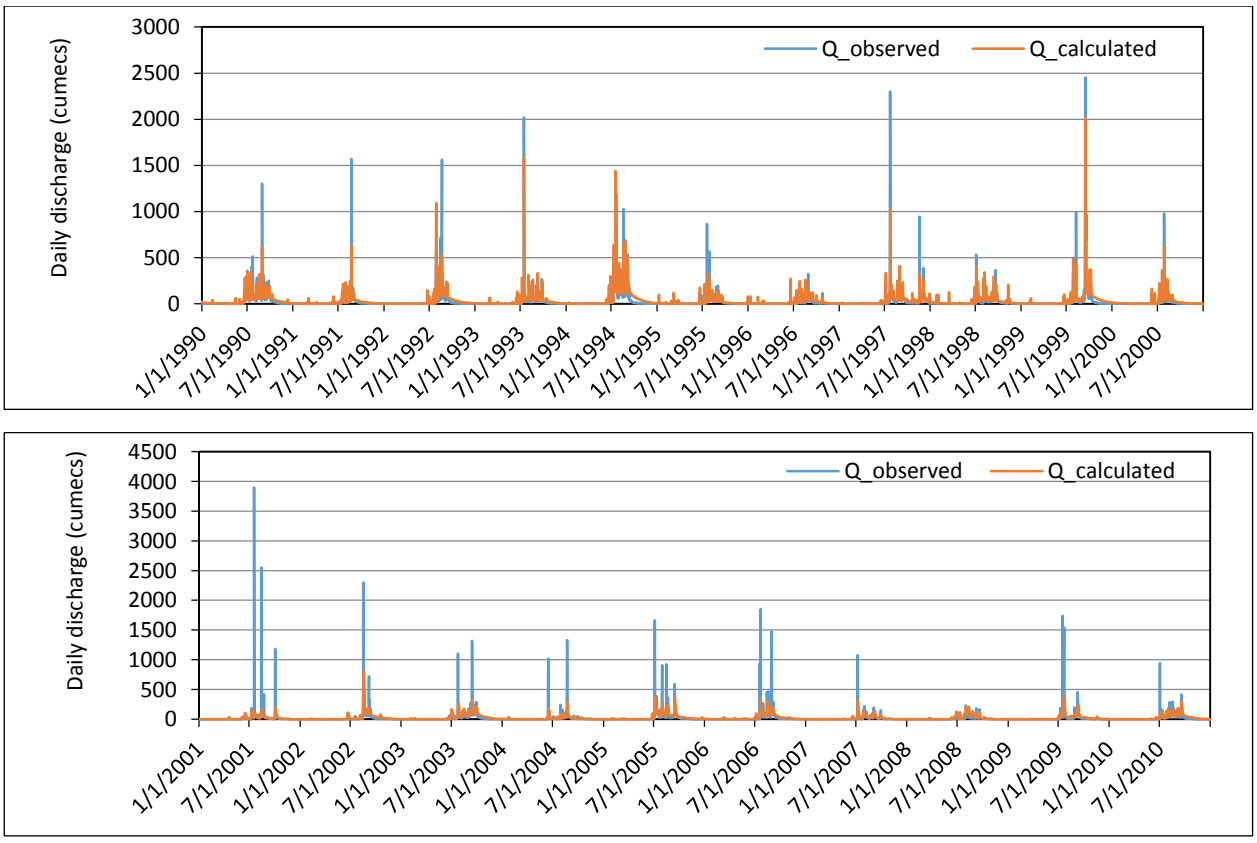

Figure 5.12: Comparison of observed and simulated runoff at Belkheri a) calibration b) validation

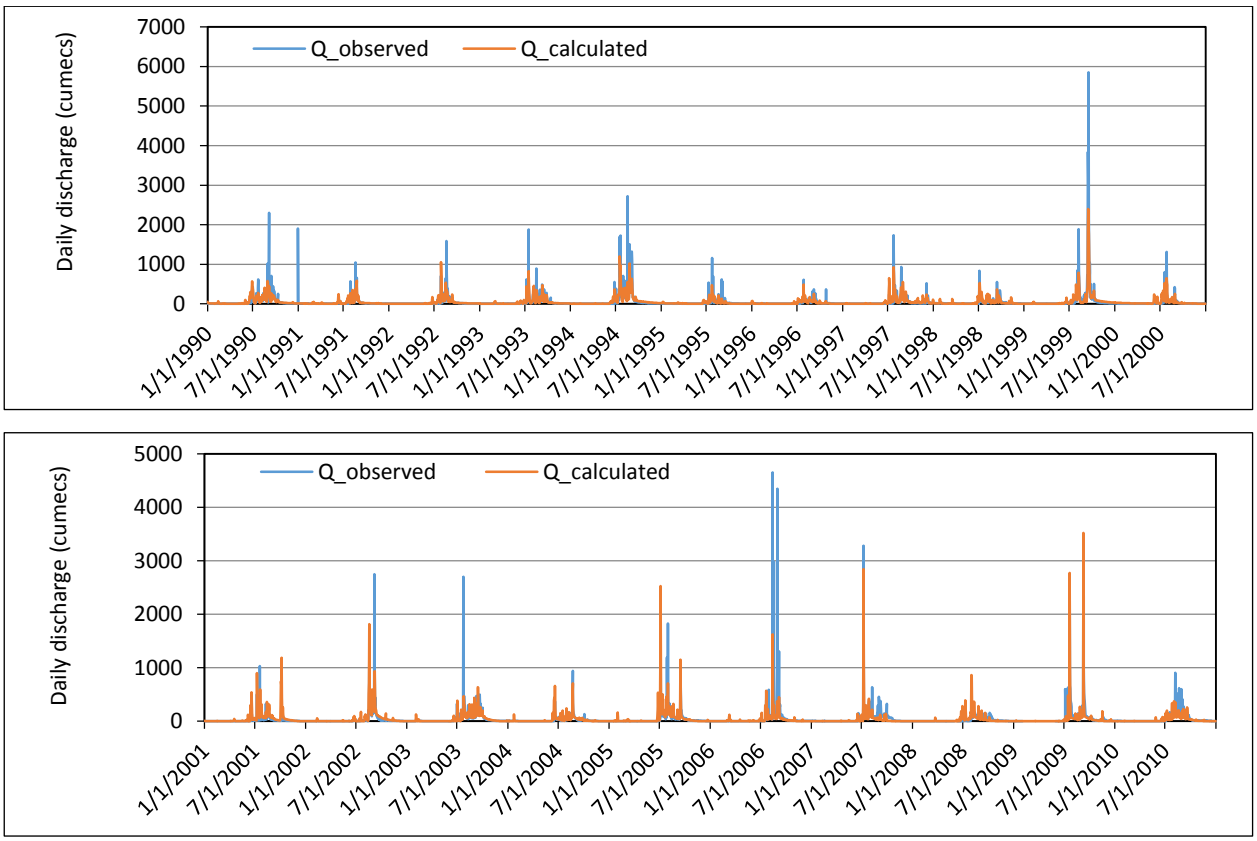

Figure 5.13: Comparison of observed and simulated runoff at Gadarwara a) calibration b) validation

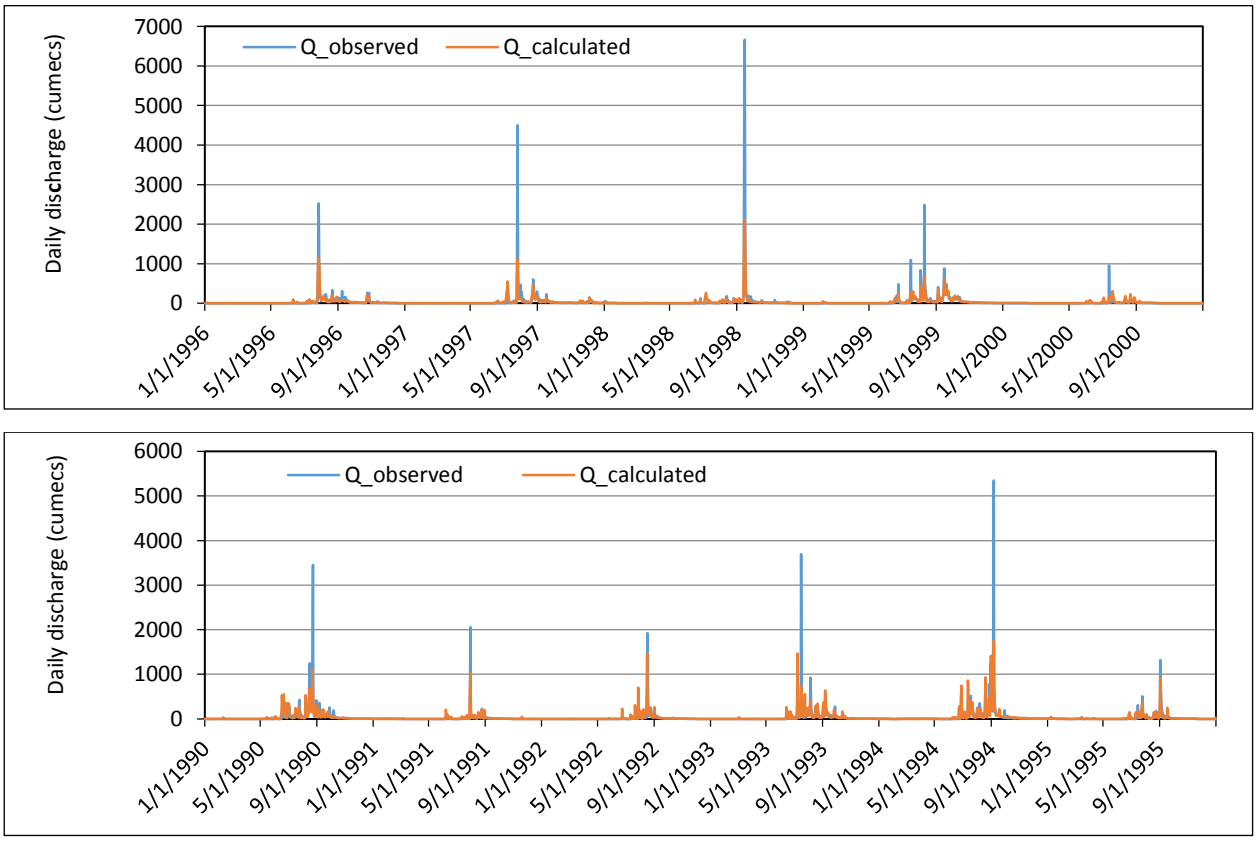

Figure 5.14: Comparison of observed and simulated runoff at Chidgaon a) calibration b) validation

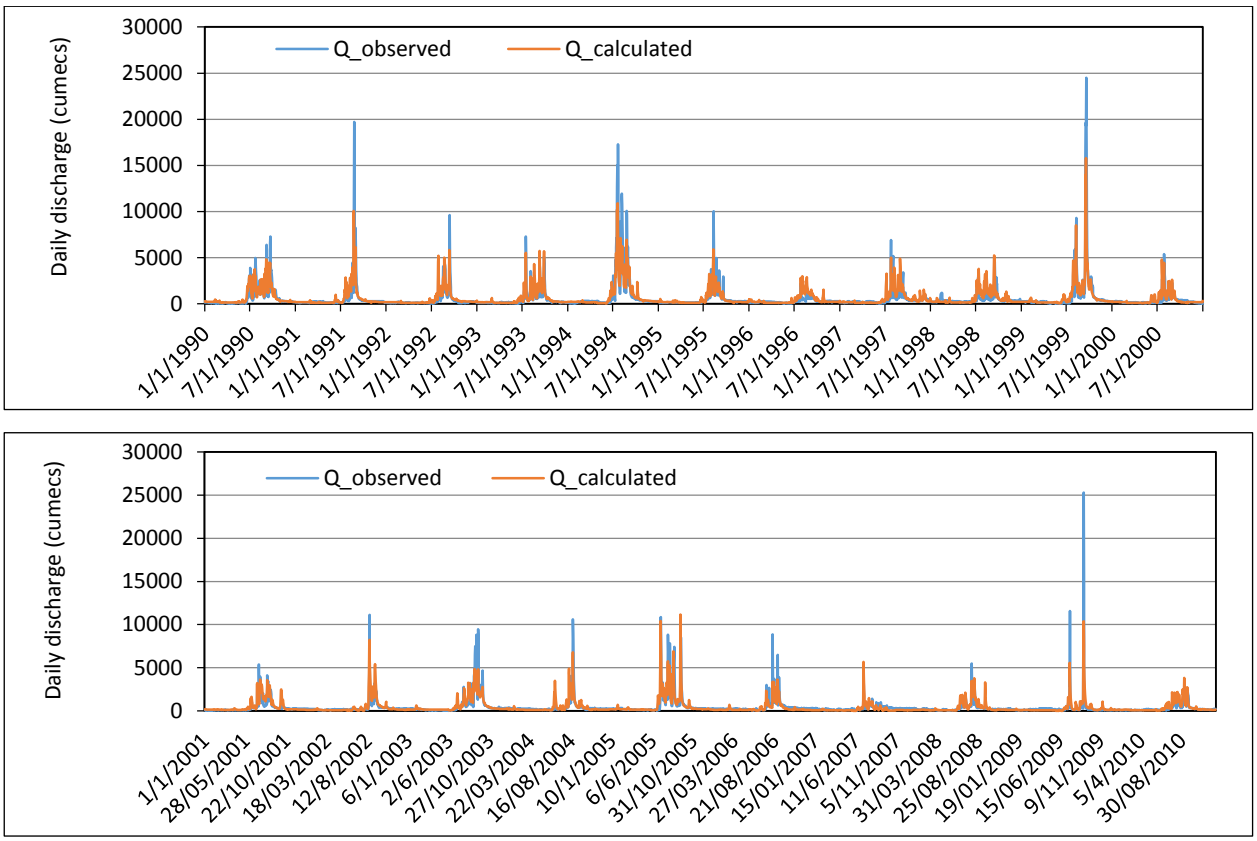

Figure 5.15: Comparison of observed and simulated runoff at Sandia a) calibration, b) validation

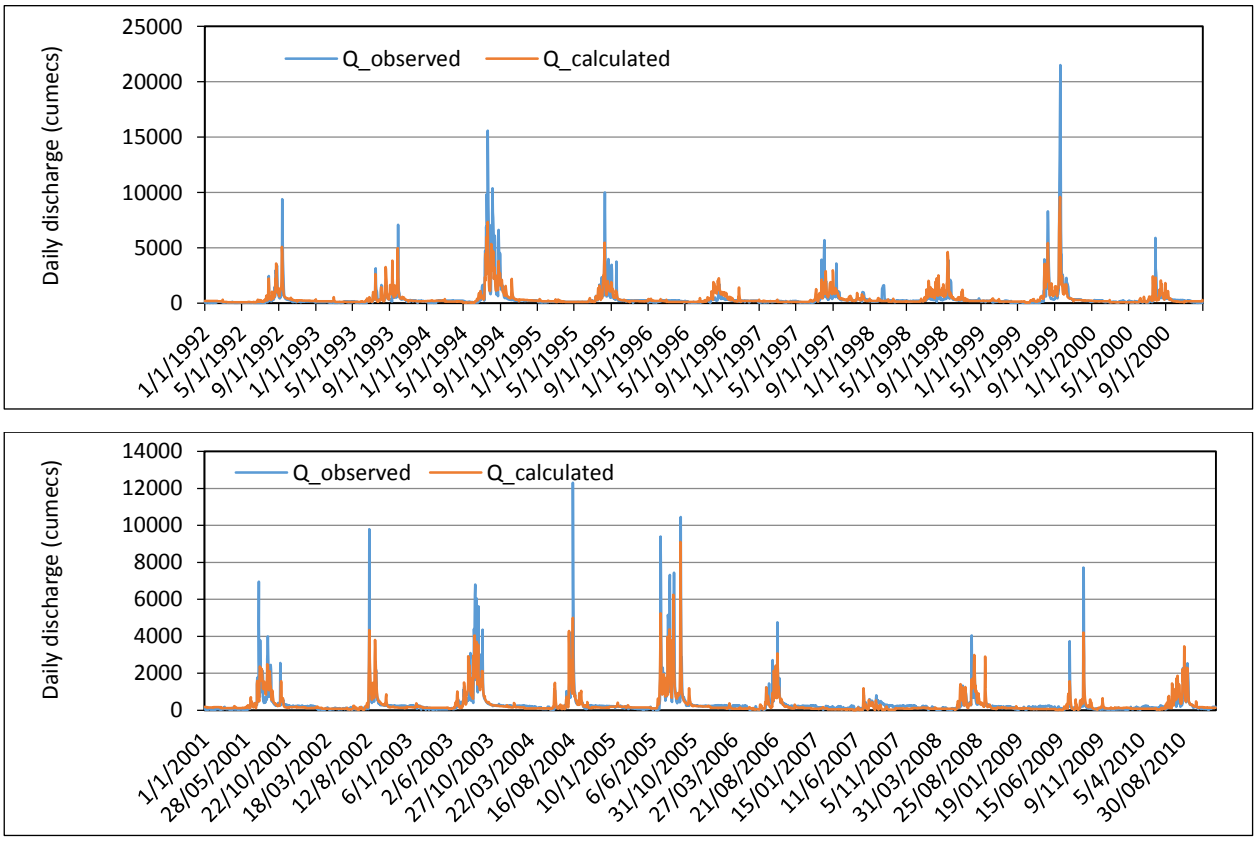

Figure 5.16: Comparison of observed and simulated runoff at Barmanghat a) calibration, b) validation

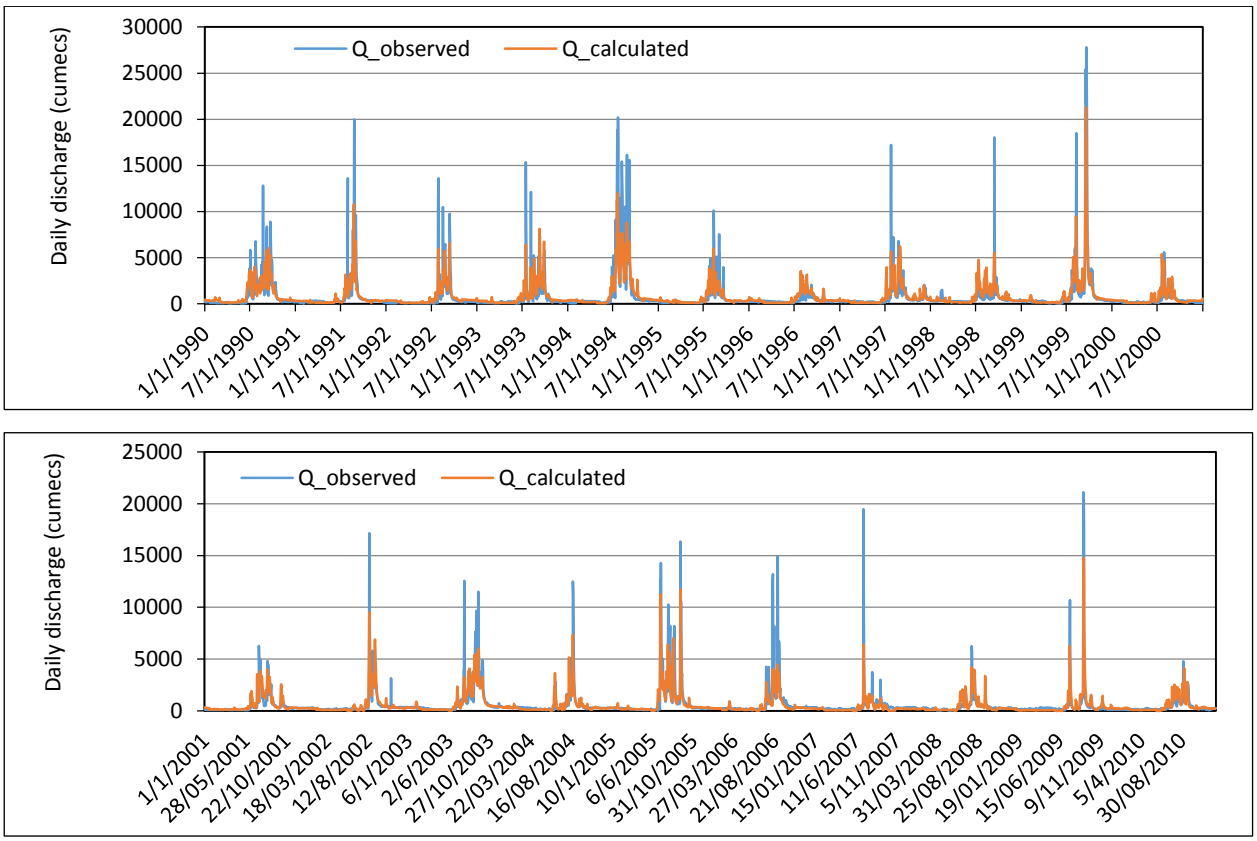

Figure 5.17: Comparison of observed and simulated runoff at Hoshangabad a) calibration b) validation

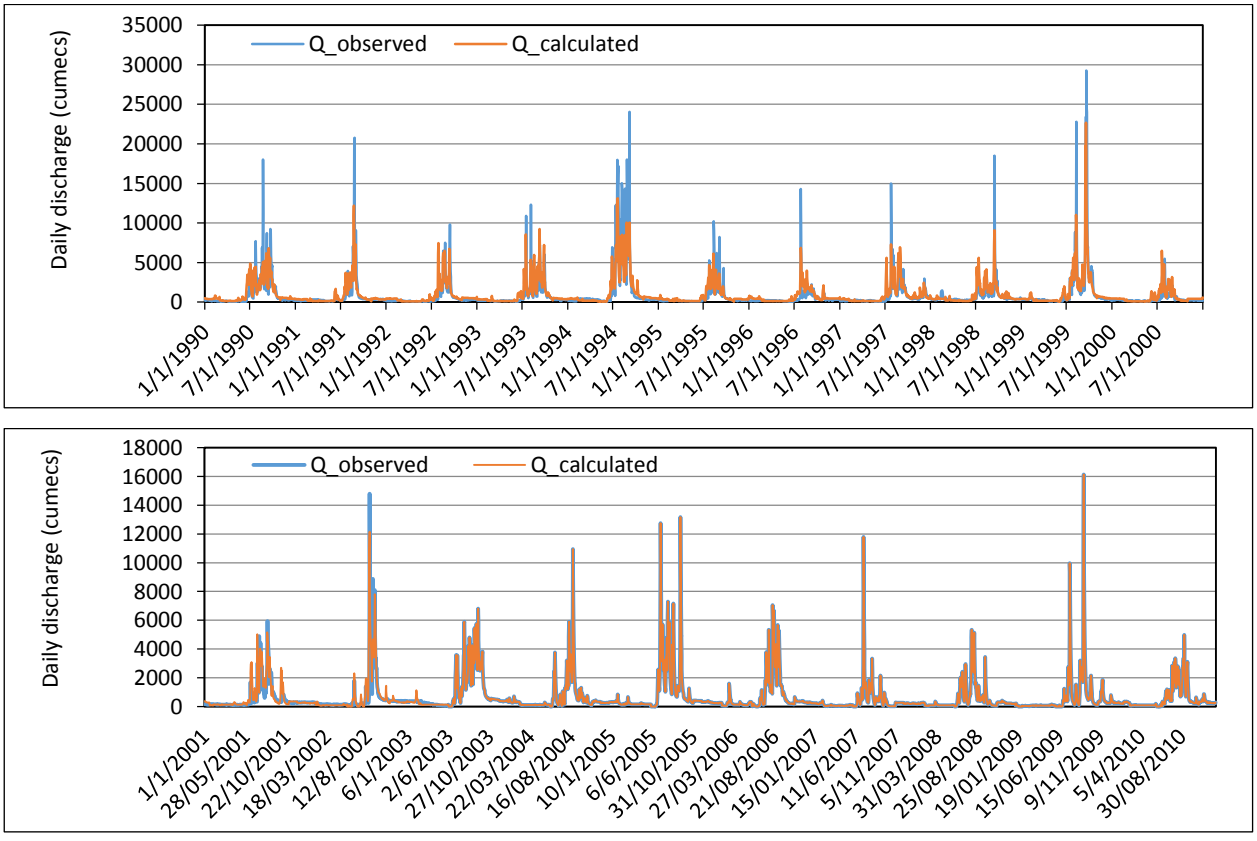

Figure 5.18: Comparison of observed and simulated runoff at Handia a) calibration, b) validation

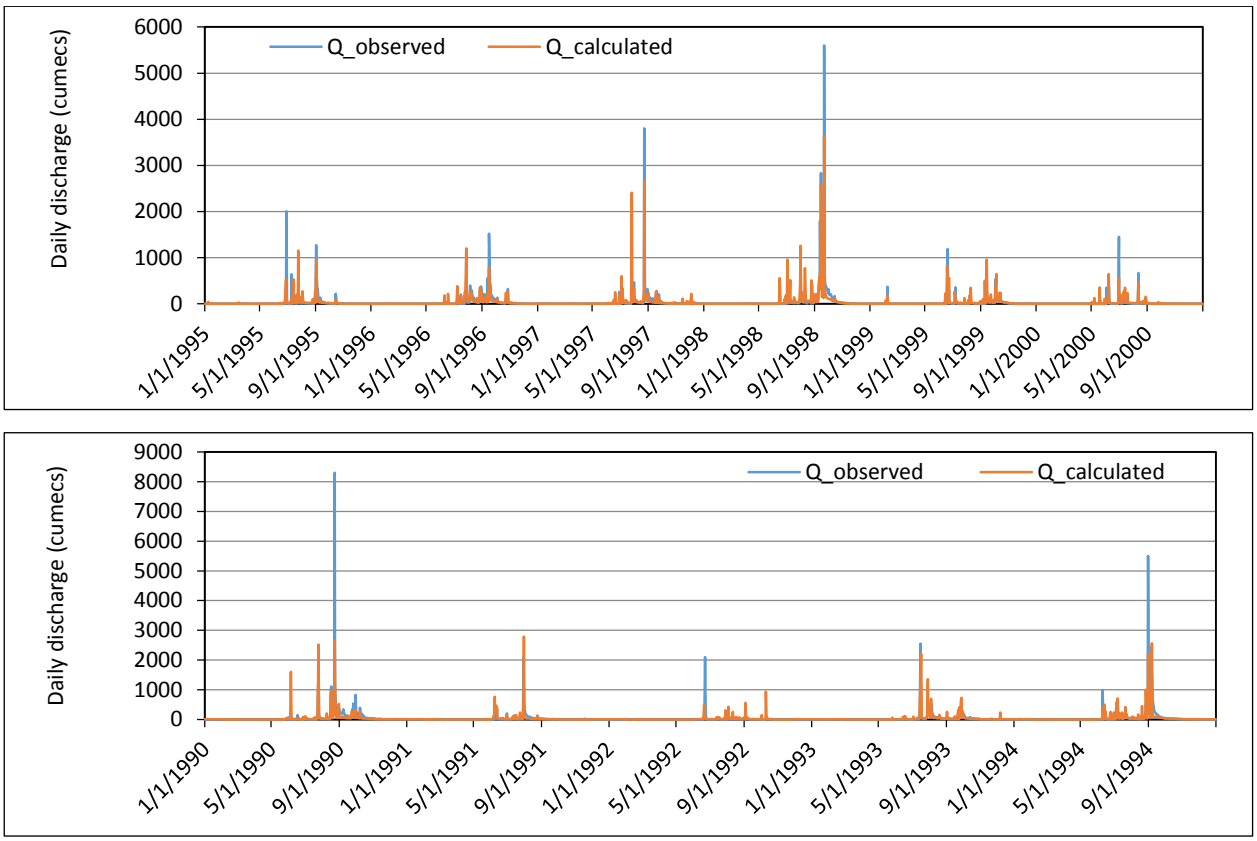

Figure 5.19: Comparison of observed and simulated runoff at Kogaon a) calibration, b) validation

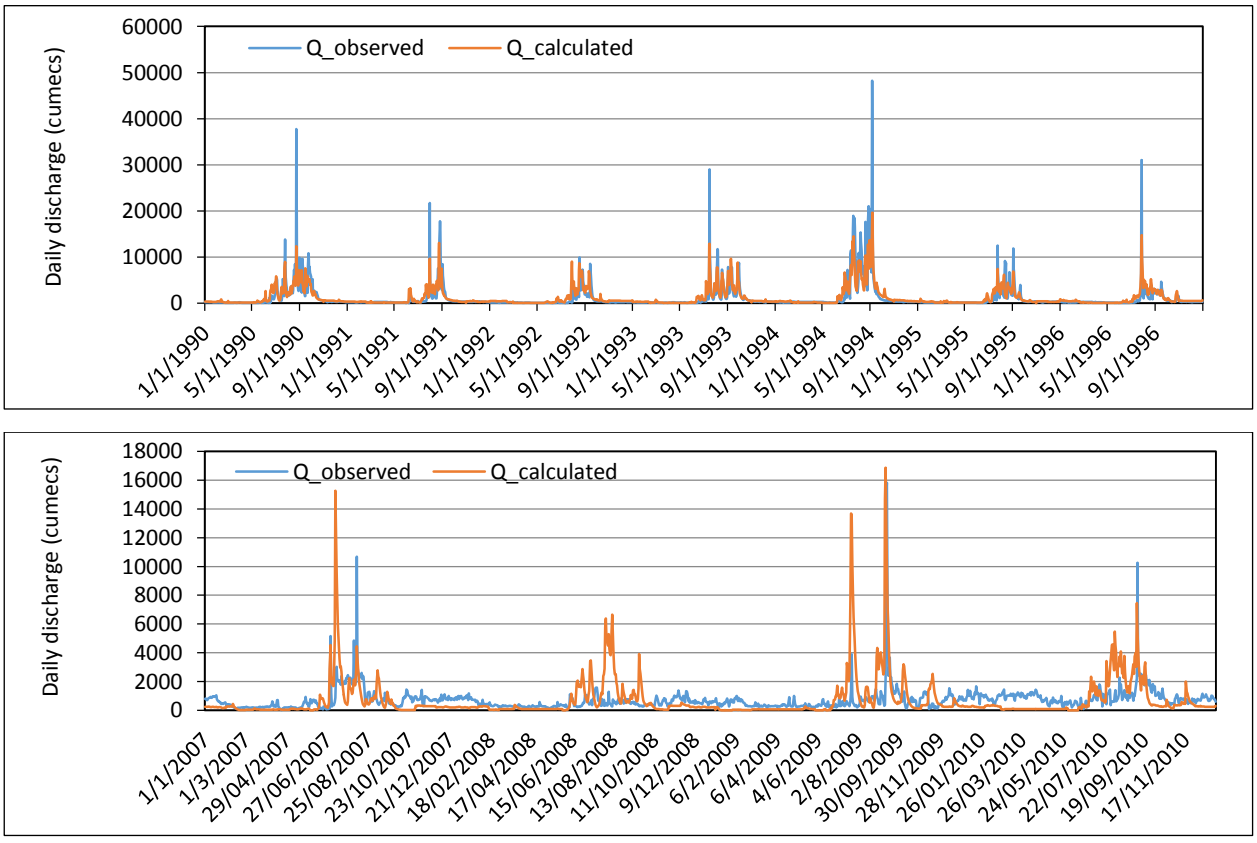

Figure 5.20: Comparison of observed and simulated runoff at Mandleshwar during a) calibration, b) validation

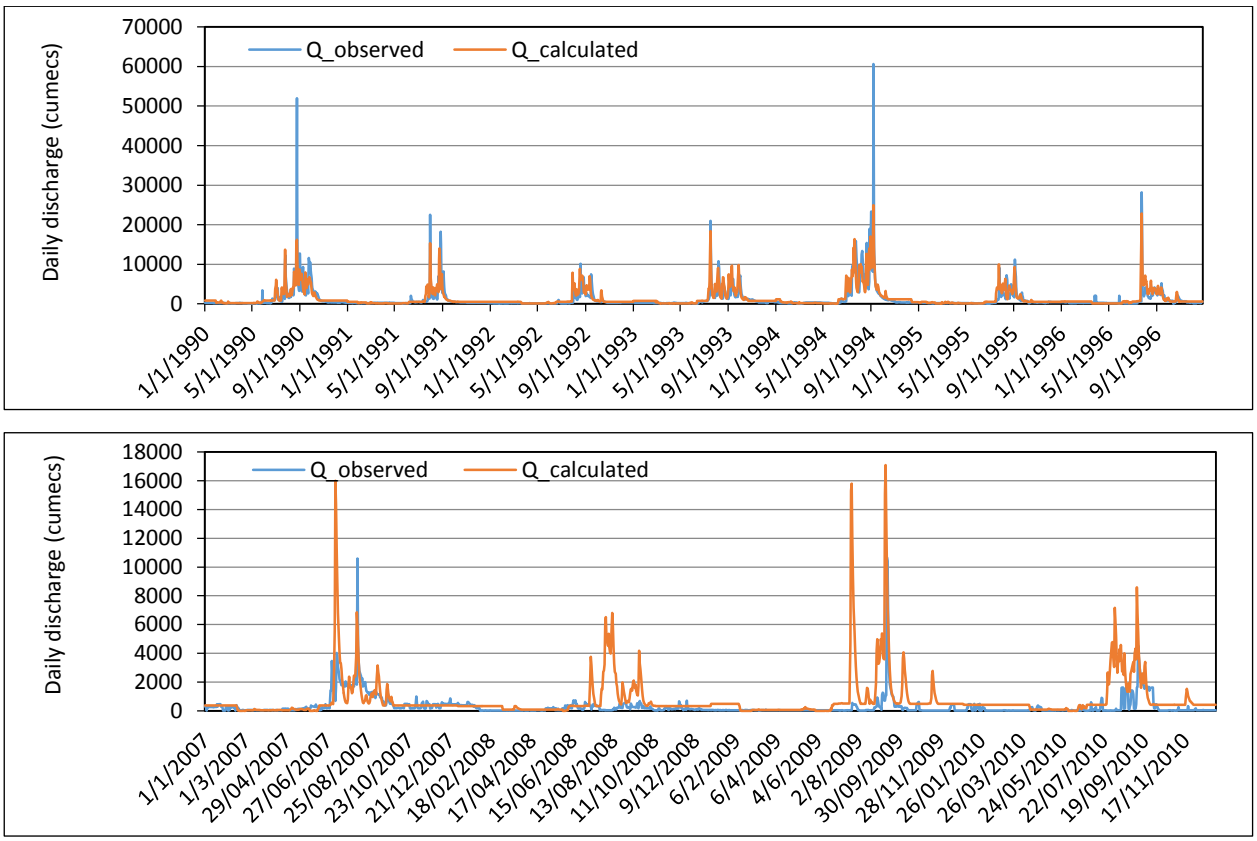

Figure 5.21: Comparison of observed and simulated runoff at Garudeshwar during a) calibration, b) validation

The performance indicators used for model performance evaluation for simulation of monthly flows include Nash Sutcliffe efficiency (NSE) presented by Nash and Sutcliffe, (1970), Percentage Bias (PBias), log Nash (LNE) and Kling-Gupta efficiency (KGE) presented by Gupta et al., (2009). The comparison of the performance of the model simulations during calibration and validation is given in Table 5.7.

GWAVA 5.1 has been simulated on a daily time scale in Narmada basin and the model performance has been evaluated based on the comparison between the observed and simulared monthly flows. The model generally performs well during both calibration and validation periods in reproducing monthly stream flow at the thirteen gauging stations. The model performance has been evaluated considering the monthly stream flow simulations. And the NSE metric ranges from 0.79 to 0.93 during calibration and from 0.65 to 0.88 during validation. During calibration, the performance is “excellent” at Manot, Patan, Hoshangabad, Handia, Mandleshwar and Garudeshwar (NSE > 0.85) whereas it is “very good” at remaining sites (NSE: 0.65 - 0.85) except for Hoshangabad which is “poor” (NSE: 0.20-0.50). However, there is a slight drop in the performance during validation with “excellent” performance being observed at Patan, and Sandia whereas it is “very good” at all the remaining sites except at Belkheri and Gadarwara with “very good” performance (NSE: 0.65 - 0.85) and Garudeshwar where the model performance is “fair”

Table 5.7: Performance evaluation of GWAVA 5.1 during calibration and validation of monthly stream flow

Catchment	Calibration					Validation				
	Period	PBias	NSE	LNE	KGE	Period	PBias	NSE	LNE	KGE
Manot	1990-2000	4.20	0.93	0.86	0.83	2001-2010	-1.40	0.84	0.93	0.78
Mohgaon	1990-1996	3.40	0.83	0.85	0.80	2001-2010	-0.20	0.84	0.87	0.78
Patan	1990-2000	12.30	0.91	0.91	0.83	2001-2010	9.30	0.88	0.92	0.86
Belkheri	1990-2000	2.50	0.84	0.71	0.80	2001-2010	22.00	0.66	0.75	0.65
Gadarwara	1990-2000	1.00	0.83	0.83	0.72	2001-2010	-12.00	0.67	0.61	0.60
Chhidgaon	1996-2000	-13.30	0.86	0.88	0.77	1990-1995	3.20	0.78	0.86	0.32
Kogaon	1995-2000	2.00	0.79	0.76	0.72	1990-1994	-5.50	0.75	0.77	0.33
Barmanghat	1992-2000	3.20	0.81	0.81	0.82	2001-2010	-3.40	0.84	0.88	0.68
Sandia	1990-2000	9.10	0.84	0.88	0.77	2001-2010	6.00	0.86	0.85	0.63
Hoshangabad	1990-2000	0.40	0.90	0.90	0.78	2001-2010	-1.80	0.85	0.89	0.79
Handia	1990-2000	9.90	0.91	0.90	0.77	2001-2010	5.40	0.85	0.89	0.72
Mandleshwar	1990-1996	4.40	0.92	0.88	0.80	2007-2010	0.10	0.75	0.89	0.76
Garudheswar	1990-1996	13.40	0.90	0.89	0.80	2007-2010	10.00	0.64	0.78	0.64

(NSE:0.50-0.65).

As NSE is biased towards high flows (peaks), the performance at Garudeshwar is “fair” due to overestimation of peak flows. Therefore the log-NSE (LNE) has also been evaluated, as it is not biased towards high flows. During calibration, the model performance based on LNE is better as compared to the evaluations based on NSE, except at Belkheri (NSE: 0.84 & LNE: 0.71) and Kogaon (NSE: 0.79 & LNE: 0.76). Similarly, the model performance has improved during validation at all sites except Gadarwara (NSE: 0.67 & LNE: 0.61), and Sandia (NSE: 0.86 & LNE: 0.85). The model performance at Garudeshwar is higher based on LNE (NSE: 0.64 & LNE: 0.78). More or less a similar model performance is seen for the evaluations based on KGE which varies between 0.72 and 0.83 during calibration and between 0.32 and 0.86 during validation.

The PBias varies between -13.3% and 13.4% during calibration and -12.0% to 22.0% during validation. The model performance at Belkheri is “poor” (PBias: 20-40%) during validation, but the NSE, LNE and KGE are 0.66, 0.75 and 0.65 respectively which suggest a “fair” model performance. The model performance at Garudeshwar is “fair” (PBias: 10-20%) during calibration and “very good” (PBias: 5-10%) during validation. Therefore based on all these four performance evaluation the model performance can be considered to vary between “very good” to “excellent” at most of the catchments except for few exceptions of “fair” performance at very few sites and “poor” performance at Hoshangabad only during calibration. The differences in the performances

may be generally due to the small scale watershed interventions in the form of minor irrigation structures, check dams, stop dams and other water conservation measures that have come up in these catchments over a period of time. However, the application of GWAVA 5.1 with improved estimation of groundwater and reservoir outflows, suggest that the model is able to represent the baseflow better in the headwater catchments and is also able to better represent the reservoir outflows and groundwater contribution to the stream flow at the gauging sites located downstream of major reservoirs. Therefore the GWAVA 5.1 can be effectively used for the assessment of climate change impacts on water availability in Narmada river basin.

5.3.3 Impact Assessment Analysis

5.3.3.1 Population increase scenario

The impact of the increase in domestic population leading to higher water demands have been evaluated for the 2050s. The comparison of the mean monthly stream flow at the various gauging sites located in the headwater catchments and in the main river channel is given in Figure 5.22. No significant deviation in monthly flows has been observed at any of the months and at any of the gauging sites.

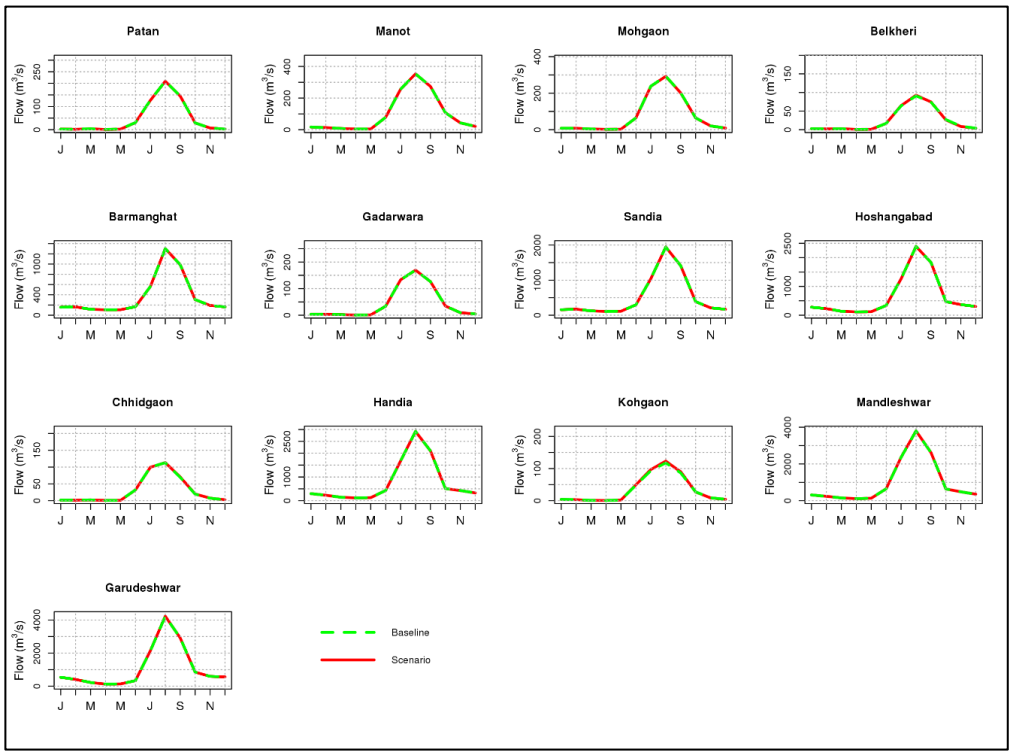

Figure 5.22: Comparison of mean monthly flow during the baseline and the population growth scenario during the 2050s

The spatial variation of the impact of population growth on the mean daily flows, high flows (Q10) and low flows (Q90) in Narmada river basin is given in Figure 5.23. It can be observed that there is no considerable change in mean flows, high flows and lows flows as a consequence of the higher

water demands due to population growth. This may be because the population growth has a miniscule impact on the future water availability in the Narmada basin, as compared to the climate change induced impacts and other major demands in the agriculture sector.

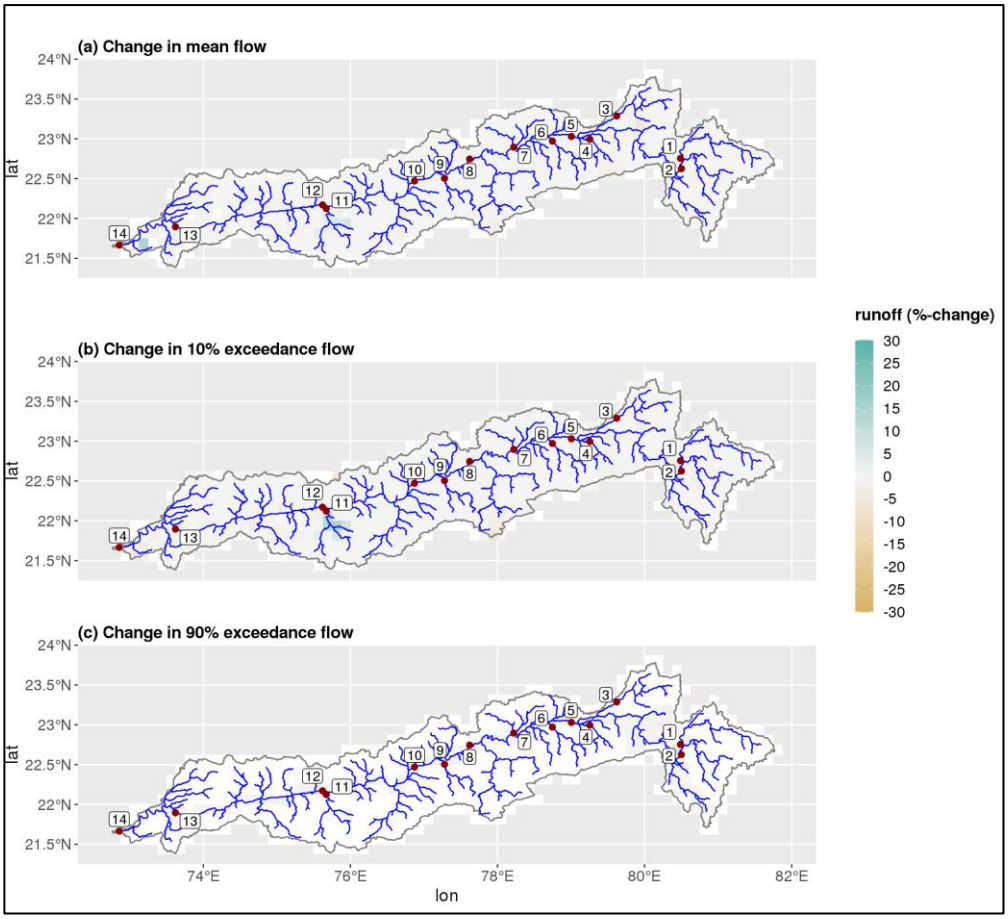

Figure 5.23: Spatial distribution of the runoff change due to population growth in 2050s: a) change in mean flow, b) change in high flows, c) change in low flows

5.3.3.2 Livestock increase scenario

The impact of the increase in livestock population leading to higher water demands have been evaluated for the 2050s based on the livestock projections for 2050 provided by FAO. No significant deviation in monthly flows has been observed at any of the months and at any of the gauging sites. The spatial variation of the impact of livestock growth on the mean daily flows, high flows (Q10) and low flows (Q90) in Narmada river basin is given in Figure 5.24. It can be observed that there is no considerable change in mean flows, high flows and lows flows as a consequence of the slightly higher water demands due to livestock growth. Therefore the livestock growth has a minimum impact on the future water availability in the Narmada basin when compared to the climate change induced impacts.

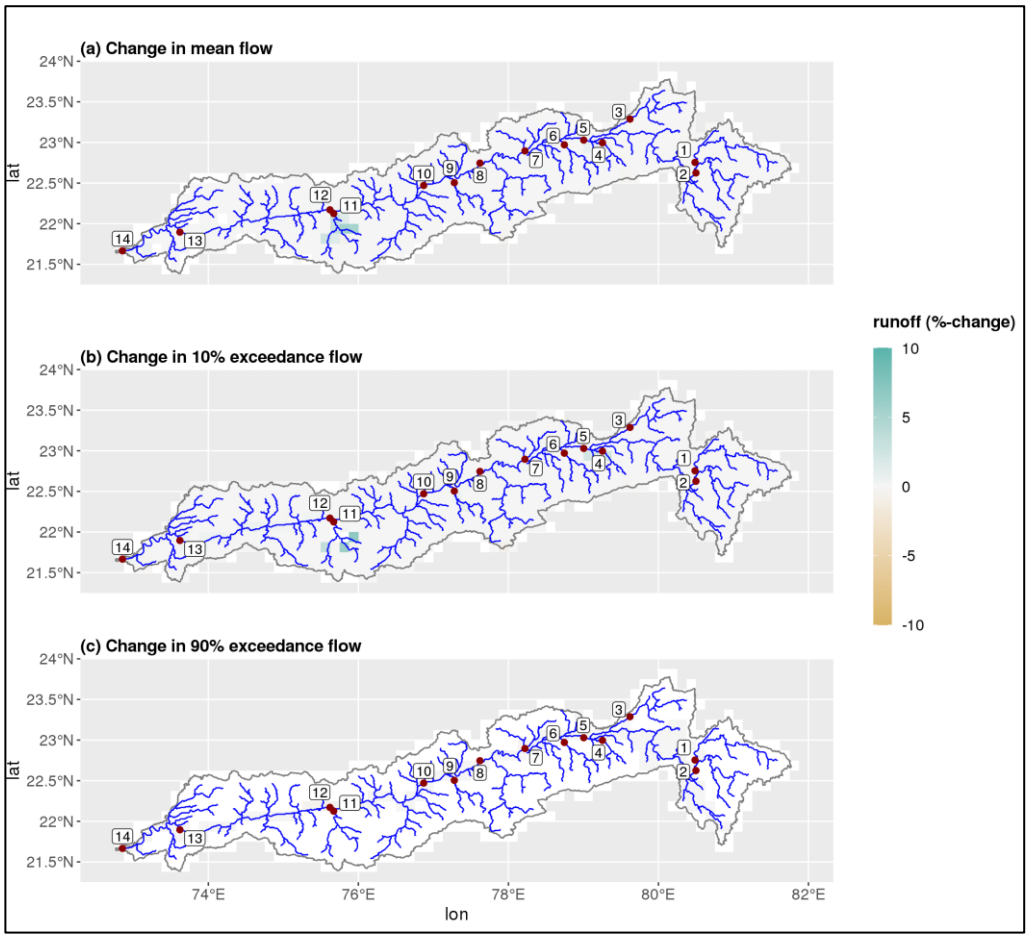

Figure 5.24: Spatial distribution of the runoff change due to livestock growth in 2050s: a) change in mean flow, b) change in high flows, c) change in low flows

5.3.3.3 Upcoming reservoirs scenario

The impact of the upcoming reservoirs on the stream flow regime in Narmada basin has been evaluated by comparing with the stream flow during the baseline scenario. In the baseline scenario, the major dams including the Bargi dam, Tawa dam, Barna Dam, Kolar Dam, ISP, OSP and SSP have been incorporated in GWAVA 5.1. The reservoir releases for multiple uses were also incorporated. The out-of-the-basin transfers including the Narmada-Shipra link, domestic water supply to Bhopal city located in Ganga basin etc., have been considered for the baseline scenario for simulation of daily runoff at the various gauging sites on the main river and its tributaries. However, for the future scenario the proposed (upcoming) reservoirs that may get implemented sooner have been incorporated in the model. The upcoming reservoirs include Upper Narmada project, Rosra project, Basania project, Chinki Project, Raghavpur project, Machrewa project and Dudhi project have been included alongwith the existing major dams considered during the baseline scenario. The out-of-basin water transfers from Narmada basin to Ganga basin via the right bank canal (RBC) of Bargi dam has also been incorporated in the model. The changes in the stream flow pattern at the various gauging sites as a consequence of the upcoming dams getting constructed and

out-of-basin water transfers has been studied by comparing the mean monthly flows during the baseline and upcoming reservoirs scenario. The comparison of the mean monthly stream flow during the baseline scenario with the upcoming reservoirs in the headwater catchments and main river channel is given in Figure 5.25.

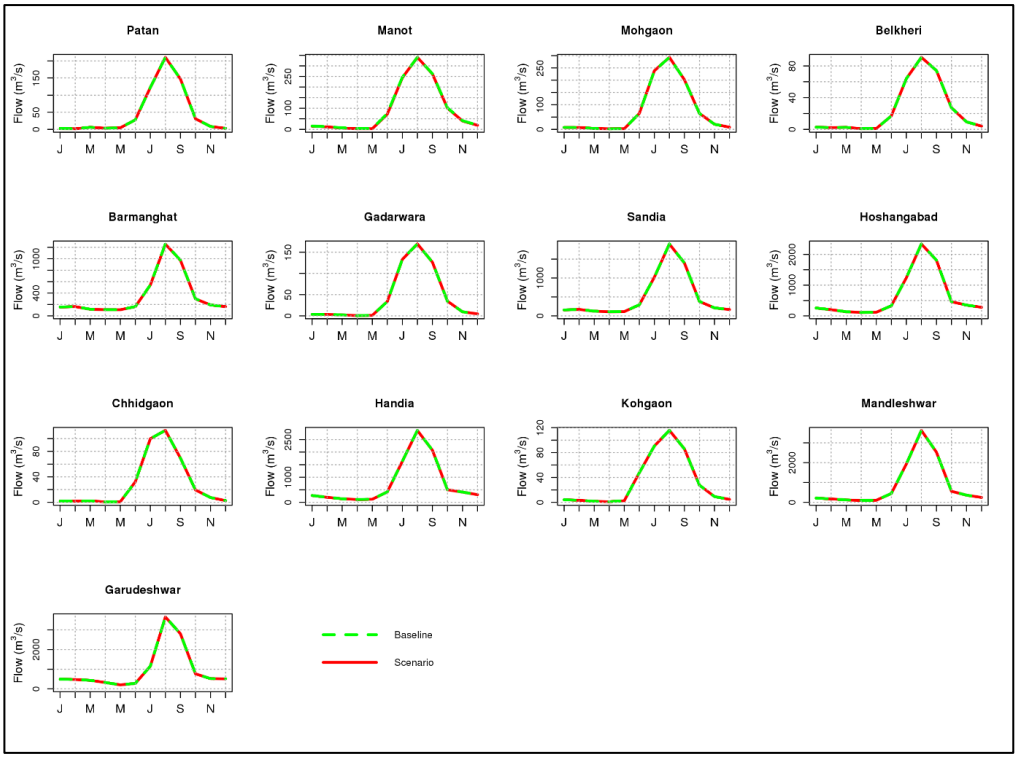

Figure 5.25: Comparison of mean monthly flow during the baseline with upcoming reservoir scenario

No major changes have been observed in mean monthly flows at any of the gauging sites. The spatial variation of the impact of upcoming reservoirs on the mean daily flows, high flows (Q10) and low flows (Q90) in Narmada river basin is given in Figure 5.26. As most of the proposed reservoirs are relatively smaller in size as compared to the existing major dams in the basin, the quantum of storage in these reservoirs is not large enough to have a likely major impact in the stream flow as a result of their construction. Therefore there is no significant change in mean flows, high flows and lows flows as a consequence of the proposed projects getting implemented.

5.3.3.4 Forestry buffer scenario

The likely impact of afforestation in the riparian areas on the stream flow was investigated for which a 400 m buffer zone was considered along the river. The prevailing land use in this buffer strip was changed to forested land use and model simulation was carried out to obtain the stream flow with this changed land use. The forestry band width was limited to 400 m based on the discussion with the experts in forest management and other stakeholders in the basin. The simulated flows obtained with the forestry buffer scenario were compared with the flows during the baseline

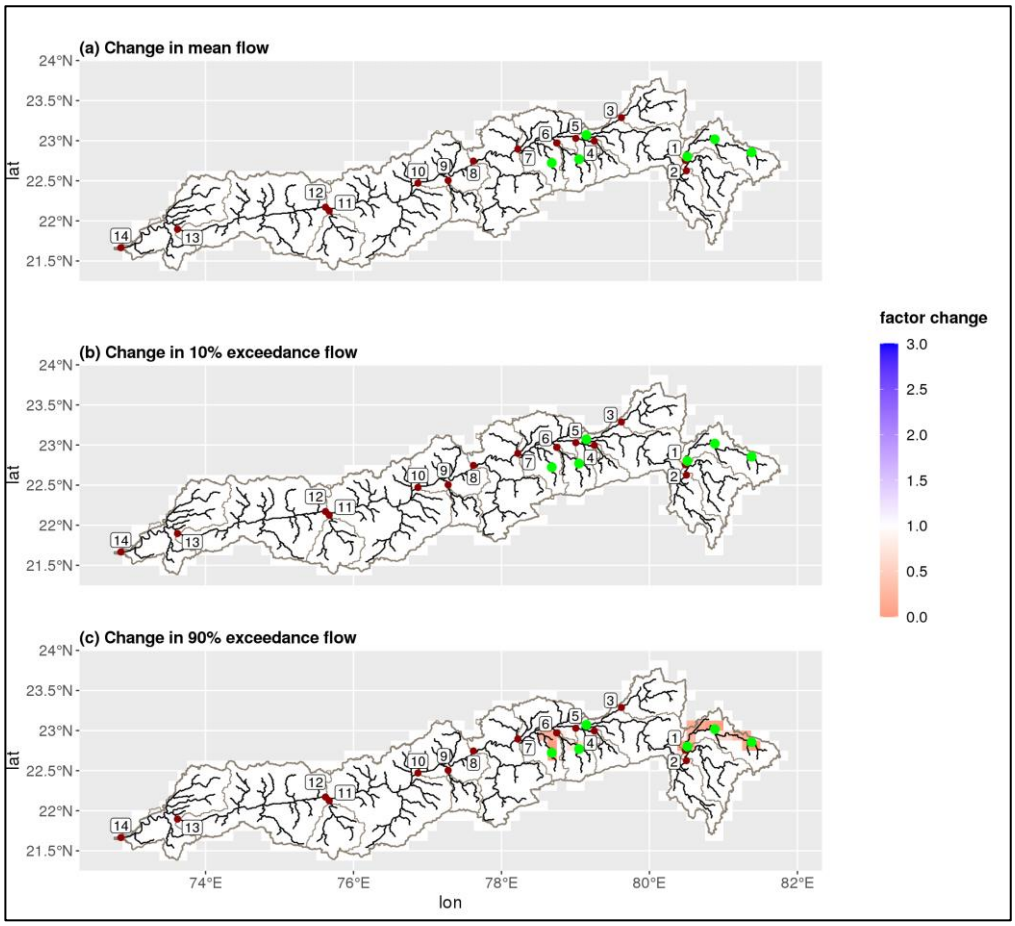

Figure 5.26: Spatial distribution of the runoff change due to upcoming reservoirs: a) change in mean flow, b) change in high flows, c) change in low flows

period to understand the likely impacts of having a forest buffer along the river. The mean monthly stream flow from the forestry buffer scenario has been compared with the baseline scenario, at the gauging sites located in the headwater catchments and main river channel and is given in Figure 5.27. No major changes have been observed in mean monthly flows at any of the gauging sites. The spatial variation of the impact of upcoming reservoirs on the mean daily flows, high flows (Q10) and low flows (Q90) in Narmada river basin is given in Figure 5.28. There is hardly any noticeable changes in the mean flows, high flows and low flows even in those grids covering the forestry buffer, as the water availability in these grids is much higher than that required by the forests plantations that may be implemented in the buffer zone. Moreover, the water availability near the river/stream is expected to be generally higher as compared to the areas located far away from the river in the basin.

5.3.3.5 Cropping pattern change scenario

The cropping pattern change scenario was also considered to study the impacts of changes in cropping pattern on the resultant stream flow. Recently, the cropping pattern in Narmada basin

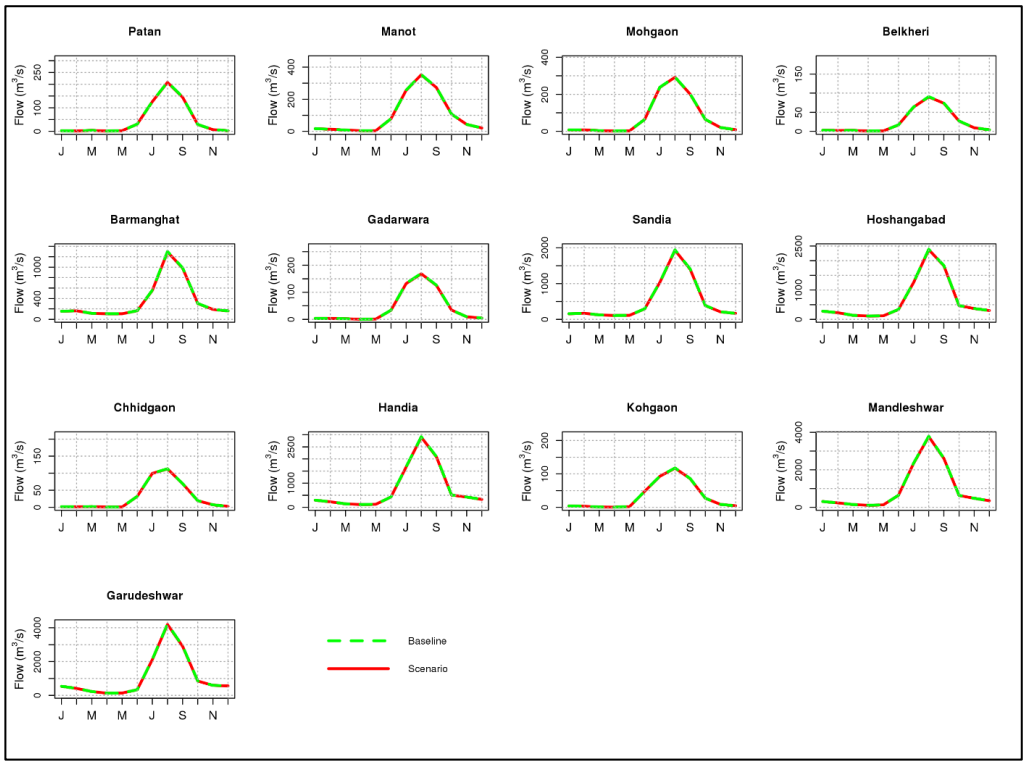

Figure 5.27: Comparison of mean monthly flow during the baseline period with forestry buffer scenario

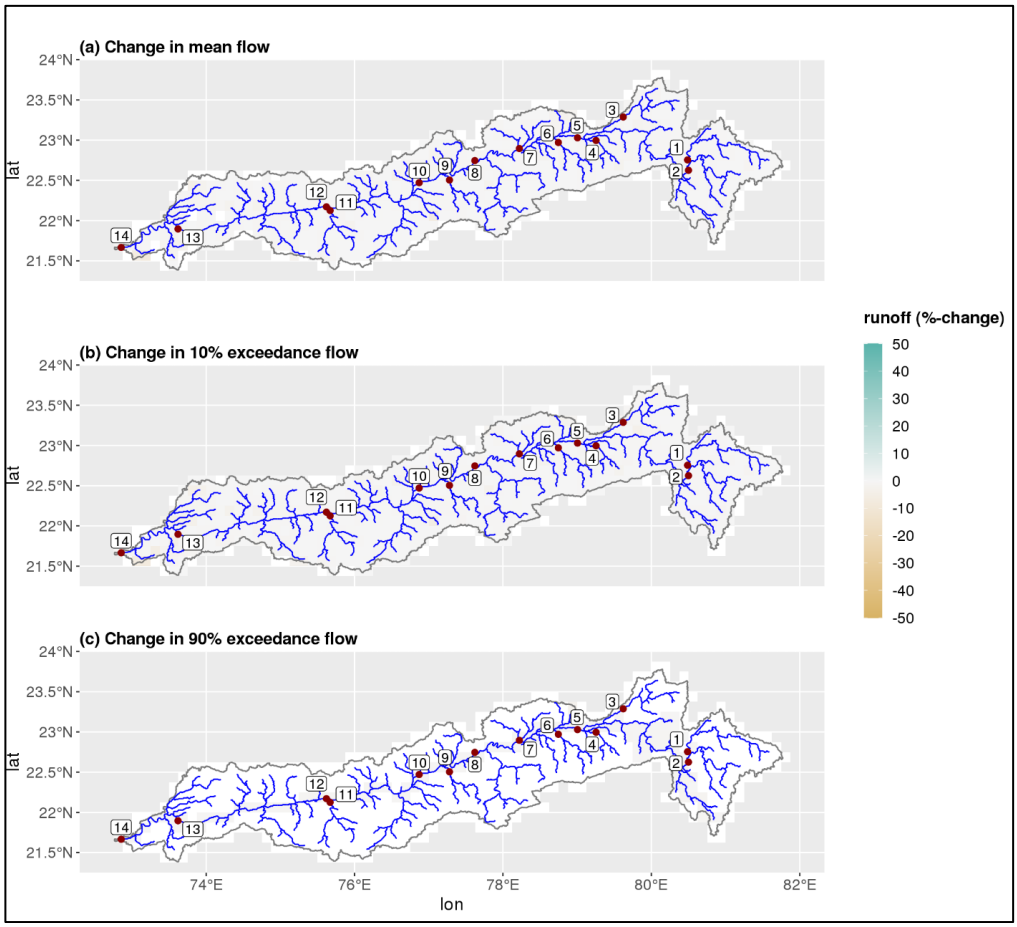

Figure 5.28: Spatial distribution of the runoff change due to forestry buffer: a) change in mean flow, b) change in high flows, c) change in low flows

particularly, in the upper and middle regions have changed, with the farming community switching over from soybean to paddy (basmati rice) in the command areas. As the basmati rice is a cash crop which fetches much higher returns, the farmers have been attracted in a big way to grow paddy. Moreover sufficient water is available at present as the water transfer to Ganga basin through the RBC is not effectively taking place due to incomplete construction of the RBC. The simulation for the cropping pattern change scenario has been carried out by changing the cropland under soyabean during the baseline period to paddy during the kharrif season for future time zones. However, no changes have been observed for the rabi crops. The comparison of the mean daily discharge during the baseline period with the crop switch scenario (soyabean cropped area to paddy) at the headwater catchment and in the main river channel is given in Figures 5.29 and Figure 5.30 respectively.

The mean flows are expected to get reduced substantially both in the headwater catchments and in the main river channel. The average reduction in the mean daily stream flow in the headwater catchments is 24.85% whereas the average reduction in the mean daily flow at the gauging sites in the main river channel is 26.04%. Therefore, the shift in the cropping pattern from soyabean to paddy will have consequences of reduced stream flow in Narmada basin. However, it will be interesting to study how the climate change related impacts translate in future and whether these additional crop water demands can be met naturally due to the climate induced impacts.

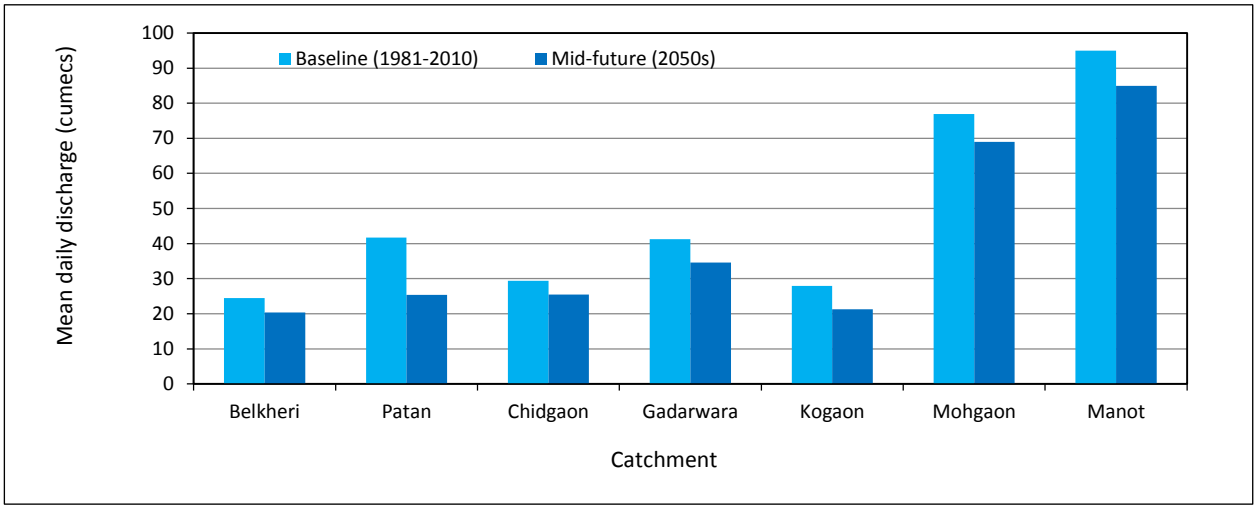

Figure 5.29: Comparison of mean daily discharge during the baseline period with crop switch scenario in headwater catchments

5.3.3.6 Climate Change Scenario

For future river flow projections, GWAVA 5.1 was forced with the daily bias-corrected future data of precipitation, maximum and minimum temperature at 0.25^{o} x 0.25^{o} spatial resolution for South Asia from the 13 GCMs that participated in the Coupled Model Intercomparison Project-6 (CMIP6) (Mishra et al., 2020). CMIP6-GCMs based precipitation, maximum and minimum

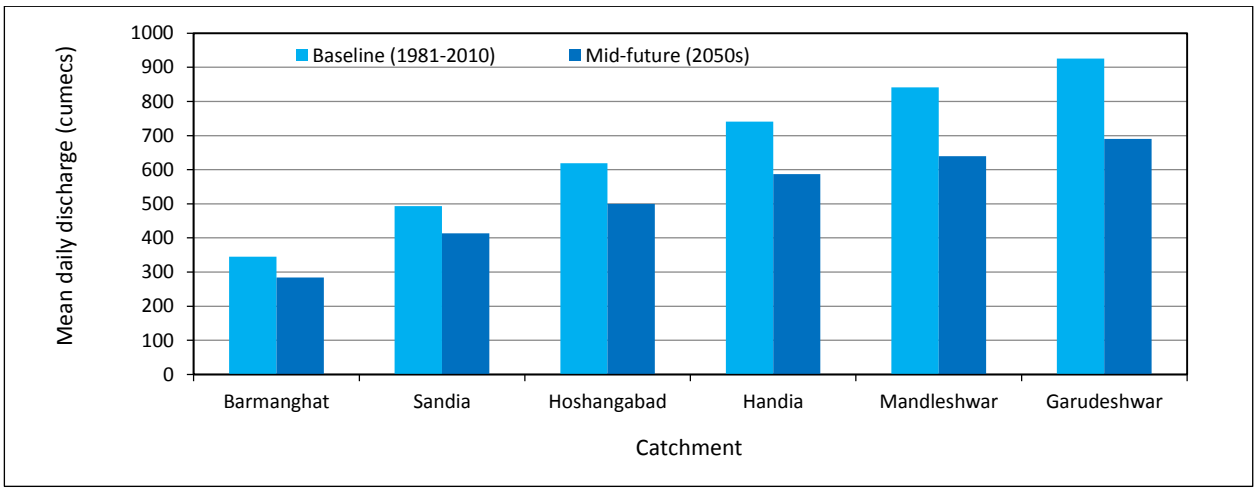

Figure 5.30: Comparison of mean daily discharge during the baseline period with crop switch scenario in in main river channel

temperature are available at various spatial resolutions viz., 0.7° for EC-Earth3 to more than 2° for CanESM5. The daily precipitation, maximum and minimum temperature for the historical (1850-2014) and future (2015-2100) climate for SSP126 (2015–2100), SSP245 (2015–2100), SSP370 (2015–2100), and SSP585 (2015–2100) scenarios under r1i1p1f1 initial condition at daily time scale (Eyring et al., 2016) was available only for 13 GCMs (Mishra et al., 2020). The scenarios used in the CMIP6 combine Shared Socioeconomic Pathways (SSP) and target radiative forcing levels at the end of the 21st century, viz., SSP126 indicates SSP-1 and target radiative forcing of 2.6 Watt/m2 at the end of 21st Century, which can be considered as a mitigation scenario. Similarly, SSP585 indicates SSP-5 and radiative forcing of 8.5 Watt/m2 at the end of the 21st Century (Giden et al., 2019). Empirical Quantile Mapping (EQM) was used to obtain the bias-corrected dataset developed using for the historic (1951–2014) and projected (2015–2100) climate for the four scenarios (SSP126, SSP245, SSP370, SSP585) from selected 13 GCMS (Mishra et al., 2020).

The climate change impact assessments on the future water availability in Narmada basin has been carried out by driving the calibrated and validated GWAVA 5.1 model with future climate data sets to obtain the future simulated stream flows. The future stream flows in the basin have been simulated using for two future 30-year time slices of 2050s (2036-2065) and 2080s (2066-2095) for SSP245 and SSP585. The Table 5.8 provides the details of the GCMs used in this study.

5.3.3.6.1 Climate change impact on precipitation

The projected changes in future climate for the 2050s and 2080s were assessed relative to the baseline period of 1981–2010. The mean annual precipitation projections across all GCMs show an increase at all sites both during 2050s and 2080s, the increase being more predominant during 2080s. There is considerable variation in mean annual precipitation between the individual GCMs,

Table 5.8: CMIP6 Global Circulation Models (GCMs) used in the study

Model Name	Institution
ACCESS-CM2	Commonwealth Scientific and Industrial Research Organisation (CSIRO) and Bureau of Meteorology (BOM), Australia
ACCESS-ESM1-5	Commonwealth Scientific and Industrial Research Organisation (CSIRO) and Bureau of Meteorology (BOM), Australia
BCC-CSM2-MR	Beijing Climate Center, China Meteorological Administration, China
CanESM5	Canadian Centre for Climate Modelling and Analysis, Canada
EC-Earth3	Swedish Meteorological and Hydrological Institute, Sweden
EC-Earth3-Veg	Swedish Meteorological and Hydrological Institute, Sweden
INM-CM4-8	Institute for Numerical Mathematics, Russian Academy of Science, Moscow
INM-CM5-0	Institute for Numerical Mathematics, Russian Academy of Science, Moscow
MPI-ESM1-2-LR	Max-Planck-Institut für Meteorologie (Max Planck Institute for Meteorology), Germany
MPI-ESM1-2-HR	Max-Planck-Institut für Meteorologie (Max Planck Institute for Meteorology), Germany
MRI-ESM2-0	Meteorological Research Institute , Japan
NorESM2-LM	Norwegian Meteorological Institute, Norway

with CanESM5 predicting substantially higher rainfall increase as compared to other GCMs. The mean annual precipitation during historical period spanning from 1970-2019 is 1091.8 mm and is projected to exceed in future, by all the GCMs, the largest increase being projected by CanESM5 as 1710 mm during 2020-2100. The ensemble mean annual rainfall for the SSP245 scenario during 2020-2100 is 1379.35 mm, an increase of 21.4%. Similarly, the ensemble mean annual rainfall for the SSP245 scenario during 2020-2100 is 1524.8 mm, an increase of 39.7%. Similarly, the consecutive 3-day rainfall in the study area is projected to increase from 180.06 mm (1970-2019) to 221.54 mm (2020-2100) which is an increase of 23%. The average rainfall intensity, which represents the rainfall during the rainy day, is also projected to increase from 17.99 mm/day to 18.60 mm/day for SSP585 scenario. The average 1-day maximum rainfall is projected to increase from 108.14 mm during 1970-2019 to 110.13 mm during 2020-2100 (SSP245) and 120.04 mm during 2020-2100 (SSP585).

5.3.3.6.2 Climate change impact on maximum and minimum temperature

The average maximum temperature is also projected to increase from 32.4^{o}C during 1970-2019 to 32.42^{o}C during 2020-2100 for SSP245 scenario and to 34.3^{o}C during 2020-2100 based on SSP585 scenario. This increase in the MaxT amounts to an increase at the rate of 1.62^{o}C/100 year for SSP245 scenario and 2.30^{o}C/100 year for SSP585 scenario. The average minimum temperature is also projected to increase in the Narmada basin at a much higher rate as compared to the increase in

maximum temperature. The average minimum temperature is also projected to increase from 19.0^{o}C during 1970-2019 to 20.9^{o}C during 2020-2100 as per SSP245 scenario and to 21.8^{o}C during 2020-2100 as per SSP585 scenario. This increase in the MinT amounts to an increase at the rate of 2.32^{o}C/100 year for SSP245 scenario and 3.39^{o}C/100 year for SSP585 scenario. Therefore the rate of increase in the minimum temperature is substantially higher than rate of increase of maximum temperature in the basin.

The maximum of MaxT is also projected to increase at a slightly higher rate from 43.6^{o}C during 1970-2019 to 44.9^{o}C during 2020-2100 for SSP245 scenario and to 45.6^{o}C during 2020-2100 for SSP585 scenario. The minimum of MinT is also projected to increase at a much higher rate as compared to the increase in average minimum temperature from 6.23^{o}C to 8.22^{o}C (SSP245) and 9.14^{o}C (SSP585). This indicates that the future temperature changes linked to global warming may be characterised by a marked asymmetry between daytime maxima and night time minima. The increases in both maximum and minimum temperature will have significant impacts on the water viz., increase in water demands for the domestic, agricultural and other water dependent sectors, considerable impacts on crop growth and crop yields, intensification of the hydrological cycle, increase spatio-temporal variability in the precipitation distribution leading to higher water deficits and water surplus scenarios.

5.3.3.6.3 Climate change impact on mean flows

The GWAVA 5.1 model was calibrated with the observed daily stream flow and validated with the independent stream flow time series. The performance evaluation of the model in simulating the daily stream flow has been well established and explained in the previous section. This model has been driven with the bias-corrected daily precipitation, maximum and minimum temperature of 13 GCMs for two future climate scenarios viz., SSP245 and SSP585. The comparison of the mean daily discharge during the baseline period (1981-2010), 2050s (2036-2065) and 2080s (2066-2095) has been carried out for the gauging sites located at the outlet of headwater catchments and also located in the main river channel.

Figure 5.31 show the comparison of mean daily stream flows at Manot during the baseline period and during the 2050s whereas Figure 5.32 shows the comparison of stream flows during the baseline period with those during the 2080s. It can be observed that the stream flow is projected to increase both during 2050s and 2080s, but the increase is more pronounced with the SSP585 scenario as compared to the SSP245 scenario. The simulated stream flow obtained by driving GWAVA 5.1 using CanESM5 gives the largest mean daily discharge as a result of its higher precipitation as compared to other GCMs. The ensemble mean of the mean daily discharge during at Manot during

the 2050s for SSP245 is 128.42 cumecs as compared to 94.97 cumecs during the baseline period, which indicates an increase of more than 35%. However, during the 2080s the mean daily discharge for SSP245 is 146.06 cumecs which translates to an increase of 54% in the mean daily discharge at Manot. The projected increase is much higher considering the SSP585 scenario with an increase of 39% during the 2050s and 82% during the 2080s.

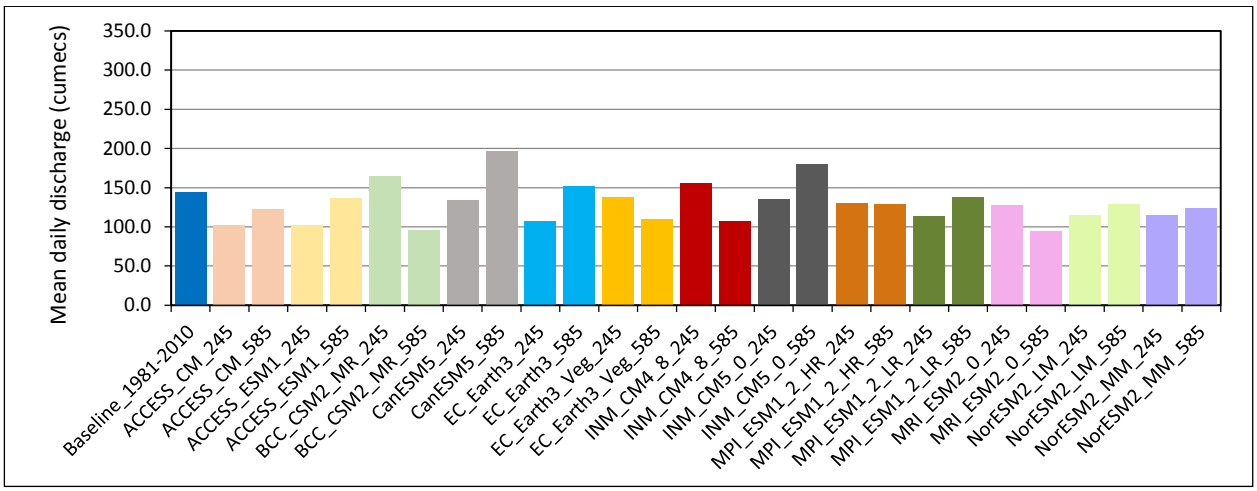

Figure 5.31: Comparison of mean daily flow during the baseline and 2050s at Manot

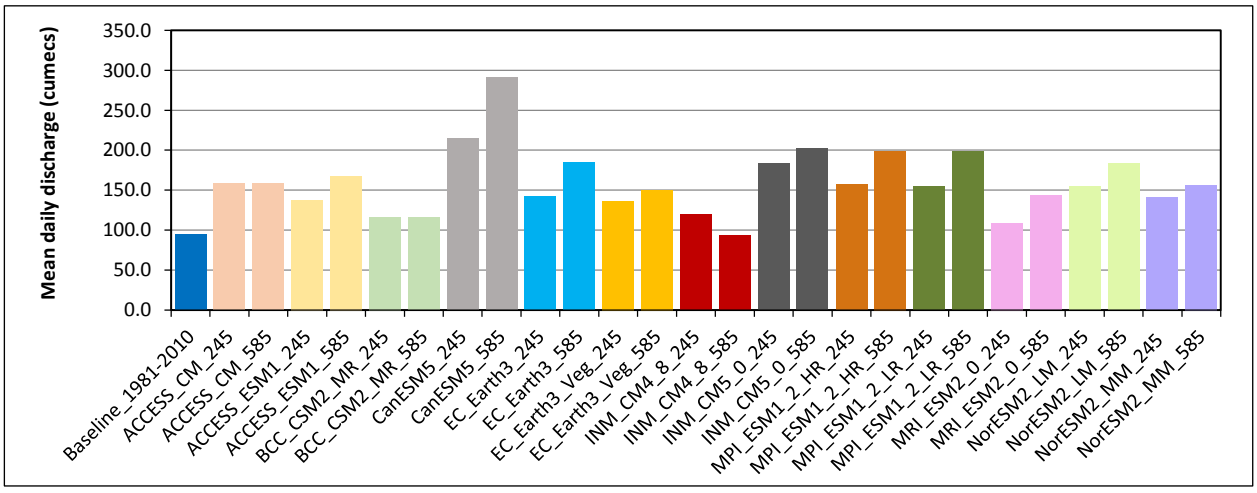

Figure 5.32: Comparison of mean daily flow during the baseline and 2080s at Manot

Figure 5.33 show the comparison of mean daily stream flow at Mohgaon during the baseline period and during the 2050s whereas Figure 5.34 shows the comparison of stream flows during the baseline period with those during the 2080s. Here too, the stream flow is projected to increase during both 2050s and 2080s, but the increase is more pronounced with the SSP585 scenario as compared to the SSP245 scenario. The ensemble mean of the mean daily discharge during at Mohgaon during the 2050s for SSP245 is 101.26 cumecs as compared to 76.94 cumecs during the baseline period, an increase of about 32%. Similarly, during the 2080s the mean daily discharge for SSP245 is 114.05 cumecs which translates to an increase of 48% in the mean daily discharge at Mohgaon. The projected

increase is much higher considering the SSP585 scenario with an increase of 37% during the 2050s and 78% during the 2080s. The simulated stream flow obtained by driving GWAVA 5.1 using CanESM5 gives the largest mean daily discharge. The projected increase in stream flow augurs

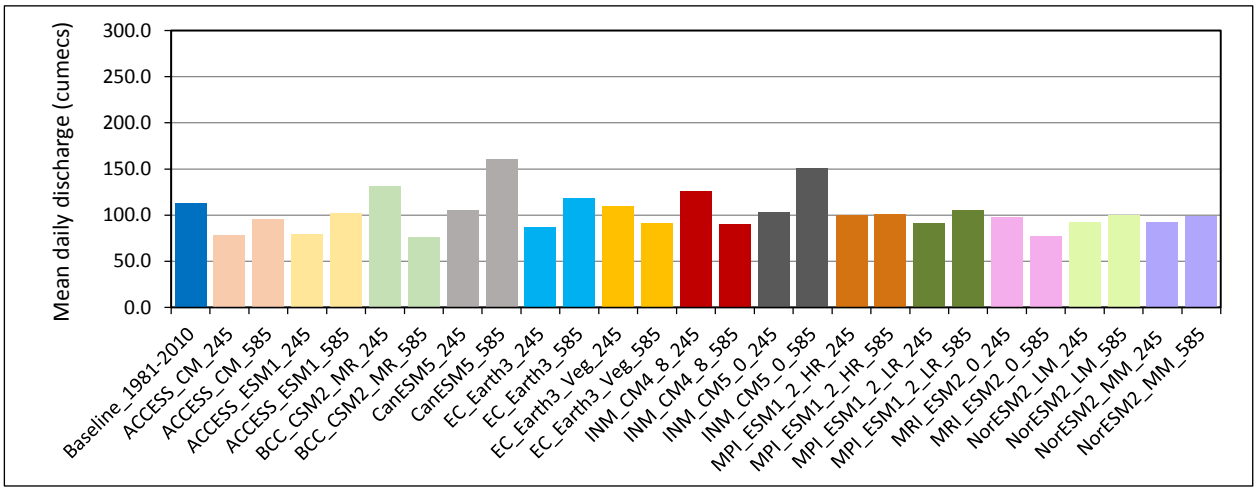

Figure 5.33: Comparison of mean daily flow during the baseline and 2050s at Mohgaon

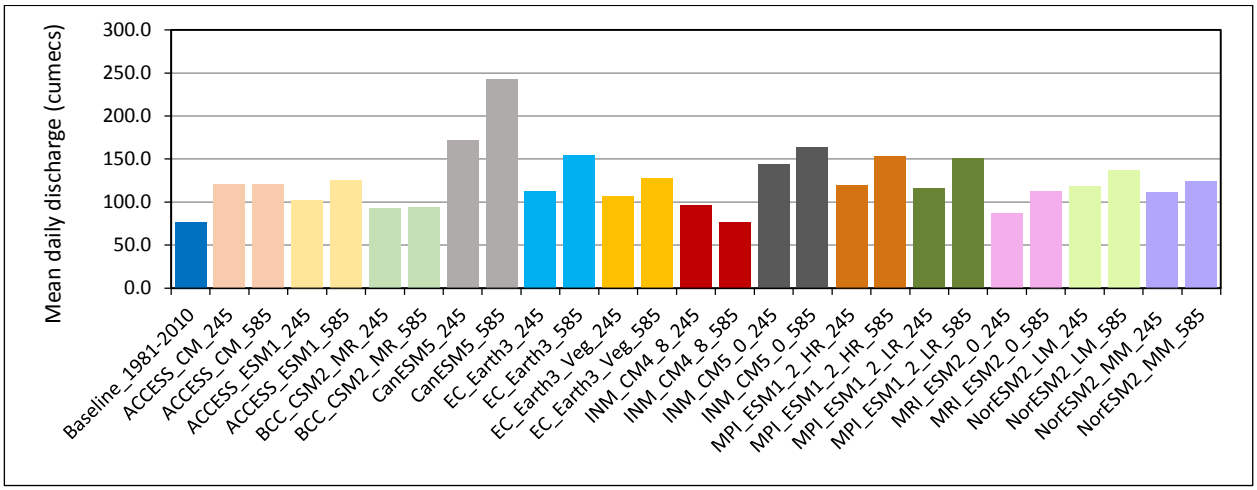

Figure 5.34: Comparison of mean daily flow during the baseline and 2080s at Mohgaon

well, as these are headwater catchments responsible for sustaining perennial flows in the Narmada river system.

Figure 5.35 show the comparison of mean daily stream flows at Belkheri during the baseline period and during the 2050s whereas Figure 5.36 shows the comparison of stream flows during the baseline period with those during the 2080s. The ensemble mean of the mean daily discharge during at Belkheri during the 2050s for SSP245 is 36.37 cumecs as compared to 24.45 cumecs during the baseline period, an increase of about 49%. Similarly, during the 2080s the mean daily discharge for SSP245 is 42.60 cumecs which translates to an increase of 74% in the mean daily discharge at

Belkheri. The projected increase is much higher considering the SSP585 scenario with an increase of 54% during the 2050s and 209% during the 2080s.

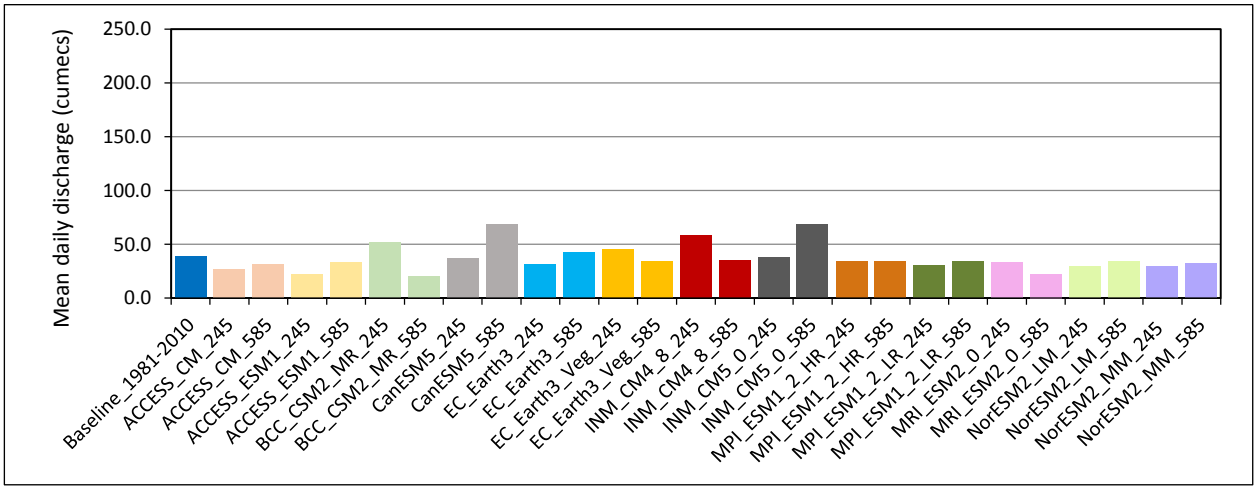

Figure 5.35: Comparison of mean daily flow during the baseline and 2050s at Belkheri

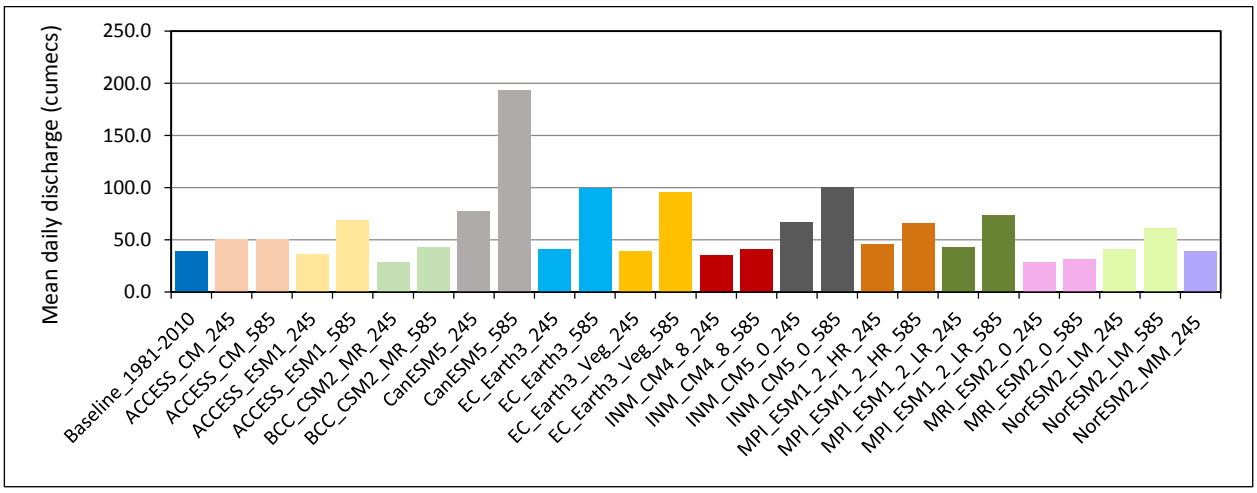

Figure 5.36: Comparison of mean daily flow during the baseline and 2080s at Belkheri

Similarly, Figure 5.37 show the comparison of stream flows at Patan during the baseline period and during the 2050s whereas Figure 5.38 shows the comparison of stream flows during the baseline period with those during the 2080s. The ensemble mean of the mean daily discharge during at Patan during the 2050s for SSP245 is 53.29 cumecs as compared to 41.71 cumecs during the baseline period, an increase of about 28%. During the 2080s the mean daily discharge for SSP245 is 61.9 cumecs which translates to an increase of 62% in the mean daily discharge at Patan. The projected increase is much higher considering the SSP585 scenario with an increase of 35% during the 2050s and 54% during the 2080s. As the stream flow in Belkheri and Patan headwater catchments are projected to increase in future, this will help to sustain the flows in the main channel of Narmada river system.

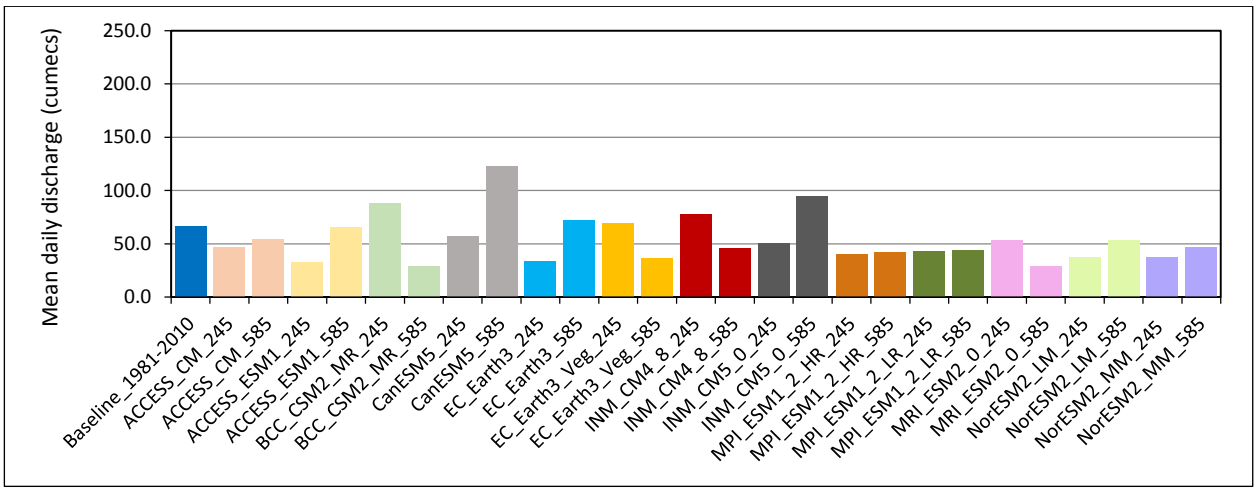

Figure 5.37: Comparison of mean daily flow during the baseline and 2050s at Patan

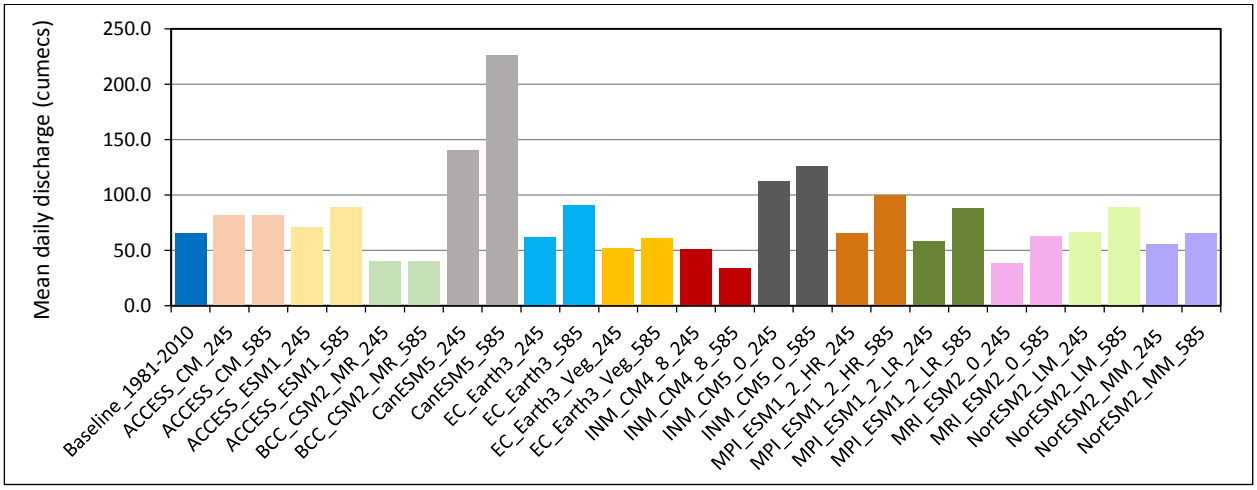

Figure 5.38: Comparison of mean daily flow during the baseline and 2080s at Patan

The comparison of the mean daily stream flow at the remaining headwater catchments viz., Gadarwara, Kogaon and Chidgaon is given in Figure 5.39 to Figure 5.44. It can be observed that the stream flows in these headwater catchments are projected to increase substantially during the future time zones. The stream flow is projected to increase substantially during the 2080s as compared to the 2050s. During the 2050s, under SSP245 scenario the stream flow at Gadarwara, Kogaon and Chidgaon is projected to increase by 45%, 58% and 31% respectively, whereas the projected increase is higher under SSP585 viz., Gadarwara (+48%), Kogaon (+74%) and Chidgaon (+36%). However, during the 2080s the projected increases in stream flow is much higher at Gadarwara, Kogaon and Chidgaon which is expected to increase by 68%, 98% and 50% respectively, whereas the projected increase is relatively higher under SSP585 viz., Gadarwara (+113%), Kogaon (+181%) and Chidgaon (+95%). The results of the analysis indicate that the mean daily stream flows in these headwater catchments are projected to increase considerably during both future time horizons, viz., the 2050s and the 2080s. This augurs well for Narmada basin as a major portion of

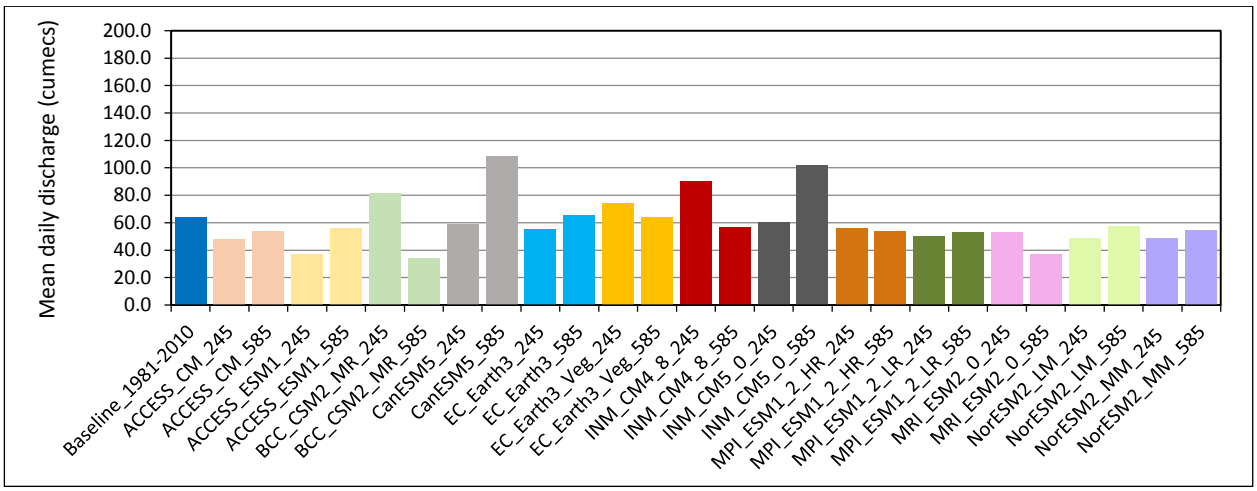

Figure 5.39: Comparison of mean daily flow during the baseline and 2050s at Gadarwara

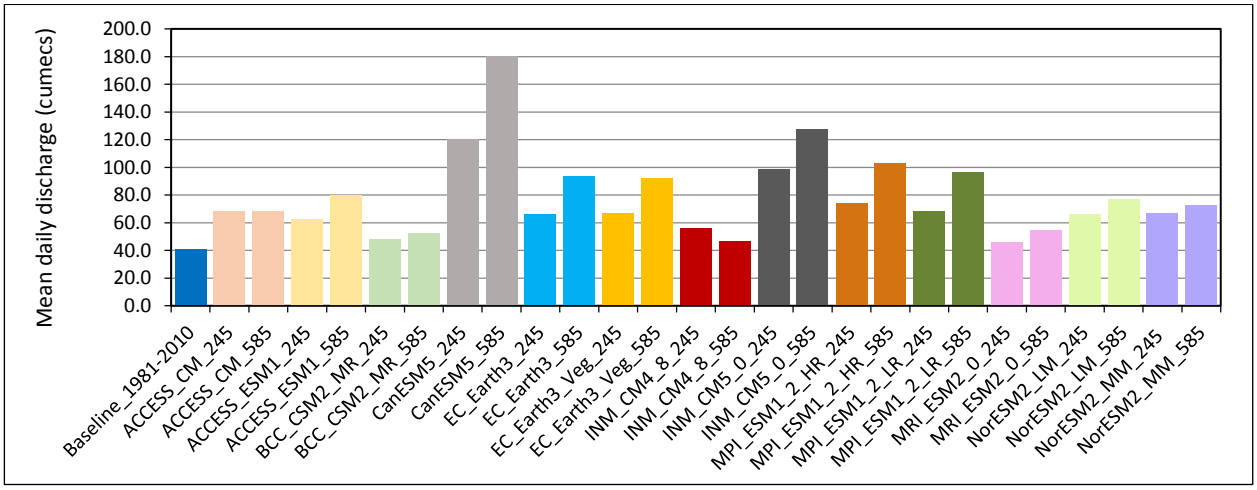

Figure 5.40: Comparison of mean daily flow during the baseline and 2080s at Gadarwara

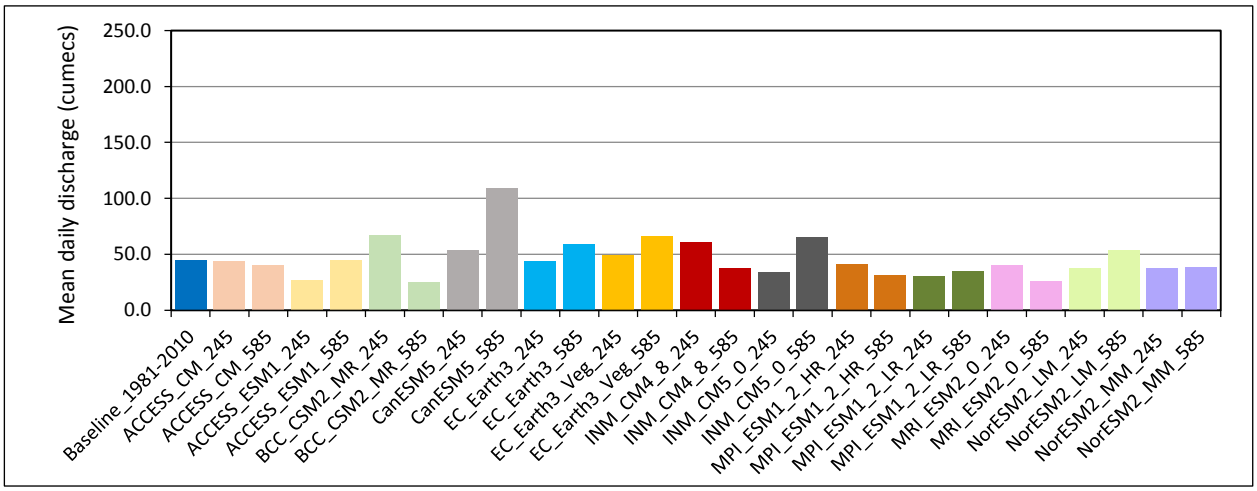

Figure 5.41: Comparison of mean daily flow during the baseline and 2050s at Kogaon

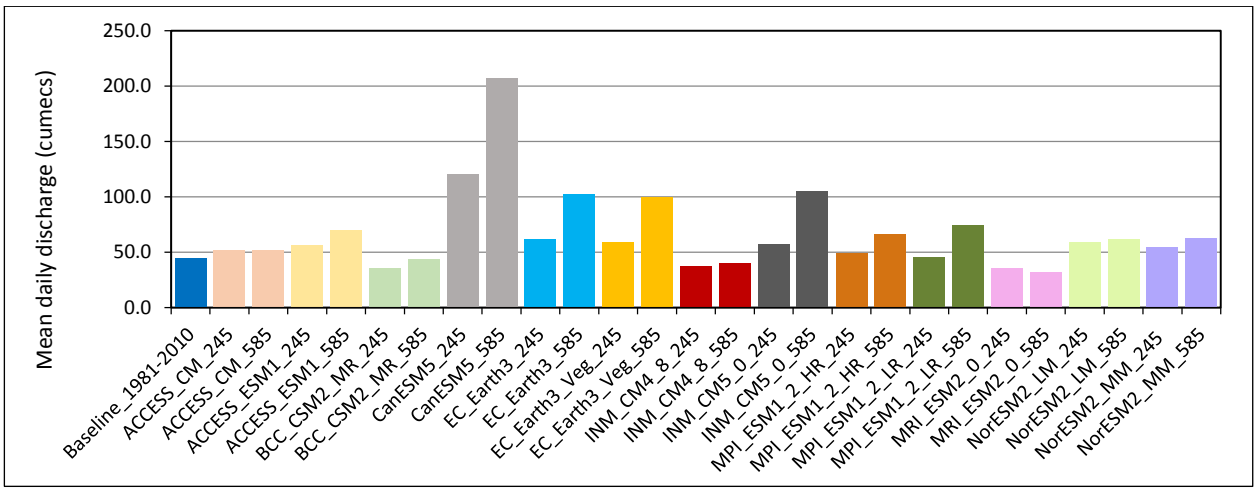

Figure 5.42: Comparison of mean daily flow during the baseline and 2080s at Kogaon

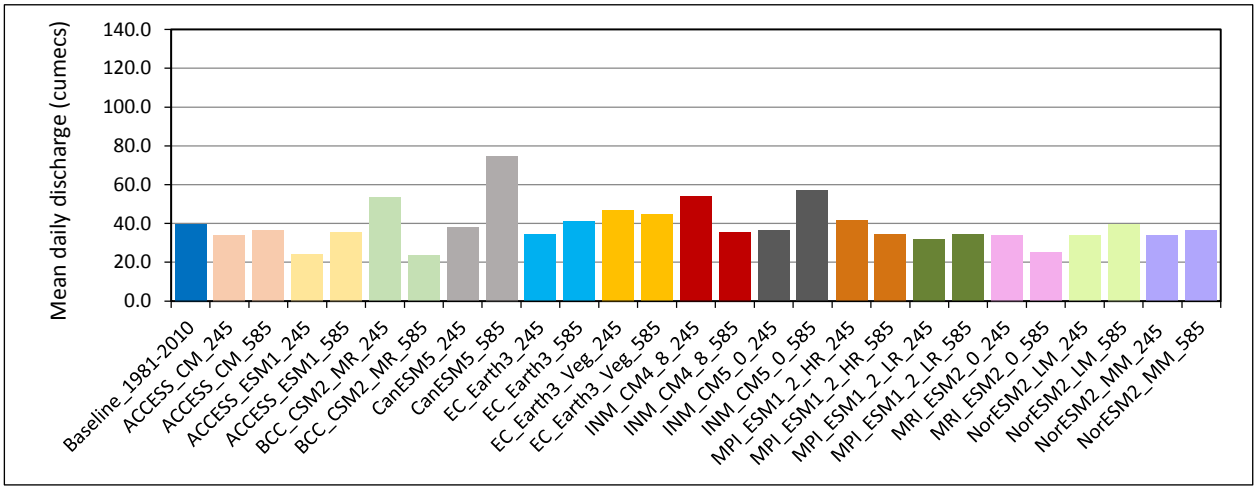

Figure 5.43: Comparison of mean daily flow during the baseline and 2050s at Chidgaon

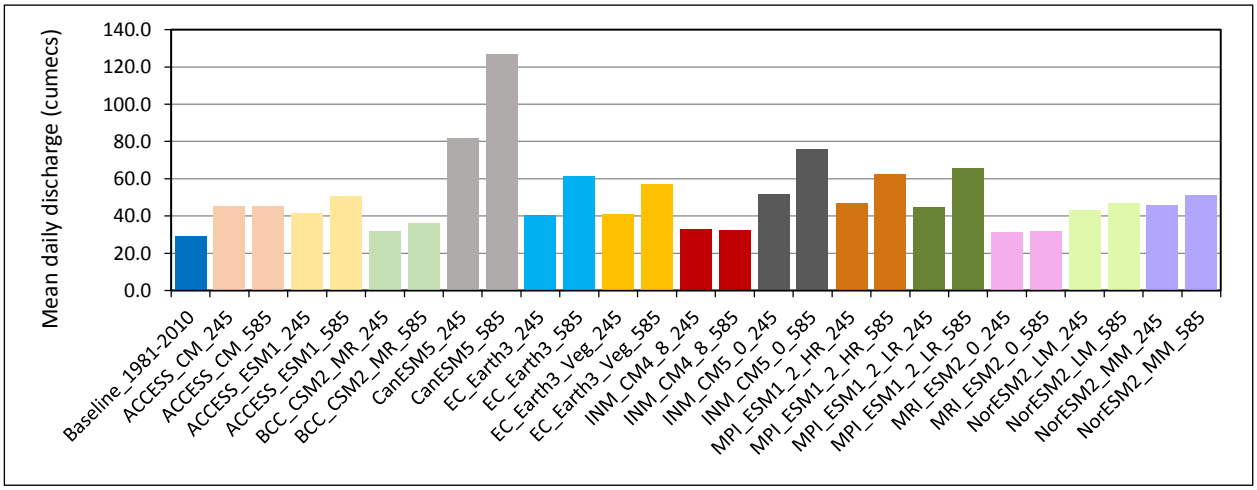

Figure 5.44: Comparison of mean daily flow during the baseline and 2080s at Chidgaon

the higher flows generated from the headwater catchments will ultimately reach the main river where major projects are located.

The comparison of the mean daily stream flow at Barmanghat during under the SSP245 and SSP585 during the 2050s and 2080s is given in Figure 5.45 and Figure 5.46 respectively. The gauging site at Barmanghat is located on the main river channel downstream of Bargi Reservoir Project, which is a major multipurpose dam. The flows in the main river at Barmanghat is therefore influenced by the reservoir storages during the filling up of the reservoir, spillway releases once the reservoir is filled completely and also influenced by the releases made for hydropower generation. These figures indicate that the simulated mean daily stream flow is higher during the 2080s as compared to the 2050s for all GCMs. The CanESM2 projects the highest increase in mean daily flow owing to the higher precipitation projected by this GCM. However, an intercomparison between scenarios, indicate a mixed response with few GCMs suggesting higher mean daily flows under SSP585 whereas many other GCMs suggest relatively lesser mean daily flows under SSP585 both during the 2050s and 2080s. The ensemble mean daily stream flow under SSP245 during

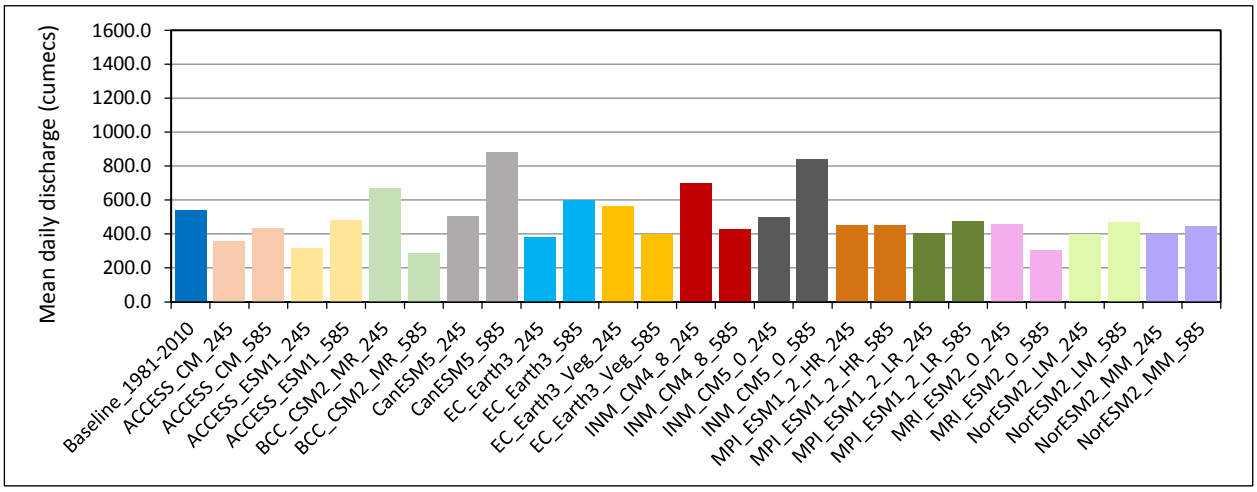

Figure 5.45: Comparison of mean daily flow during the baseline and 2050s at Barmanghat

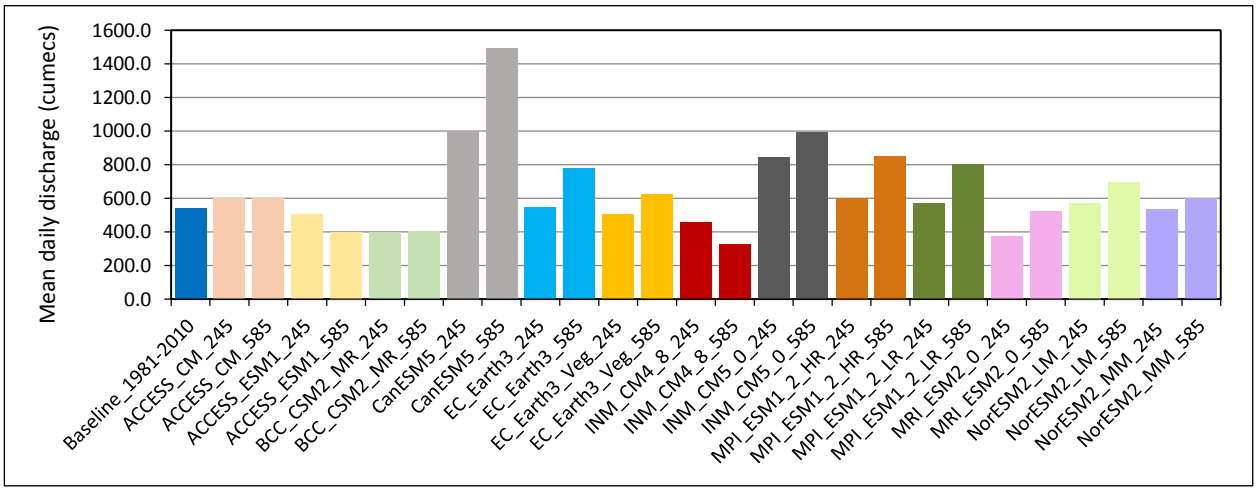

Figure 5.46: Comparison of mean daily flow during the baseline and 2080s at Barmanghat

2050s and 2080s is 478.58 cumecs and 498.75 cumecs respectively, an increase of 39% and 45% during 2050s and 2080s respectively. Similarly, the ensemble mean daily stream flow under SSP585 is 569.38 cumecs and 699.13 cumecs, (increase of 65% and 103%) respectively during the 2050s and 2080s.

The comparison of the mean daily stream flow at Sandia during under the SSP245 and SSP585 during the 2050s and 2080s is given in Figure 5.47 and Figure 5.48 respectively. The gauging site at Sandia is located on the main river channel downstream of Barmanghat. The flows in the main river at Sandia is therefore influenced by the reservoir storages and reservoir releases from the Bargi Reservoir Project and also on the generation and withdrawal of water from the main river located within the intermediate catchment. The ensemble mean daily stream flow at Sandia under SSP245 during 2050s and 2080s is 688.44 cumecs and 713.13 cumecs respectively, an increase of 40% and 45% during 2050s and 2080s respectively. Similarly, the ensemble mean daily

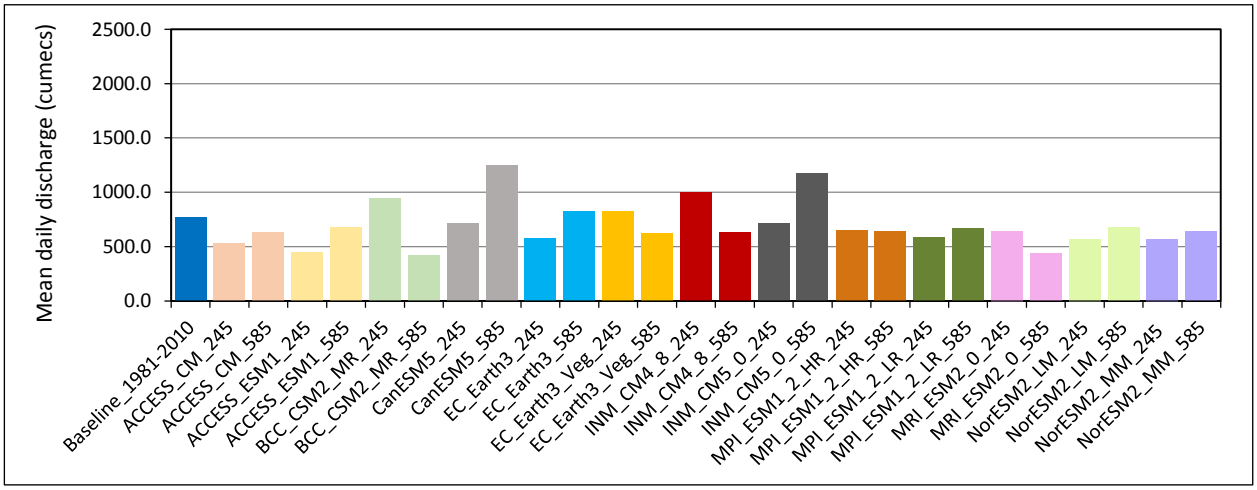

Figure 5.47: Comparison of mean daily flow during the baseline and 2050s at Sandia

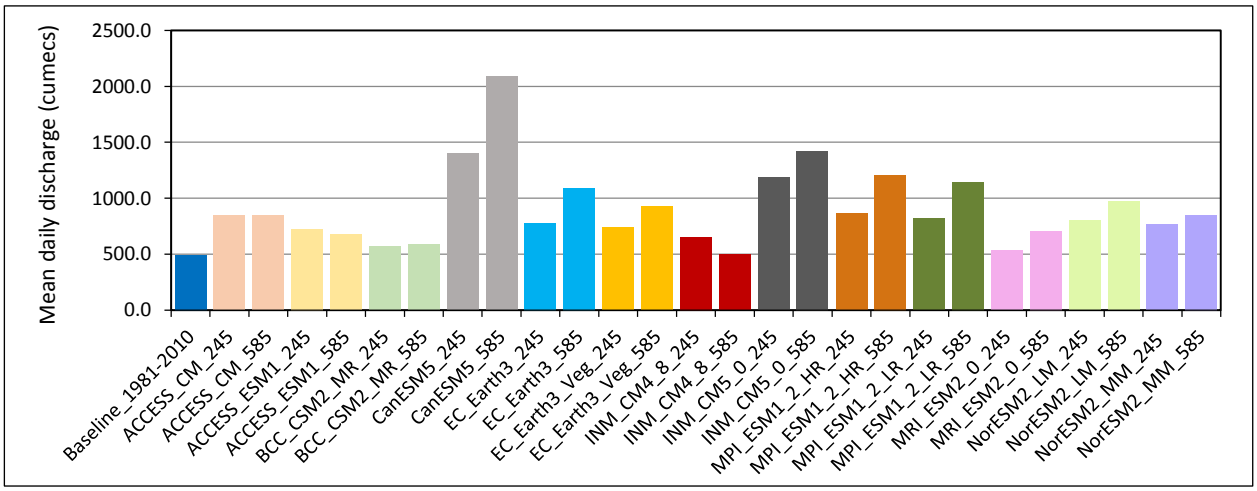

Figure 5.48: Comparison of mean daily flow during the baseline and 2080s at Sandia

stream flow at Sandia under SSP585 is 569.38 cumecs and 699.13 cumecs, (increase of 65% and 103%) respectively during the 2050s and 2080s. Figure 5.47 and Figure 5.48 indicate that the simulated mean daily stream flow is higher during the 2080s as compared to the 2050s for all GCMs. The CanESM2 projects the highest increase in mean daily flow owing to the higher precipitation projected by this GCM. However, an inter-comparison between scenarios, indicate a mixed response with few GCMs suggesting higher mean daily flows under SSP585 whereas many other GCMs suggest relatively lesser mean daily flows under SSP585 both during the 2050s and 2080s.

The gauging site at Hoshangabad is located on the main river channel downstream of Sandia. This site is also situated downstream of Tawa Reservoir Project and Barna dam, both of which are principally irrigation projects. The flows in the main river at Hoshangabad is therefore influenced by the reservoir storages and reservoir releases from the Tawa Reservoir Project and Barna dam and also to some extent from Bargi Reservoir Project. Spills from these dams are managed in a coordinated manner by staggering the releases based on the time of travel from the dam to Hoshangabad, to prevent flooding at Hoshangabad. An inter-comparison between scenarios, indicate a mixed response with majority of the GCMs suggesting higher mean daily flows under SSP585 whereas few other GCMs also suggest relatively lesser mean daily flows under SSP585 both during the 2050s and 2080s (Figure 5.49 & Figure 5.50). The ensemble mean daily stream

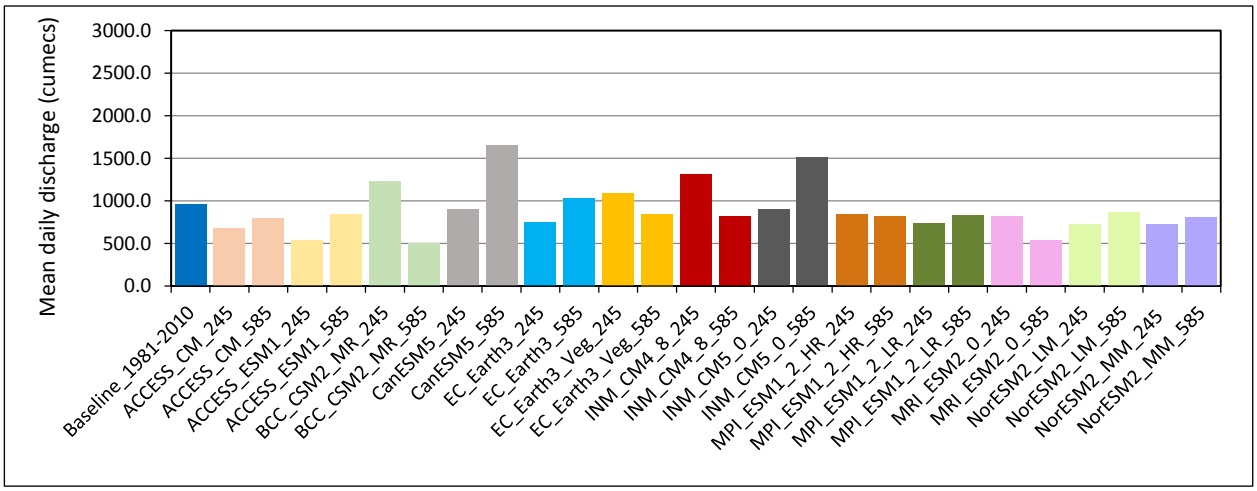

Figure 5.49: Comparison of mean daily flow during the baseline and 2050s at Hoshangabad

flow under SSP245 during 2050s and 2080s is 879.93 cumecs and 1039.4 cumecs respectively, an increase of 42% and 68% during 2050s and 2080s respectively. Similarly, the ensemble mean daily stream flow under SSP585 is 911.23 cumecs and 1310.77 cumecs, an increase of 47% and 111% respectively during the 2050s and 2080s.

The comparison of the mean daily flow during baseline period and future periods 2050s and

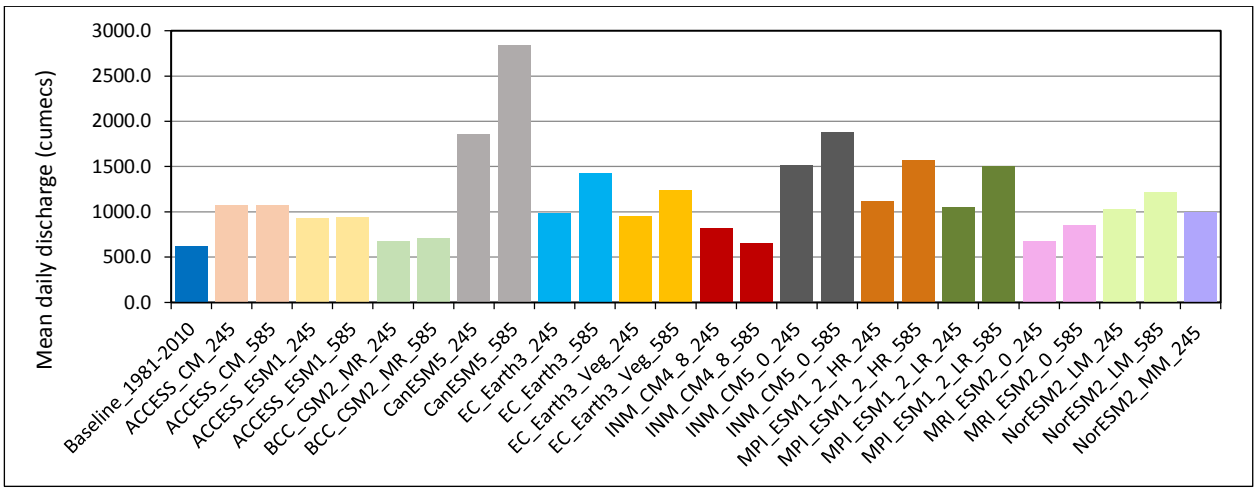

Figure 5.50: Comparison of mean daily flow during the baseline and 2080s at Hoshangabad

2080s at Handia, and Mandleshwar, both all located on the main river channel is given in Figure 5.51 to Figure 5.54. It can be seen that the flows are projected to be higher during the 2080s

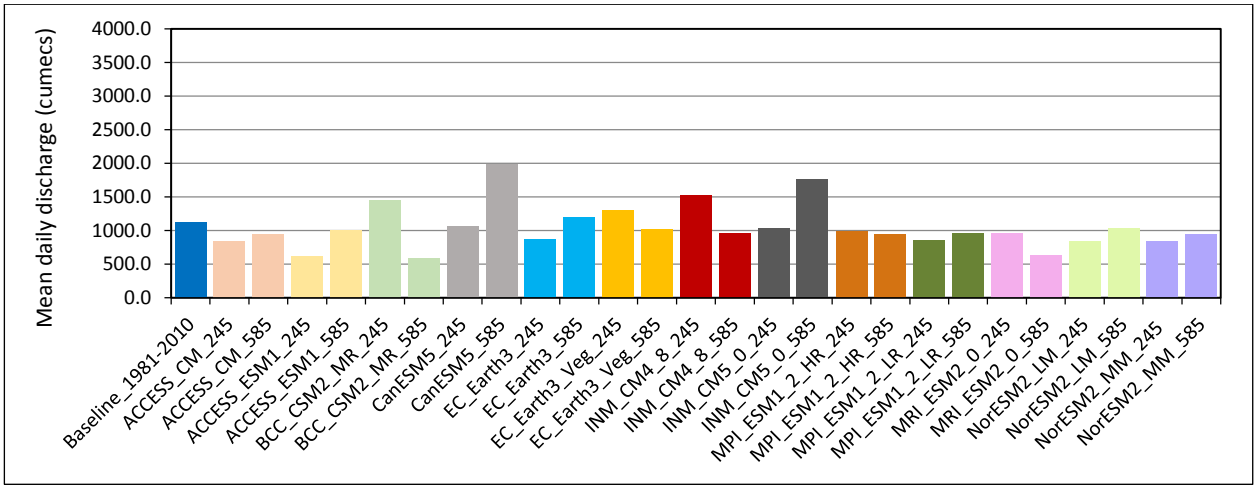

Figure 5.51: Comparison of mean daily flow during the baseline and 2050s at Handia

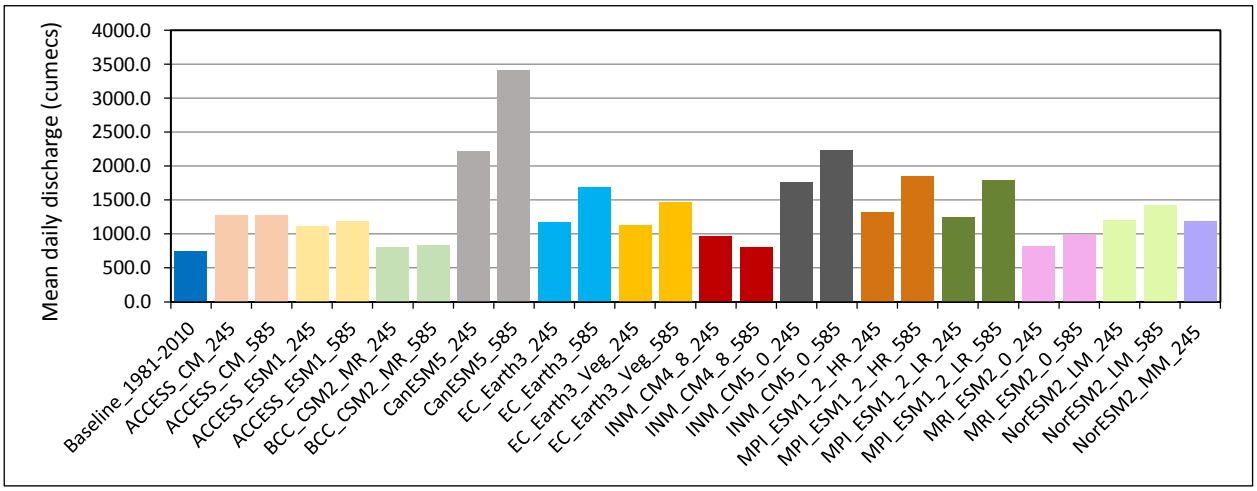

Figure 5.52: Comparison of mean daily flow during the baseline and 2080s at Handia

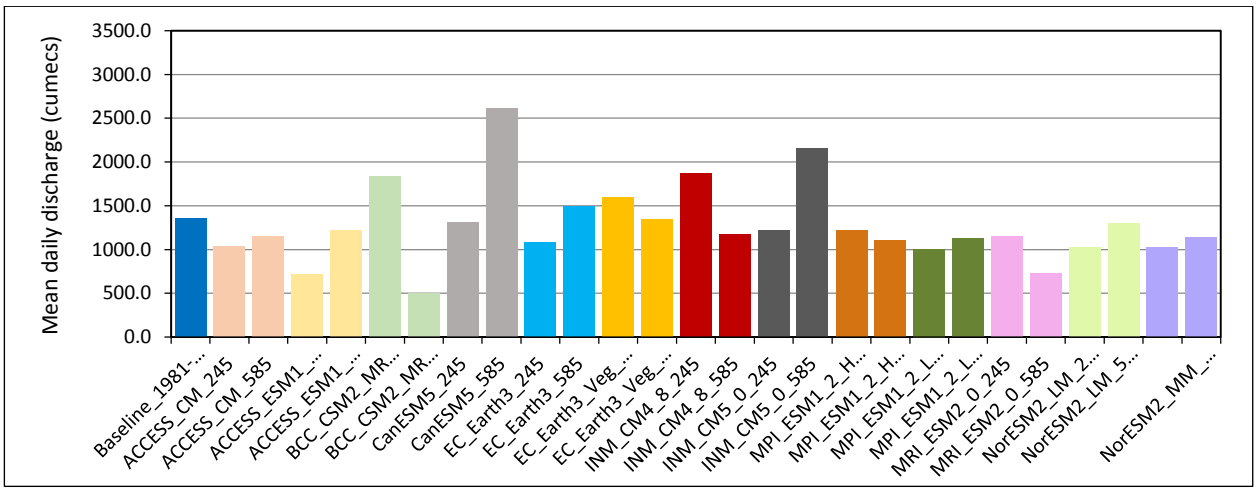

Figure 5.53: Comparison of mean daily flow during the baseline and 2050s at Mandleshwar

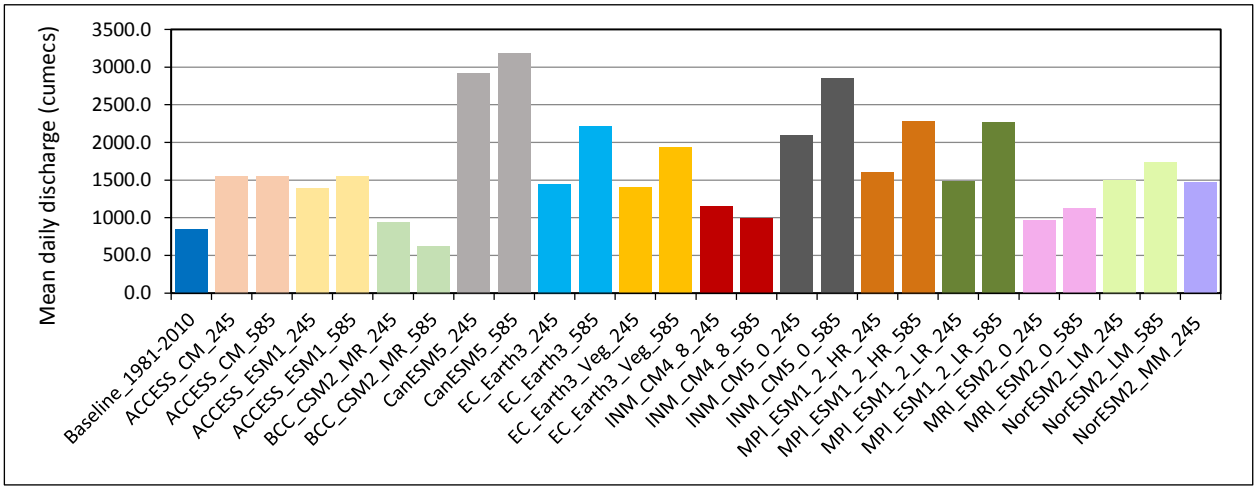

Figure 5.54: Comparison of mean daily flow during the baseline and 2080s at Mandleshwar

as compared to that during the 2050s at these gauging sites. The Mandleshwar gauging site is located below the Indira Sagar Project (ISP) and Omkareshwar Project (OSP) and therefore the stream flow at Mandleshwar GD site depend on the reservoir storage and release pattern from these major projects. The ensemble mean daily stream flow under SSP245 during 2050s and 2080s is 1262.07 cumecs and 1515.48 cumecs respectively, an increase of 56% and 80% during 2050s and 2080s respectively. Similarly, the ensemble mean daily stream flow under SSP585 is 1309.60 cumecs and 1844.44 cumecs, an increase of 55% and 120% respectively during the 2050s and 2080s.

The Garudeshwar gauging site is located below the Sardar Sarovar Project (SSP) which is a major multipurpose reservoir and therefore the stream flow at Garudeshwar GD site depend on the reservoir storage and release pattern from SSP. The comparison of the mean daily flow during baseline period and future periods 2050s and 2080s at Garudeshwar located on the main river channel is given in Figure 5.55 and Figure 5.56.

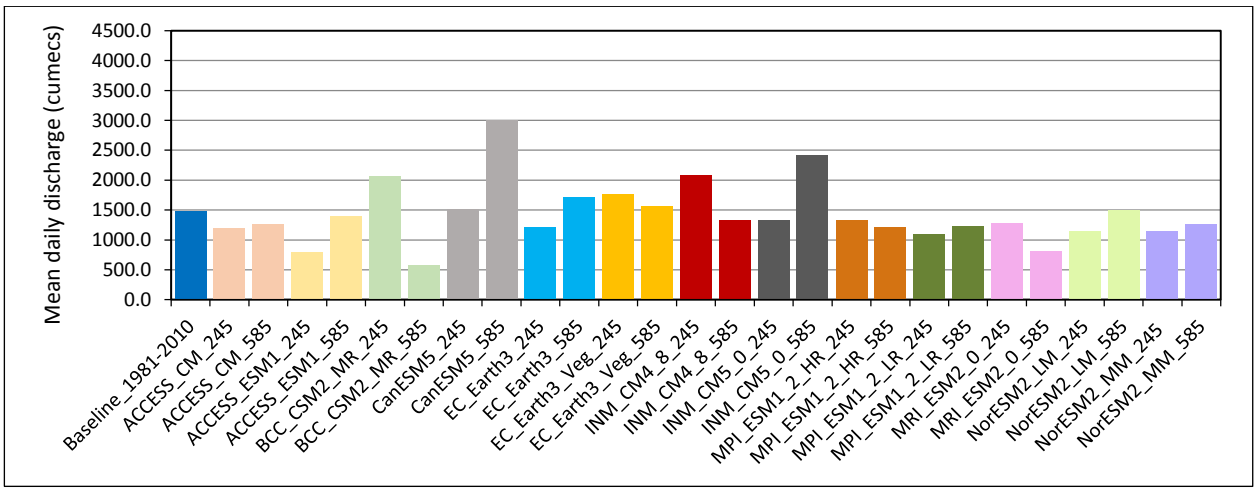

Figure 5.55: Comparison of mean daily flow during the baseline and 2050s at Garudeshwar

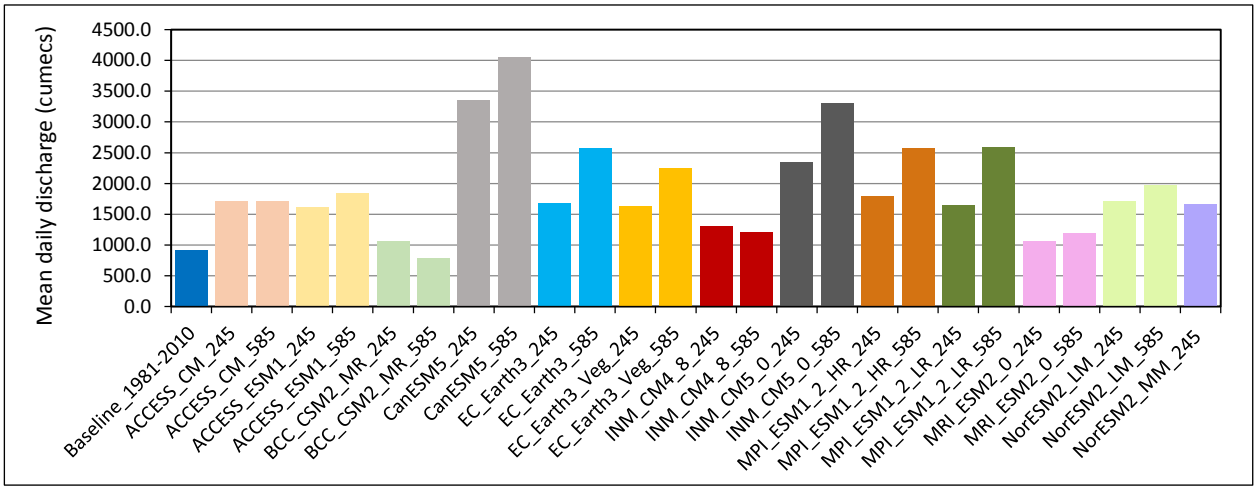

Figure 5.56: Comparison of mean daily flow during the baseline and 2080s at Garudeshwar

The ensemble mean daily stream flow under SSP245 during 2050s and 2080s is 1409.11 cumecs and 1720.64 cumecs respectively, an increase of 52% and 86% during 2050s and 2080s respectively. Similarly, the ensemble mean daily stream flow under SSP585 is 1483.72 cumecs and 2152.43 cumecs, an increase of 55% and 132% respectively during the 2050s and 2080s.

The overall comparison of the mean daily flows for SSP245 and SSP585 during the 2050s and 2080s for the headwater catchments is given in Figure 5.57. It can be observed that the mean daily discharge is increasing under both scenarios and both time zones as compared to the mean daily flow during the baseline period. The increase in the mean daily stream flow is projected to be much higher during the 2080s as compared to the baseline period and the 2050s. Among these headwater catchments, the projected rate of increase in the mean daily flow is lower for both SSP245 and SSP585 scenarios at Manot and Mohgaon, which are large sized catchments as compared to Belkheri, Gadarwara, Patan, Kogaon and Chidgaon.

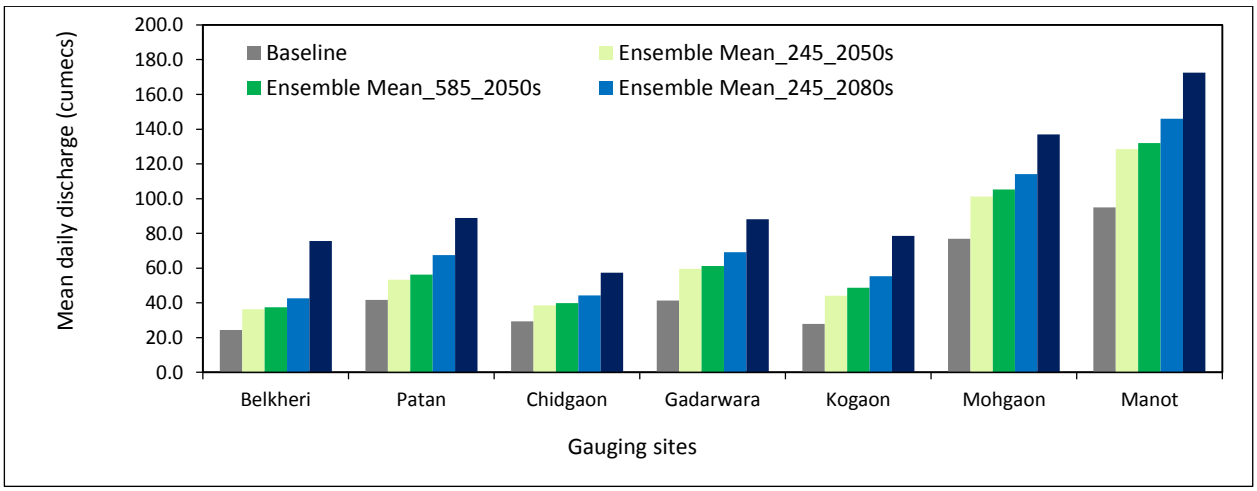

Figure 5.57: Comparison of mean daily discharge during 2050s & 2080s in the headwater catchments

The overall comparison of the mean daily flows for SSP245 and SSP585 during the 2050s and 2080s for the gauging sites on the main river channel is given in Figure 5.58. The mean daily discharge is increasing under both scenarios and both time zones as compared to the mean daily flow during the baseline period. Not much variability is observed rate of increase in the mean daily flow at the various gauging sites with the exception at Garudeshwar which depicts highest rate of increase in mean daily river flows. Therefore the analysis suggests that the mean daily stream flow is projected to increase both in the headwater catchments as well as bigger catchments corresponding to the gauging sites on the main river channel.

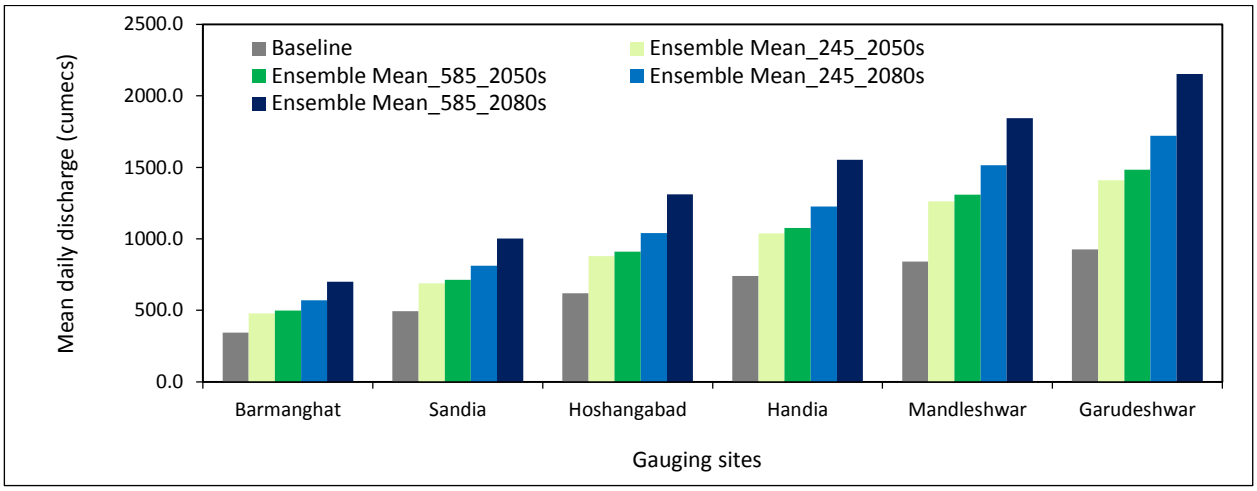

Figure 5.58: Comparison of mean daily discharge during baseline, 2050s & 2080s in main river channel

The factor change, which is the proportion future mean daily flow to the baseline mean daily flow has been evaluated at each of the grids in the Narmada basin. The spatial variation of the mean daily precipitation in Narmada basin is given in Figure 5.59. It can be observed that the mean daily

flow is increasing everywhere in the basin but the increase is more pronounced during the 2080s. The highest increase in the mean daily flows is projected SSP585 is projected during the 2080s under SSP585 scenario. Also, as depicted by the factor change, the increases in mean flows are comparitively much higher in the lower plains regions of the basin.

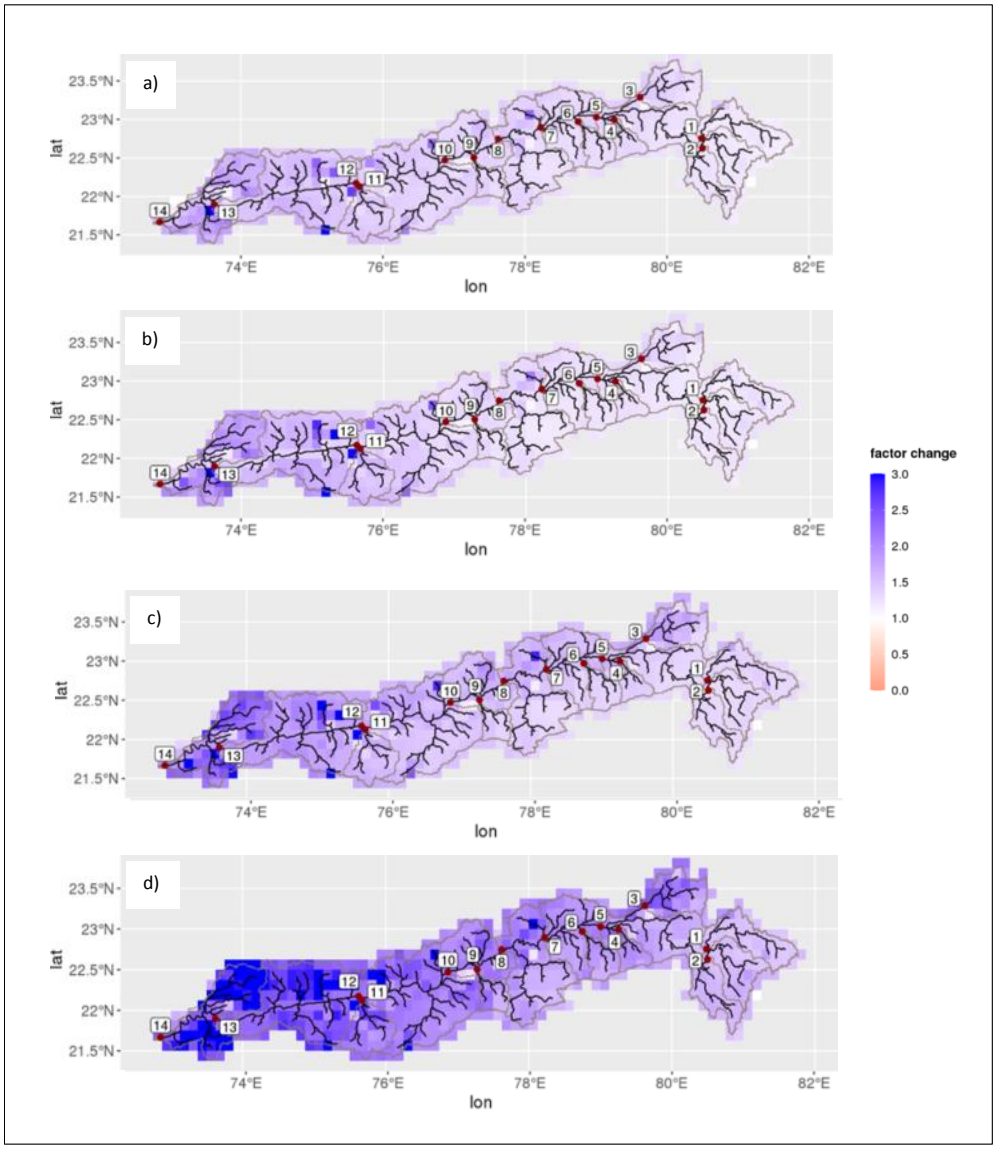

Figure 5.59: Spatial variation of mean flow a) SSP245-2050s, b) SSP585-2050s, c) SSP245-2080s, d) SSP585-2080s

The mean monthly discharge has been estimated for all the headwater catchments and all gauging sites located on the main river channel to understand the temporal distribution of the rainfall in the study area. The mean monthly discharge at two of the headwater catchments under SSP245 and SSP585 during 2050s and 2080s at Manot is given in Figure 5.60 whereas Figure 5.61

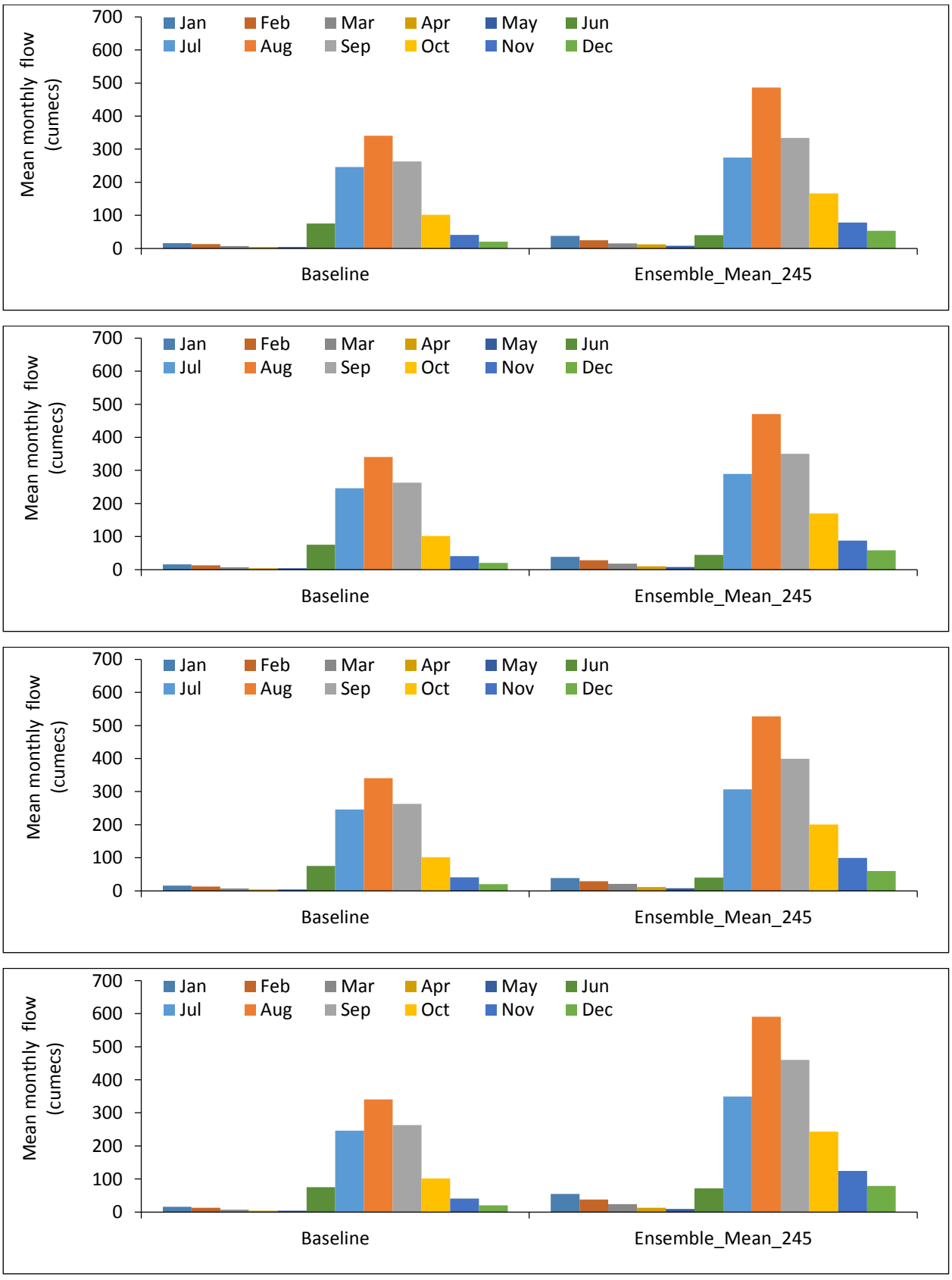

Figure 5.60 : Comparison of the mean monthly flow during the baseline and future time periods at Manot: a) SSP245-2050s, b) SSP585-2050s, c) SSP245-2080s, d) SSP585-2080s

shows the distribution of the mean monthly rainfall at Mohgaon. It can be observed that the mean monthly flow in June is decreasing in both catchments whereas the mean monthly flows are

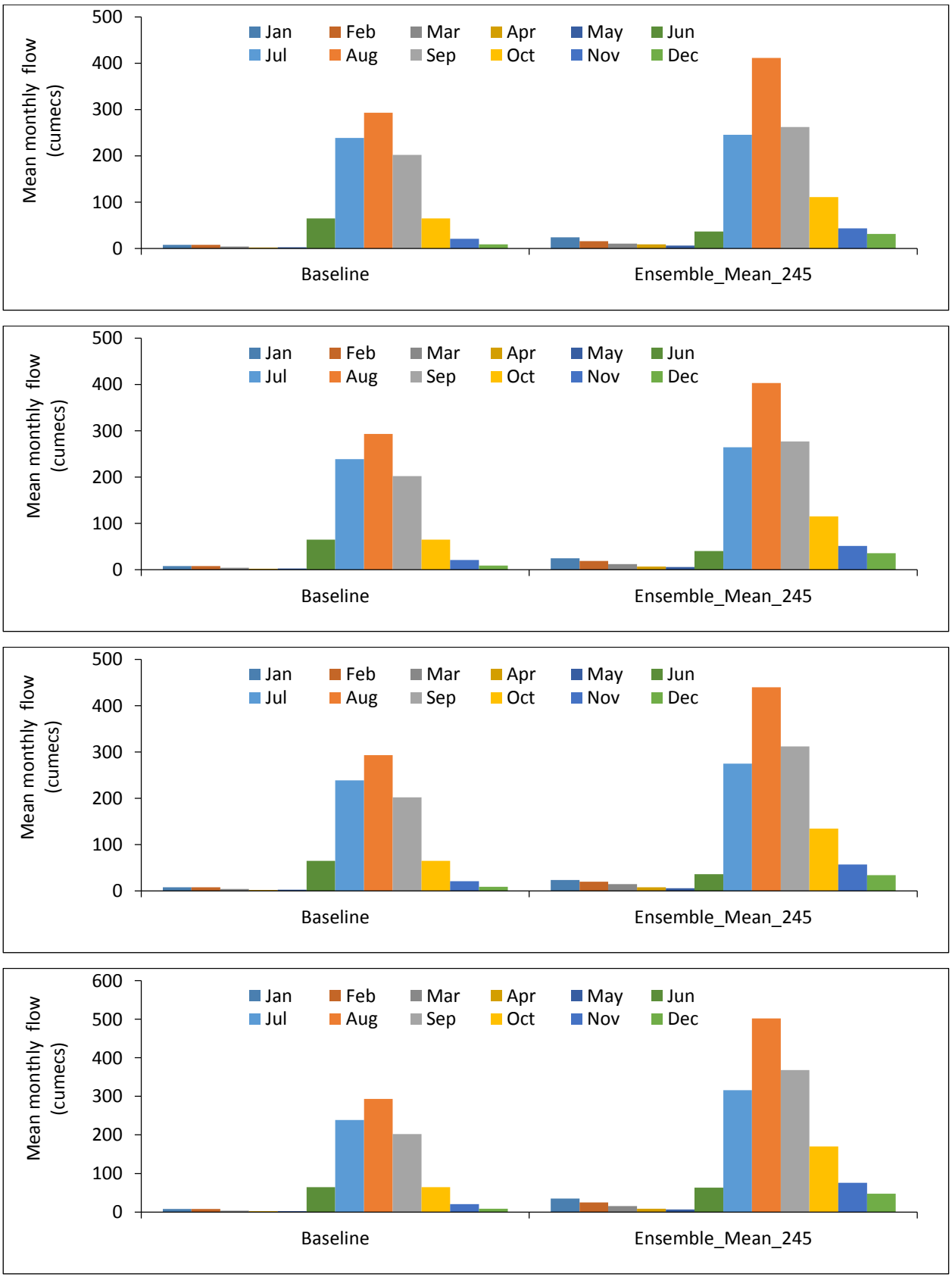

Figure 5.61 : Comparison of the mean monthly flow during the baseline and future time periods at Mohgaon: a) SSP245-2050s, b) SSP585-2050s, c) SSP245-2080s, d) SSP585-2080s

increasing in all other months during the 2050s and 2080s. These figures depicting the temporal variation of the rainfall indicates that higher rainfall is projected during the principal monsoon

months viz., July and August which will help to maintain the water availability in the minor and medium hydraulic structures in these headwater catchments. The winter rainfall is also projected to increase which will be beneficial for irrigation in the rain-fed areas as well as project command areas. A similar type of increase in mean monthly rainfall in all the months except in June is seen for the remaining five headwater catchments of Belkheri, Patan, Gadarwara, Kogaon and Chidgaon.

Similarly, the mean monthly discharge at two gauging sites located on the main river channel under SSP245 and SSP585 during 2050s and 2080s at Barmanghat and Mandleshwar is given in Figure 5.62 and Figure 5.63 respectively. During the 2050s, the mean monthly rainfall is increasing under both SSP scenarios at all the months except in June as was observed for the headwater catchments. Substantial increases are projected in the mean monthly flows during the monsoon months and winter months at all the gauging sites located on the main river channel. However a different pattern is seen during the 2080s under SSP585 scenario wherein even the mean monthly flow during June is also projected to increase along with the mean monthly flows in all other months. All these gauging sites are located below the major dams existing on the main river and a projected increase in the monthly flows in the river at these locations will provide additional water in the river system in most of the months, which can be utilised foe meeting the increased water demands in future.

5.3.3.6.4 Climate change impact on high flows

The analysis has been carried out for the assessment of impacts on the high flows based on the 10% dependable flow (Q10) during the baseline period (1981-2010) and future time periods viz., 2050s (2035-2065) and 2080s (2066-2095). The comparison of Q10 for the various headwater catchments is given in Figure 5.64. The Q10 is projected to increase in all future time horizons as compared to the baseline period under SSP245 and SSP585 scenarios during 2050s and 2080s.

The comparison of Q10 during the baseline period with Q10 during 2050s and 2080s along with the projected percentage increase for the various headwater catchments is given in Table 5.9. The high flows as represented by Q10 are projected to increase at all the headwater catchments in Narmada basin. During the 2050s, the projected increase in the high flows as compared to the baseline period, varies between +18.2% at Patan to +102.3% at Kogaon catchments under SSP245 which is expected to further increase under SSP585 viz., Patan (+24.3%) and Kogaon (+140.6%). During the 2050s, the average of projected increase in these seven headwater catchments is 44.5% under SSP245 and 52.8% under SSP585.

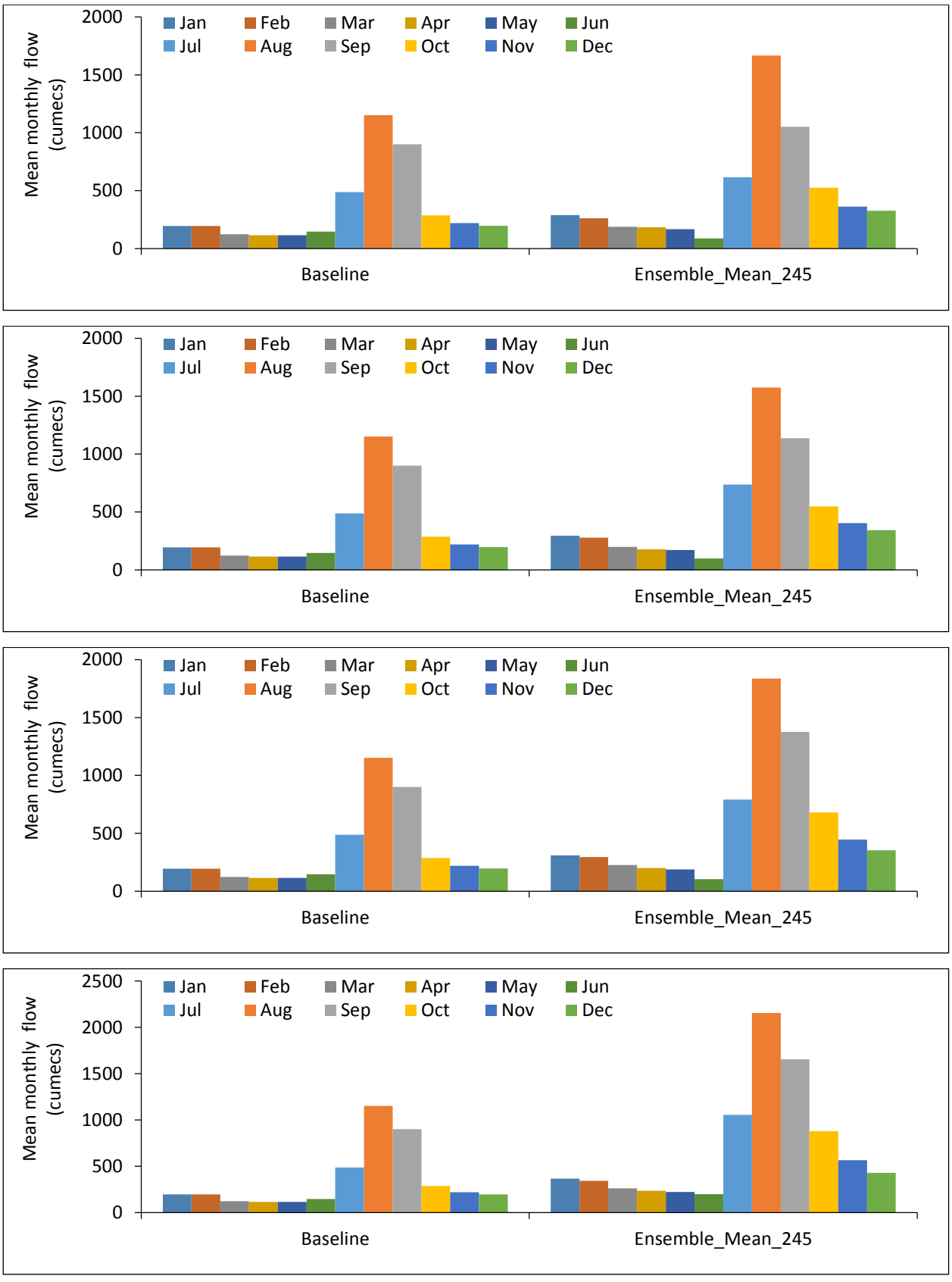

Figure 5.62: Comparison of the mean monthly flow during the baseline and future time periods at Barmanghat: a) SSP245-2050s, b) SSP585-2050s, c) SSP245-2080s, d) SSP585-2080s

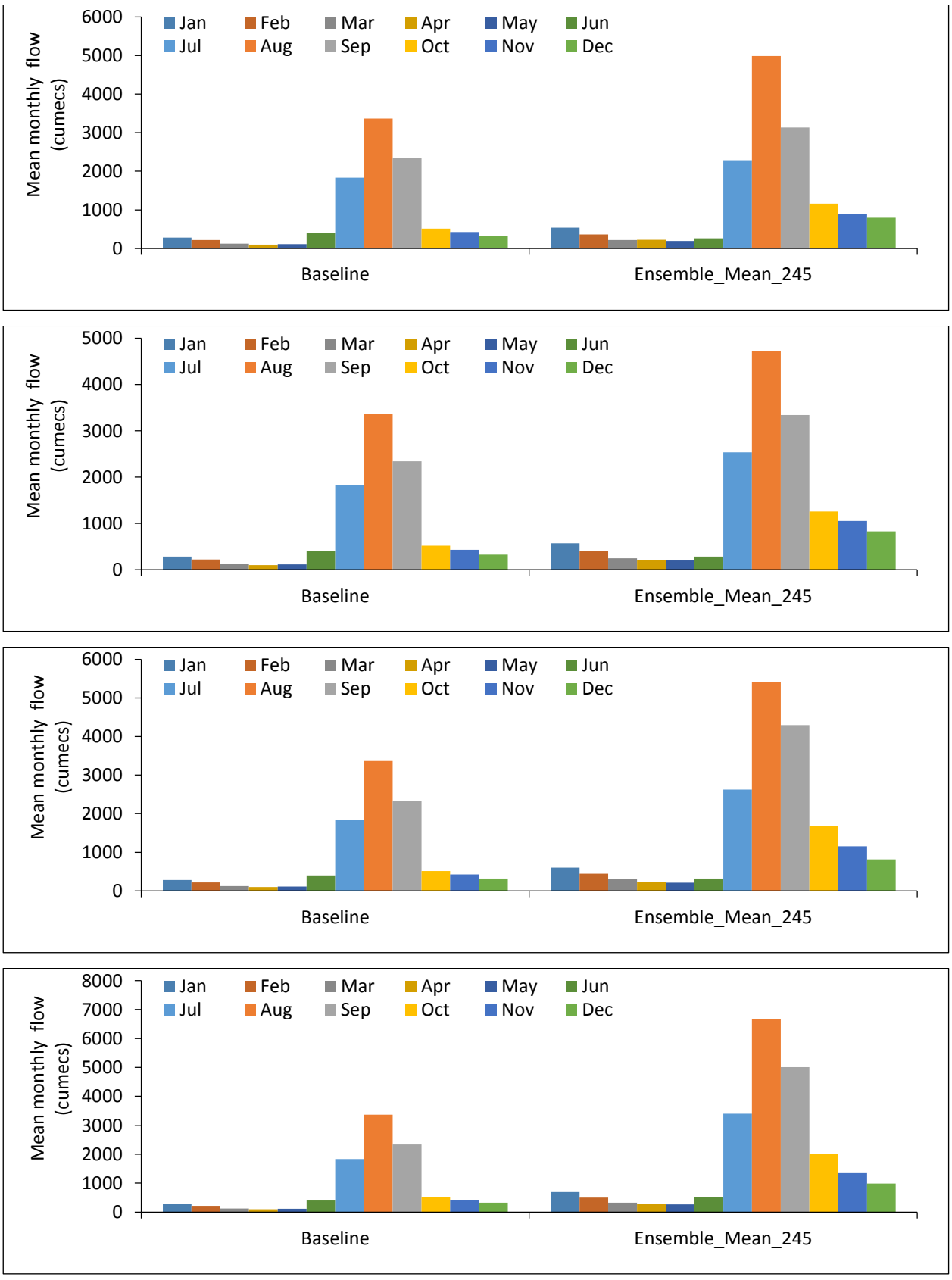

Figure 5.63: Comparison of the mean monthly flow during the baseline and future time periods at Mandleshwar: a) SSP245-2050s, b) SSP585-2050s, c) SSP245-2080s, d) SSP585-2080s

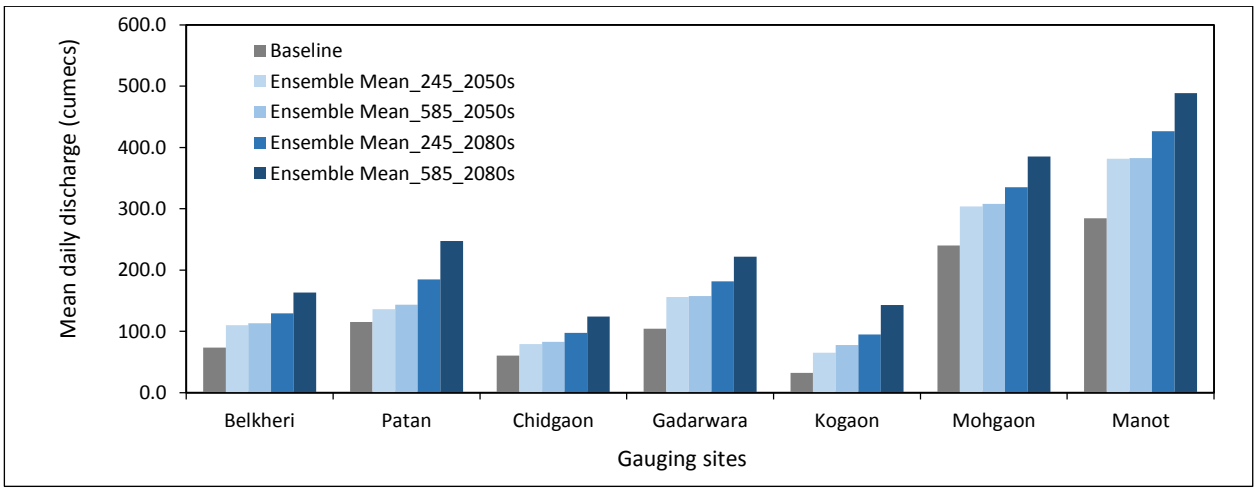

Figure 5.64: Comparison of Q10 during 2050s & 2080s in the headwater catchments

However, during the 2080s, a higher increase in the high flows is projected ranging between +39.6% at Mohgaon to +195% at Kogaon under SSP245 which is expected to further increase under SSP585 viz., Mohgaon (+60.5%) and Kogaon (344.4%). The average flows in these headwater catchments is projected to increase further to +79.4% under SSP245 and +133.1% under SSP585. Therefore, it can be observed that the high flows in these seven headwater catchments are projected to increase under both SSP245 and SSP585 scenarios, with higher increases projected under SSP 585 scenario. Similarly, during the end term, i.e. the high flows will be more intense in the 2080s as compared to the 2050s in these headwater catchments.

Table 5.9: Comparison of Q10 during baseline period, 2050s and 2080s at the headwater catchments

Catchment	Baseline	2050s (2036-2065)				2080s (2066-2095)			
		Q10_SSP245	% Increase	Q10_SSP585	% Increase	Q10_SSP245	% Increase	Q10_SSP585	% Increase
Belkheri	73.5	110.1	*49.7*	113.1	*53.8*	129.4	76.0	163.5	*122.3*
Patan	115.3	136.3	*18.2*	143.4	*24.3*	184.8	60.3	247.2	*114.4*
Chidgaon	60.6	79.2	*30.7*	83.1	*37.1*	97.3	60.6	124.4	*105.3*
Gadarwara	104.1	155.9	*49.7*	157.5	*51.3*	181.8	74.6	221.8	*113.0*
Kogaon	32.2	65.1	*102.3*	77.4	*140.6*	94.9	195.0	143.0	*344.4*
Mohgaon	240.2	303.7	*26.4*	307.9	*28.2*	335.4	39.6	385.5	*60.5*
Manot	284.6	381.7	*34.1*	382.6	*34.4*	426.7	49.9	488.6	*71.7*
Average increase			***44.5***		***52.8***		***79.4***		***133.1***

The comparison of Q10 for the various gauging sites on the main Narmada river is given in Figure 5.65. The Q10 is projected to increase in all future time horizons as compared to the baseline period under SSP245 and SSP585 scenarios for both 2050s and 2080s. The comparison of Q10 during the baseline period with Q10 during 2050s and 2080s along with the projected percentage increase for the various headwater catchments is given in Table 5.10.

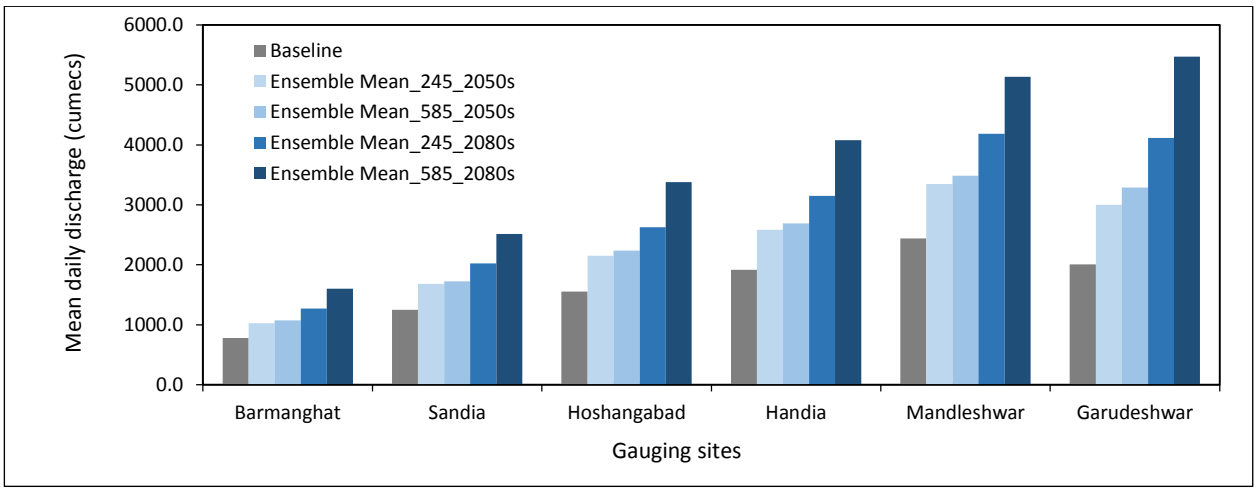

Figure 5.65: Comparison of Q10 during 2050s & 2080s in main river channel

Table 5.10: Comparison of Q10 during baseline period, 2050s and 2080s at GD sites in main river channel

GD Site	Baseline	2050s (2036-2065)				2080s (2066-2095)			
		Q10_SSP245	% Increase	Q10_SSP585	% Increase	Q10_SSP245	% Increase	Q10_SSP585	% Increase
Barmanghat	778.1	1025.5	*31.8*	1072.9	*37.9*	1271.6	*63.4*	1600.2	*105.7*
Sandia	1250.2	1678.2	*34.2*	1722.8	*37.8*	2020.8	*61.6*	2512.5	*101.0*
Hoshangabad	1550.2	2149.5	*38.7*	2234.4	*44.1*	2627.1	*69.5*	3377.3	*117.9*
Handia	1917.3	2583.7	*34.8*	2688.8	*40.2*	3147.6	*64.2*	4077.2	*112.7*
Mandleshwar	2436.3	3348.2	*37.4*	3487.2	*43.1*	4183.5	*71.7*	5135.6	*110.8*
Garudeshwar	2009.1	2999.6	*49.3*	3287.9	*63.6*	4112.8	*104.7*	5469.4	*172.2*
Average increase			***37.7***		***44.5***		***72.5***		***120.0***

The high flows represented by Q10 are projected to increase at all the gauging sites located on the main river channel as was the case for the headwater catchments in Narmada basin. During the 2050s, the projected increase in the high flows as compared to the baseline period, varies between +34.2% at Sandia to +49.3% at Garudeshwar under SSP245 which is expected to further increase under SSP585 viz., Sandia (+37.8%) and Garudeshwar (+49.3%). It can be observed that there is not much variability in the projected increases among the individual gauging sites both under SSP245 and SSP585 scenarios. The average of projected increase in these six gauging sites located on main river during the 2050s, is 37.7% under SSP245 and 44.5% under SSP585.

Much higher increase in the high flows is projected during the 2080s, the projected increase ranging between +61.6% at Sandia to +104.7% at Garudeshwar under SSP245 which is expected to further increase under SSP585 viz., Sandia (+101.0%) and Garudeshwar (172.2%). The average flows in these catchments is projected to increase to +72.5% under SSP245 and +120.0% under SSP585, which is much higher as compared to the average high flows during 2050s. Therefore it can be seen that the high flows at these six gauging sites located on the main river channel, which

are also influenced by the reservoir releases from the major projects are projected to increase under both SSP245 and SSP585 scenarios, with higher increases projected under SSP585 scenario. Similarly, the high flows will be more intense in the 2080s as compared to the 2050s in these catchments.

5.3.3.6.5 Climate change impact on low flows

The analysis has been carried out for the assessment of impact of climate change on the low flows represented by 90% dependable flow (Q90). The Q90 during the baseline period (1981-2010) has been compared with the Q90 during the future time periods viz., 2050s (2035-2065) and 2080s (2066-2095) to identify the marked changes. The comparison of Q90 for the various headwater catchments is given in Figure 5.66. The low flows (Q90) projected in future time periods show a mixed trend at different catchments. The future low flows are expected to decrease at many locations but are also expected to increase at few locations during the 2050s and 2080s.

The comparison of Q90 during the baseline period with the Q90 during the 2050s and 2080s along with the projected increase for the various headwater catchments is given in Table 5.11. During the 2050s and under SSP245 scenario, the low flows in headwater catchments of Narmada basin is projected to increase only for two catchments viz., Manot (+31.1%) and Mohgaon

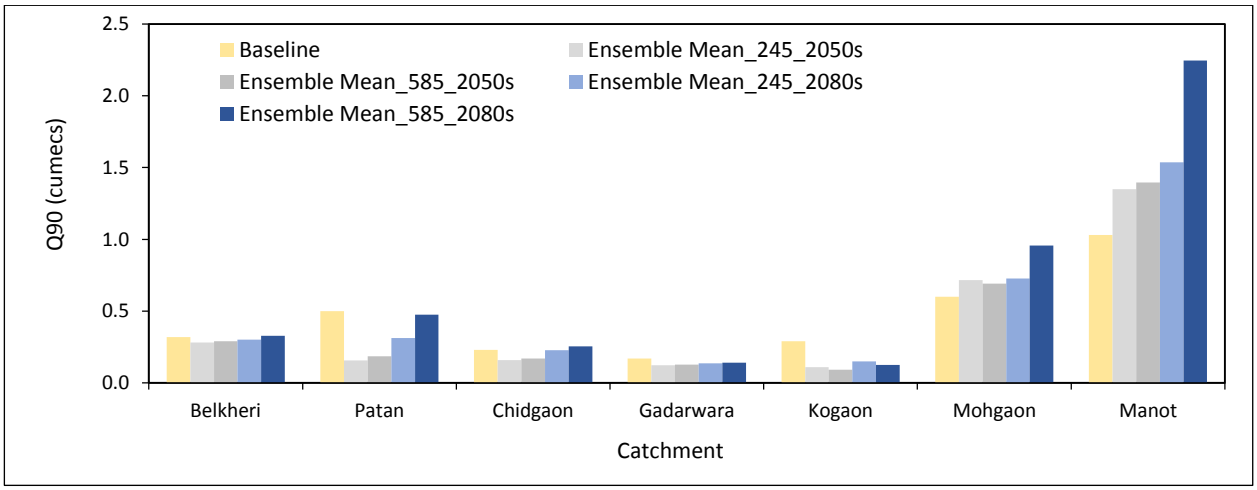

Figure 5.66: Comparison of Q90 during 2050s & 2080s in the headwater catchments

(+19.5%), whereas it is projected to decrease in the other four catchments viz., Belkheri (-11.7%), Patan (-68.9%), Chidgaon (-30.7%), Gadarwara (-27.1%) and Kogaon (-62.1%). A similar pattern is noticed for the low flows under SSP585 scenario with projected increases at Manot (+35.6%) and Mohgaon (+15.2%) and projected decreases at Belkheri (-9.4%), Patan (-63.0%), Chidgaon (-25.6%), Gadarwara (-24.6%) and Kogaon (-67.9%). Therefore the water availability at five out of the seven headwater catchments is projected to be lower during the 2050s under both SSP245 and

Table 5.11: Comparison of Q90 during baseline period, 2050s and 2080s at the headwater catchments

Catchment	Baseline	2050s (2036-2065)				2080s (2066-2095)			
		Q10_SSP245	*% Increase*	Q10_SSP585	*% Increase*	Q10_SSP245	*% Increase*	Q10_SSP585	*% Increase*
Belkheri	0.32	0.28	*-11.7*	0.29	*-9.4*	0.30	*-6.0*	0.33	*2.4*
Patan	0.50	0.16	*-68.9*	0.19	*-63.0*	0.31	*-37.4*	0.47	*-5.1*
Chidgaon	0.23	0.16	*-30.7*	0.17	*-25.6*	0.23	*-0.7*	0.25	*10.4*
Gadarwara	0.17	0.12	*-27.1*	0.13	*-24.6*	0.14	*-19.5*	0.14	*-17.2*
Kogaon	0.29	0.11	*-62.1*	0.09	*-67.9*	0.15	*-48.0*	0.12	*-57.0*
Mohgaon	0.60	0.72	*19.5*	0.69	*15.2*	0.73	*21.4*	0.96	*59.5*
Manot	1.03	1.35	*31.1*	1.40	*35.6*	1.54	*49.1*	2.25	*118.1*

SSP585 climate scenarios.

During the 2080s under SSP245 scenario, the low flows in headwater catchments of Narmada basin is projected to increase only at Manot (+49.1%) and Mohgaon (+21.4%), whereas it is projected to decrease at the remaining four catchments viz., Belkheri (-6.0%), Patan (-37.4%), Chidgaon (-0.70%), Gadarwara (-19.5%) and Kogaon (-48.0%). A similar pattern is noticed for the projected low flows under SSP585 scenario with higher increases as compared to SSP245 at Manot (+118.1%) and Mohgaon (+59.5%) and lower decreases at Belkheri (+2.4%), Patan (-5.1%), Chidgaon (+10.4%), Gadarwara (-17.2%) and Kogaon (-57.0%). During the 2080s, the low flows at Manot and Mohgaon is projected to increase as compared to the baseline period and the 2050s. Also the water availability during the 2080s and under the SSP245 scenario has improved at Belkheri, Patan, Chidgaon, Gadarwara as compared to the 2050s, but still it is lower as compared to the baseline period. However, during the 2080s and under SSP585 scenario, Belkheri and Chidgaon along with Manot and Mohgaon are projected to have higher low flows. Therefore, some of the headwater catchments depict lower Q90 whereas other few catchments depict higher lower flows. Only the Manot and Mohgaon headwater catchments show higher low flows under both climate scenarios and both future time periods. This is good for the availability of sustainable flows in the river system as the Narmada river is sustained mainly by the substantial flows generated in the head water catchments that are located in the Upper Narmada basin.

The comparison of Q90 at the gauging sites located on the main river channel is given in Figure 5.67. The low flows (Q90) projected in future time periods show a mixed trend at different gauging sites. The comparison of Q90 during the baseline period with the Q90 during the 2050s and 2080s along with the projected increase for the various headwater catchments is given in Table 5.12. During the 2050s, the low flows at the gauging sites located on the main river channel in Narmada basin, under SSP245 scenario is projected to decrease at all locations viz., Barmanghat

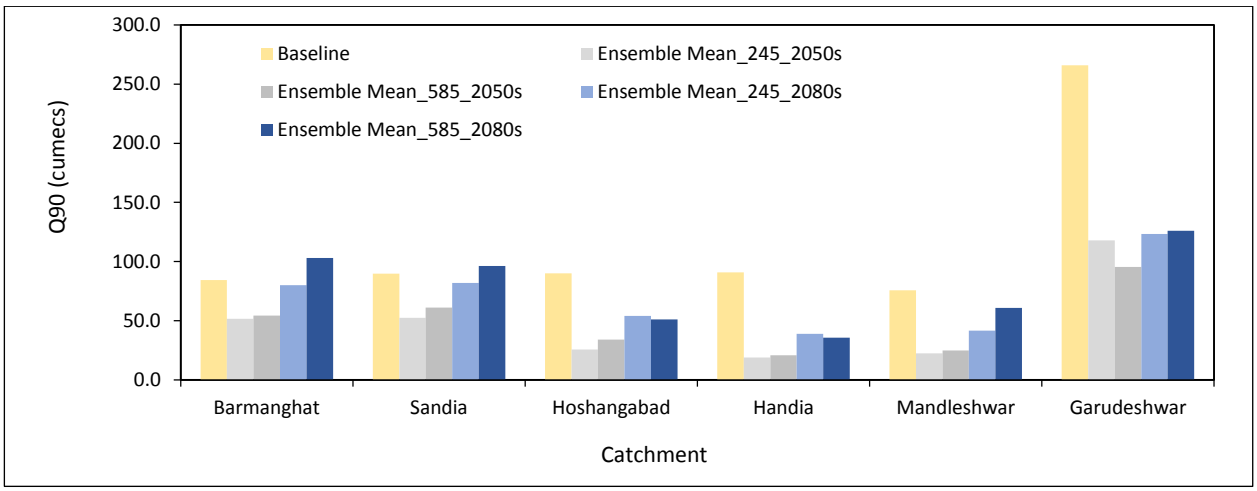

Figure 5.67: Comparison of Q90 during 2050s & 2080s in main river channel

Table 5.12: Comparison of Q90 during baseline period, 2050s and 2080s at GD sites in main river channel

Catchment	Baseline	2050s (2036-2065)				2080s (2066-2095)			
		Q10_SSP245	*% Increase*	Q10_SSP585	*% Increase*	Q10_SSP245	*% Increase*	Q10_SSP585	*% Increase*
Barmanghat	84.40	51.81	*-38.6*	54.26	*-35.7*	80.01	*-5.20*	102.99	*22.0*
Sandia	89.71	52.52	*-41.5*	61.18	*-31.8*	81.99	*-8.60*	96.24	*7.30*
Hoshangabad	90.07	25.71	*-71.5*	34.14	*-62.1*	54.16	*-39.9*	51.11	*-43.3*
Handia	90.87	19.08	*-79.0*	20.79	*-77.1*	39.10	*-57.0*	35.73	*-60.7*
Mandleshwar	75.84	22.43	*-70.4*	24.83	*-67.3*	41.58	*-45.2*	60.74	*-19.9*
Garudeshwar	265.8	118.07	*-55.6*	95.58	*-64.0*	123.31	*-53.6*	126.10	*-52.6*

(-38.6%), Sandia (-41.5%), Hoshangabad (-71.5%), Handia (-79.0%), Mandleshwar (-70.4%) and Garudeshwar (-118.1%). A similar pattern lower projected low flows is seen under SSP585 scenario with lower decrease in low flows as compared to SSP245 scenario viz., Barmanghat (-35.7%), Sandia (-31.8%), Hoshangabad (-62.1%), Handia (-77.1%), Mandleshwar (-67.3%) and Garudeshwar (-64.0%). Even though the low flows are projected to decrease under both scenarios, there is a slight improvement under the SSP585 scenario during the 2050s owing to higher precipitation resulting in marginally better low flows. But in general, the water availability based on the Q90 is projected to decrease during the 2050s as compared to the baseline period at all the gauging sites in the main river channel.

During the 2080s, the low flows at the gauging sites located on the main river channel is projected to decrease at all locations under SSP245 scenario viz., Barmanghat (-5.2%), Sandia (-8.6%), Hoshangabad (-39.9%), Handia (-57.0%), Mandleshwar (-45.2%) and Garudeshwar (-53.6%). However, the projected low flows under SSP585 scenario has seen higher increases as compared to SSP245 at Barmanghat +22.0%), Sandia (+7.3%), Hoshangabad (-43.3%), Handia

(-60.7%), Mandleshwar (-19.9%) and Garudeshwar (-52.6%). During the 2080s, the low flows at Barmanghat and Sandia is projected to increase under SSP585 as compared to the 2050s. Also, the water availability during the 2080s at Hoshangabad, Handia, Mandleshwar, and Garudeshwar is projected to improve under the SSP245 scenario, as compared to the 2050s, but still it is lower as compared to the low flows in the baseline period. However, under SSP585 scenario during the 2080s, Hoshangabad, Handia, Mandleshwar, and Garudeshwar is projected to have higher low flows as compared to the 2050s. Therefore, some of the gauging sites located on the main river channel depict a lower Q90 whereas other few gauging sites project higher lower flows as compared to the baseline period. The Barmanghat and Sandia depict higher low flows only under SSP585 scenarios and only during the 2080s. As Barmanghat and Sandia are located in the Upper Narmada basin, the improved low flows at these gauging sites augur well for the availability of regular flows in the river Narmada system.

6.0 Conclusions

The climate change impact assessments in highly regulated large river basins is one of the key challenges for water practitioners, for the proper planning of water resources development and management policies in accordance, and to devise the most favourable adaptation strategies. Large scale hydrological models are one of the essential tools used to derive future stream flow in river basins, for the assessment of climate change impacts. Even though many large hydrological models are in use, many of them are quite data intensive with large number of parameters and require high proficiency to use them. It is in the backdrop of these considerations, GWAVA model was selected for hydrological modelling in the Narmada basin in two phases. The Phase I covered the application of GWAVA, a simple and semi-distributed model along with MIKE-SHE, a complex and fully-distributed model in Upper Narmda Basin upto Hoshangabad. The Phase II covered the application of the refined GWAVA 5.1 to include the full Narmada basin. The refined GWAVA 5.1 included better representation of reservoir operation and groundwater modules. The GAWVA 5.1 setup for Narmada basin, was driven by the CMIP6 bias-corrected future climate data of 13 GCMs under two SSP scenarios, viz., SSP245 and SSP585.

The 13 GCM ensemble indicates that as compared to the baseline period (1981-2010), the average maximum and minimum temperature are projected to increase in the basin during the 2050s (1936-1965) and 2080s (1966-2095). The increase in maximum temperature during the 2080s is projected to be +1.62^{o}C/100 year under SSP245 scenario and +2.30^{o}C/100 year under SSP585 scenario. The average minimum temperature is also projected to increase at a much higher rate as compared to the increase in maximum temperature, at a rate of +2.32^{o}C/100 year for SSP245 scenario and +3.39^{o}C/100 year for SSP585 scenario in the 2080s. This indicates that the future temperature changes linked to global warming may be characterised by a marked asymmetry between daytime maxima and night time minima. The increases in both maximum and minimum temperature will have significant impacts on the water demands viz., increase in water demands for the domestic, agricultural and other water dependent sectors, considerable impacts on crop growth and crop yields due to change in temperature and higher consumptive use requirements, intensification of the hydrological cycle, increase spatio-temporal variability in precipitation distribution leading to higher water deficits and water surpluses.

The average annual rainfall based on the 13 GCM ensemble is projected to increase both during the 2050s and 2080s as compared to the baseline. The increased magnitude of the monsoon rainfall has implications for the availability and management water resources within the basin. The 1-day maximum rainfall, the extreme events (>200mm/day), very heavy rainfall events (>100 mm/day) and heavy rainfall events (>50 mm/day) are all projected to increase in the future time

horizons for both scenarios, but highest the highest increase is projected during 2080s under SSP585 scenario. The projected increase in all the above rainfall indices, indicate a more intense monsoon but relatively over a shorter period. This is true for both the headwater catchments and at gauging sites located on the main river channel.

The projected increases in rainfall are supported by the analysis of simulated stream flow during the future time horizons which also shows and increase. The mean daily flows are expected to increase in all future time horizons. The comparison of the mean monthly flow indicates an increase in the mean monthly flows for all the months except June, which is showing decreased flows in future. The high flows evaluated by the 10% dependable flows are projected to increase in all future time horizons for the headwater catchments and at gauging sites located on the main river channel; the highest increase being projected during the 2080s under SSP585 scenario. This may lead to flash floods and severe flooding in vulnerable areas as the existing as riverine infrastructure, including small-scale interventions, may not currently have the capacity to both store and utilise the projected increase in precipitation.

However, the low flows characterised by 90% dependable flows (Q10) shows a mixed trend with many headwater catchments except Manot and Mohgaon, and most of the sites on the main river channel projecting lower water availability scenario in future. Outside of command areas and reservoir-fed regions, this has the potential to lead to greater water stress during the dry season, as water may not be available at the time when it is most required. The sectoral demands are likely to rise with a growing population and the need for more food and power generation exacerbating the impact of climate on flows across the hydrological regime. This calls for better planning for optimal water resources development and management for storage of excess water generated during the monsoon season to provide assured water supplies to the multiple competing water users during the lean season.

This study provides an overall insight and direction as to what the future holds for the basin, in respect of the climate and future water availability scenario. However, the GCM climate projections are inherently uncertain, from the SSP scenarios, through to the GCM model structure, the downscaling methodology, re-gridding, and bias-correction techniques employed. Moreover, understanding both current and future changes for the Indian climate, and specifically the Indian Summer Monsoon Rainfall (ISMR), remains a major challenge. Even the weather forecasts at shorter lead times, are many a times quite challenging and therefore these projections for longer time periods based on the GCM outputs have to be used keeping in mind the chain of uncertainties involved in the modelling processes. This element of uncertainty is also supported by the high inter-

variability amongst the 13 GCMs, wherein the CanESM5 model projects future annual rainfall way ahead of all other models used for impact assessments. However, all the GCMs project an increased rainfall scenario for the future. Obviously, the simulated flows arrived at by forcing the hydrological model with these GCM inputs, will have these uncertainties translated to the hydrological model outputs (stream flow) as well.

Many other alternate scenarios were also explored including the adoption of a 400 m buffer plantation along the main river, population growth, livestock growth, upcoming reservoirs and change in cropping pattern. The change in cropping pattern from soyabean to paddy in the kharrif season, which has already taken place in the upper and middle regions of the basin, is projected to increase the future water demands on a standalone basis. However no major changes in water demands are anticipated due to the other scenarios. Climate change is the most significant factor affecting the future water resources in the basin. Considering all the inherent uncertainties in the model projections, the sustainability of water resources is however, vital for agriculture and socio-economic development in Narmada basin. The projected alterations in flow could have a significant impact on water resources and other water dependent sectors for which an appropriate adaptation strategy needs to be devised to best equip the basin and the stakeholders for the future projected changes.

References

1. Abbott MB, Bathurst JC, Cunge JA, O'Conncll PE, Rasmussen J (1986a). An introduction to the European hydrological system-Syste`me Hydrologique Europe´en ''SHE''. 1: history and philosophy of a physically based distributed modelling system. J. Hydrol., 87:45–59.

2. Abbott MB, Bathurst JC, Cunge JA, O'Conncll PE, Rasmussen J (1986b). An introduction to the European hydrological system-Syste`me Hydrologique Europe´en ''SHE''. 2: structure of a physically based distributed modelling system. J. Hydrol., 87:61–77.

3. Acreman, M. and Dunbar, M. J. (2004). Defining environmental river flow requirements – a review, Hydrology and Earth System Sciences, 8, 861–876.

4. Ahrends, H., Mast, M., Rodgers, C. and Kunstmann, H. (2008). Coupled hydrological–economic modelling for optimised irrigated cultivation in a semi-arid catchment of West Africa, Environmental Modelling & Software, 23, 385–395.

5. Alfieri, L.; Burek, P.; Dutra, E.; Krzeminski, B.; Muraro, D.; Thielen, J.; Pappenberger, F. (2013). GloFAS–global ensemble streamflow forecasting and flood early warning. Hydrol. Earth Syst. Sci., 17, 1161–1175.

6. Allen, R.G., Pereira, L.S., Raes, D. and Smith, M. (1998). Crop evapotranspiration - Guidelines for computing crop water requirements - FAO Irrigation and Drainage paper 56, Rome: FAO.

7. Anand, J.; Gosain, A.K.; Khosa, R.; Srinivasan, R. (2018). Regional scale hydrologic modeling for prediction of water balance, analysis of trends in streamflow and variations in streamflow: The case study of the Ganga River basin. J. Hydrol. Reg. Stud., 16, 32–53.

8. Andersen, J., Refsgaard, J.C. and Jensen, K.H. (2001). Distributed hydrological modelling of the Senegal River Basin – model construction and validation, Journal of Hydrology, 247, 200–214.

9. Anis, R.; Razavi, M.; Wheater, S. (2017). Howard An integrated modelling framework for regulated river systems in Land Surface Hydrological Models. EGU Gen. Assem. Conf. Abstr., 19, 9753.

10. Asokan, S.M.; Dutta, D. (2008). Analysis of water resources in the Mahanadi River Basin, India under Projected climate conditions. Hydrol. Process., 22, 3589–3603.

11. Beven, K.J.; Cloke, H.L. (2012). Comment on Hyper resolution global land surface modeling: Meeting a Grand challenge for monitoring Earth's terrestrial water" by Eric F. Wood et al. Water Resour. Res., 48.

12. Butts MB, Payne JT, Kristensen M, Madsen H (2004). An evaluation of the impact of model structure on hydrological modelling uncertainty for stream flow simulation, J. Hydrol., 298, 242–266.

13. Chow, V.T. (1959). Open Channel Hydraulics, New York: McGraw-Hill.

14. Clapp, R.B. and Hornberger, G.M. (1978). Empirical equations for some soil hydraulic properties, Water Resources Research, 14, 601–604.

15. Clark, M.J.R. (2003). British Columbia Field Sampling Manual. Victoria, BC, Canada: Water, Air, and Climate Change Branch, Ministry of Water, Land, and Air Protection.

16. De Couet, T.; Maurer, T. (2009). Surface freshwater fluxes into the world oceans. Glob. Runoff Data Cent. Fed. Inst. Hydrol. (BfG), 2596–2614.

17. Delorit, J.; Gonzalez Ortuya, E.C.; Block, P. (2017). Evaluation of model-based seasonal streamflow and water allocation forecasts for the Elqui Valley, Chile. Hydrol. Earth Syst. Sci., 21, 4711–4725.

18. Demetriou C, Punthakey JF (1999). Evaluating sustainable groundwater management options using the MIKE SHE integrated hydrogeological modelling package. Environ Model Softw 14:129–140.

19. Doorenbos, J.; Pruitt, W.O. (1977). Guidelines for prediction of crop water requirements. FAO Irrig. Drain. Pap., 24, 144.

20. DHI-WE (2009) MIKE SHE User Manual. Volume 2: Reference Guide, Hørsholm: DHI Water and Environment.

21. Eyring, V. et al. (2016). Overview of the Coupled Model Intercomparison Project Phase 6 (CMIP6) experimental design and organization, Geosci. Model Dev., 9, 1937–1958.

22. Food and Agricultural Organization AQUASTAT. Available online: http://www.fao.org/nr/water/aquastat/main/index.stm (accessed on 21 April 2020).

23. Frei, C., Christensen, J.H., Déqué, M., Jacob, D., Jones, R.G. and Vidale, P.L. (2003). Daily precipitation statistics in regional climate models: Evaluation and intercomparison for the European Alps, Journal of Geophysical Research, 108(D3), 4124.

24. Frei, C. and Schär, C. (1998). A precipitation climatology of the Alps from high-resolution rain-gauge observations, International Journal of Climatology, 18, 873–900.

25. Gidden, M. J. et al. (2019). Global emissions pathways under different socioeconomic scenarios for use in CMIP6: A dataset of harmonized emissions trajectories through the end of the century, Geosci. Model Dev., 12, 1443–1475.

26. Gosain, A.K.; Rao, S.; Basuray, D. (2006). Climate change impact assessment on hydrology of Indian river basins. Curr. Sci., 346–353.

27. Gosling, S.N., Taylor, R.G., Arnell, N.W. and Todd, M.C. (2011). A comparative analysis of projected impacts of climate change on river runoff from global and catchment-scale hydrological models, Hydrology and Earth System Sciences, 15, 279–294.

28. Government of India. Indian Livestock Census; Ministry of Agriculture & Farmers Welfare, Government of India: New Delhi, India, 2007.

29. Government of India. Indian Population Census; Ministry of Home Affairs, Government of India: New Delhi, India, 2011.

30. Government of India. National Water Policy; Department of Water Resources, Government of India: New Delhi, India, 2012.

31. Government of India Ministry of Water Resources (2014). Narmada Basin [Online] Water Resources Information System of India Available from: http://www.india-wris.nrsc.gov.in/wris.html.

32. Government of India. Department of Water Resources India-WRIS. Available online: http://indiawris.gov.in/wris/#/DataDownload (accessed on 23 April 2020).

33. Graham, D.N. and Butts, M.B. (2005). Flexible integrated watershed modeling with MIKE SHE, In: Singh, V.P. and Frevert, D.K. (eds.) Watershed Models, Boca Raton: CRC Press, 245–272.

34. Guo, Z.; Dirmeyer, P.A.; Hu, Z.-Z.; Gao, X.; Zhao, M. (2006). Evaluation of the Second Global Soil Wetness Project soil moisture simulations: Sensitivity to external meteorological forcing. J. Geophys. Res., 111.

35. Gupta, H.; Chakrapani, G.J. (2005). Temporal and spatial variations in water flow and sediment load in Narmada River Basin, India: Natural and man-made factors. Environ. Geol., 48, 579–589.

36. Gupta, N.; Pandey, P.; Hussain, J. (2017). Effect of physicochemical and biological parameters on the quality of river water of Narmada, Madhya Pradesh, India. Water Sci., 31, 11–23.

37. Hagemann, S., Chen, C., Clark, D.B., Folwell, S., Gosling, S.N., Haddeland, I., Hanasaki, N., Heinke, J., Ludwig, F., Voss, F. and Wiltshire, A.J. (2013). Climate change impact on available water resources obtained using multiple global climate and hydrology models, Earth System Dynamics, 4, 129–144.

38. Havnø, K., Madsen, M.N. and Dørge, J. (1995). MIKE 11 – A generalized river modelling package, In: Singh, V.P. (ed.) Computer Models of Watershed Hydrology, Highlands Ranch, Colorado: Water Resources Publications, 733–782.

39. Henriksen, H.J., Troldborg, L., Højberg, A.L. and Refsgaard, J.C. (2008). Assessment of exploitable groundwater resources of Denmark by use of ensemble resource indicators and a numerical groundwater–surface water model, Journal of Hydrology, 348, 224–240.

40. Henriksen, H.J., Troldborg, L., Nyegaard, P., Sonnenborg, T.O., Refsgaard, J.C. and Madsen, B. (2003). Methodology for construction, calibration and validation of a national hydrological model for Denmark, Journal of Hydrology, 280, 52–71.

41. Ho, J.T., Thompson, J.R. and Brierley, C. (2015). Projections of hydrology in the Tocantins-Araguaia Basin, Brazil: uncertainty assessment using the CMIP5 ensemble, Hydrological Sciences Journal, Author Manuscript Online.

42. Immerzeel, W.W.; van Beek, L.P.H.; Bierkens, M.F.P. (2010). Climate change will affect the Asian water towers. Science, 328, 1382–1385.

43. Immerzeel, W.W., Beek, L.P.H., Konz, M., Shrestha, A.B. and Bierkens, M.F.P. (2012a). Hydrological response to climate change in a glacierized catchment in the Himalayas, Climatic Change, 110, 721–736.

44. Immerzeel, W.W., Pellicciotti, F. and Shrestha, A.B. (2012b). Glaciers as a Proxy to Quantify the Spatial Distribution of Precipitation in the Hunza Basin, Mountain Research and Development, 32, 30–38.

45. India-WRIS (2013a). Bargi (Rani Avanti Bai Lodhi Sagar) Major Irrigation Project JI00740 [Online] Available from: http://india-

wris.nrsc.gov.in/wrpinfo/index.php?title=Bargi(Rani_Avanti_Bai_Lodhi_Sagar)Major_Irrigation_Project_JI00740 [Accessed 23 February 2016].

46. India-WRIS (2013b). Barna Major Irrigation Project JI00745 [Online] Available from: http://india-wris.nrsc.gov.in/wrpinfo/index.php?title=Barna_Major_Irrigation_Project_JI00745 [Accessed 23 February 2016].

47. India-WRIS (2015). Narmada [Online] Available from: http://india-wris.nrsc.gov.in/wrpinfo/index.php?title=Narmada [Accessed 23 February 2016].

48. IPCC AR5 Climate Change 2013: The Physical Science Basis—IPCC. Available online: https://www.ipcc.ch/report/ar5/wg1/.

49. Jain, S.K., Storm, B., Bathurst, J.C., Refsgaard, J.C. and Singh, R.D. (1992). Application of the SHE to catchments in India Part 2. Field experiments and simulation studies with the SHE on the Kolar subcatchment of the Narmada River, Journal of Hydrology, 140, 25–47.

50. Jain, S.K., Agarwal, P.K. and Singh, V.P. (2007). Ganga Basin, In: Hydrology and Water Resources of India, Dordrecht: Springer Netherlands, 333–418.

51. Jayatilaka CJ, Storm B, Mudgway LB (1998). Simulation of water flow on irrigation bay scale with MIKE-SHE. J Hydrol 208:108–130.

52. Johnston, R. and Smakhtin, V. (2014). Hydrological Modeling of Large River Basins: How Much is Enough?, Water Resources Management, 28, 2695–2730.

53. Kalantari, Z., Lyon, S.W., Folkeson, L., French, H.K., Stolte, J., Jansson, P.E. and Sassner, M. (2014). Quantifying the hydrological impact of simulated changes in land use on peak discharge in a small catchment', The Science of the total environment, 466-467, 741–754.

54. Kauffeldt, A.; Wetterhall, F.; Pappenberger, F.; Salamon, P.; Thielen, J. (2016). Technical review of large-scale hydrological models for implementation in operational flood forecasting schemes on continental level. Environ. Model. Softw., 75, 68–76.

55. Khare, D.; Patra, D.; Mondal, A.; Kundu, S. Impact of landuse/land cover change on run-off in the catchment of a hydro power project. Appl. Water Sci., 7, 787–800.

56. Kumar, R.; Singh, R.D.; Sharma, K.D. Water resources of India. Curr. Sci. 2005, 89, 798–811.

57. Lehmann, K. (2016). Sampling of riverine or marine bacterial communities in remote locations: from field to publication, In: Bourlat, S.J., (ed.) Marine genomics: methods and protocols. New York, Springer Science and Business Media, 1–18. (Methods in Molecular Biology). (July 2016).

58. Lindström, G.; Pers, C.; Rosberg, J.; Strömqvist, J.; Arheimer, B. (2010). Development and testing of the HYPE (Hydrological Predictions for the Environment) water quality model for different spatial scales. Hydrol. Res., 41, 295–319.

59. Loch, A.; Adamson, D.; Dumbrell, N.P. The fifth stage in water management: Policy lessons for water governance. Water Resour. Res. 2020, 56, e2019WR026714.

60. Loucks, D.P. and van Beek, E. (2005). Water Resources Systems Planning and Management: An Introduction to Methods, Models and Applications, Paris: United Nations Educational, Scientific and Cultural Organization.

61. Lu J (2006). Modelling hydrologic responses to forest management and climate change at contrasting watersheds in the South-eastern United States. Dissertation, North Carolina State University, Raleigh, NC, USA, p 147.

62. Madsen H (2003). Parameter estimation in distributed hydrological catchment modelling using automatic calibration with multiple objectives, Adv. Water. Resour., 26, 205–216.

63. Madhusoodhanan, C.G.; Sreeja, K.G.; Eldho, T.I. (2016). Climate change impact assessments on the water resources of India under extensive human interventions, Ambio, 45, 725–741.

64. Mall, R.K.; Gupta, A.; Singh, R.; Singh, R.S.; Rathore, L.S. (2006). Water resources and climate change: An Indian perspective, Curr. Sci., 90, 1610-1626.

65. Masood, M., Yeh, P.J.F., Hanasaki, N. and Takeuchi, K. (2015). Model study of the impacts of future climate change on the hydrology of Ganges–Brahmaputra–Meghna basin, Hydrology and Earth System Sciences, 19, 747–770.

66. McCartney, M.P. and Acreman, M.C. (2009). Wetlands and Water Resources, In: Maltby, E. and Barker, T. (eds.) The Wetlands Handbook, Chichester: Wiley-Blackwell.

67. McMichael CE, Hope AS (2007). Predicting streamflow response to fire-induced landcover change: implications of parameter uncertainty in the MIKE SHE model, J. Environ. Manag., 84, 245-256.

68. Mishra, S.K.; Sahany, S.; Salunke, P. (2017). CMIP5 vs. CORDEX over the Indian region: How much do we benefit from dynamical downscaling?, Theor. Appl. Climatol., 133, 1-9.

69. Mishra, V.; Bhatia, U., Tiwari, A.D. (2020). Bias-corrected climate projctions from Coupled Model Intercompariosn Project-6 (CMIP6) for South Asia, Atmospheric and Oceanic Physics, 1-28.

70. Mukherjee, S.; Aadhar, S.; Stone, D.; Mishra, V. (2018). Increase in extreme precipitation events under Anthropogenic warming in India. Weather Clim. Extrem., 20, 45-53.

71. Müller Schmied, H.; Eisner, S.; Franz, D.; Wattenbach, M.; Portmann, F.T.; Flörke, M.; Döll, P. (2014). Sensitivity of simulated global-scale freshwater fluxes and storages to input data, hydrological model structure, human water use and calibration. Hydrol. Earth Syst. Sci., 18, 3511–3538.

72. Nash, I.E. and Sutcliffe, I.V. (1970). River flow forecasting through conceptual models, J. Hydrol., 10, 282-290.

73. Nelder, J.A. (1965). Mead, R. A Simplex Method for Function Minimization. Comput. J., 7, 308–313.

74. Norman, D.W. and Dixon, J. (1995). Sustainable dryland cropping in relation to soil productivity - FAO soils bulletin 72, Rome: Food and Agriculture Organization of the United Nations.

75. Pai, D., Sridhar, L., Rajeevan, M., Sreejith, O.P., Satbhai, N.S. and Mukhopadhyay, B. (2014). Development of a new high spatial resolution (0.25° × 0.25°) long period (1901-2010) daily gridded rainfall data set over India and its comparison with existing data sets over the region', Mausam, 65, 1–18.

76. Paithankar, K.R. and Prasad, K.S.N. (1991). Precipitation of DNA by polyethylene glycol and ethanol, Nucleic Acids Research, 19, 1346.

77. Pappenberger, F.; Thielen, J.; Del Medico, M. (2011). The impact of weather forecast improvements on large scale hydrology: Analysing a decade of forecasts of the European Flood Alert System. Hydrol. Process., 25, 1091–1113.

78. Patel, J., Patel, H. and Bhatt, C. (2014). ECALTOOL: fuzzy logic based computer program to calibrate the Hargreaves equation for accurate estimation of evapotranspiration, Agricultural Engineering International: CIGR Journal, 16, 245–250.

79. Pathak, H.; Pramanik, P.; Khanna, M.; Kumar, A. (2014). Climate change and water availability in Indian agriculture: Impacts and adaptation. Indian J. Agric. Sci., 84, 671–679.

80. Payasi, Y.K. (2015). Diversity and Distribution of Phytoplankton in the River Hiran, Global Journal for Research Analysis, 4.

81. Prudhomme, C. and Davies, H. (2009). Assessing uncertainties in climate change impact analyses on the river flow regimes in the UK. Part 1: baseline climate, Climatic Change, 93, 177–195.

82. Prudhomme, C.; Parry, S.; Hannaford, J.; Clark, D.B.; Hagemann, S.; Voss, F. (2011). How Well Do Large-Scale Models Reproduce Regional Hydrological Extremes in Europe? J. Hydrometeor, 12, 1181–1204.

83. Rahman, M.M.; Thompson, J.R.; Flower, R.J. (2020**).** Hydrological impacts of climate change on rice cultivated riparian wetlands in the Upper Meghna River Basin (Bangladesh and India). *Hydrol. Sci. J.*, *65*, 33–56.

84. Rajaguru, S.N., Gupta, A., Kale, V.S., Mishra, S., Ganjoo, R.K., Ely, L.L., Enzel, Y. and Baker, V.R. (1995). Channel form and processes of the flood-dominated Narmada River, India, Earth Surface Processes and Landforms, 20, 407–421.

85. Raje, D.; Priya, P.; Krishnan, R. (2017). Macroscale hydrological modelling approach for study of large scale hydrologic impacts under climate change in Indian river basins. Hydrol. Process. 2014, 28, 1874–1889.

86. Räsänen, T.A., Koponen, J., Lauri, H. and Kummu, M. (2012). Downstream Hydrological Impacts of Hydropower Development in the Upper Mekong Basin, Water Resources Management, 26, 3495–3513.

87. Refsgaard JC (1997). Parameterization, calibration, and validation of distributed hydrological models. J Hydrol 198:69–97.

88. Refsgaard, J.C. and Henriksen, H.J. (2004). Modelling guidelines-terminology and guiding principles, Advances in Water Resources, 27, 71–82.

89. Refsgaard, J.C., Storm, B. and Clausen, T. (2010). Système Hydrologique Europeén (SHE): review and perspectives after 30 years development in distributed physically-based hydrological modelling, Hydrology Research, 41, 355-377.

90. Rijsberman, F.R. (2006). Water scarcity: Fact or fiction? Agric. Water Manag., 80, 5–22.

91. Richter, B.D., Baumgartner, J.V., Wigington, R. and Braun, D.P. (1997). How much water does a river need?, Freshwater Biology, 37, 231-249.

92. Saleth, R.M. (2011). Water scarcity and climatic change in India: The need for water demand and supply management. Hydrol. Sci. J., 56, 671–686.

93. Schumacher, M.; Forootan, E.; van Dijk, A.I.J.M.; Müller Schmied, H.; Crosbie, R.S.; Kusche, J.; Döll, P. (2018). Improving drought simulations within the Murray-Darling Basin by combined calibration/assimilation of GRACE data into the WaterGAP Global Hydrology Model. Remote Sens. Environ., 204, 212–228.

94. Simonovic, S.P. (2012). World Water Resources at the Beginning of the Twenty-First Century; University Press: Cambridge, UK.

95. Singh, C.R., Thompson, J.R., Kingston, D.G. and French, J.R. (2011). Modelling water-level options for ecosystem services and assessment of climate change: Loktak Lake, northeast India, Hydrological Sciences Journal, 56, 1518-1542.

96. Singh R, Subramanian K, Refsgaard JC (1999). Hydrological modelling of a small watershed using MIKE-SHE for irrigation planning, Agric. Water Manag., 41, 149-166.

97. SMHI Climate Change Is Affecting Water Supply in India. Available online: https://www.smhi.se/en/research/research-news/climate-change-is-affecting-water-supply-in-india-1.34468.

98. Srivastava, A.K., Rajeevan, M. and Kshirsagar, S.R. (2009). Development of a high resolution daily gridded temperature data set (1969-2005) for the Indian region, Atmospheric Science Letters, 10, 249-254.

99. Stisen, S., Jensen, K.H., Sandholt, I. and Grimes, D.I.F. (2008). A remote sensing driven distributed hydrological model of the Senegal River basin, Journal of Hydrology, 354, 131-148.

100. Tan, B., Ng, C., Nshimyimana, J.P., Loh, L.L., Gin, K.Y.H. and Thompson, J.R. (2015). Next-generation sequencing (NGS) for assessment of microbial water quality: current progress, challenges, and future opportunities, Frontiers in Microbiology, 6: 1027, doi: 10.3389/fmicb.2015.01027.

101. Thompson, J.R., Green, A.J. and Kingston, D.G. (2014a). Potential evapotranspiration-related uncertainty in climate change impacts on river flow: An assessment for the Mekong River basin, Journal of Hydrology, 510, 259–279.

102. Thompson, J.R., Green, A.J., Kingston, D.G. and Gosling, S.N. (2013) 'Assessment of uncertainty in river flow projections for the Mekong River using multiple GCMs and hydrological models', Journal of Hydrology, 486, 1–30.

103. Thompson, J.R., Laizé, C.L.R., Green, A.J., Acreman, M.C. and Kingston, D.G. (2014b). Climate change uncertainty in environmental flows for the Mekong River, Hydrological Sciences Journal, 59, 935–954.

104. Thompson JR, Sorenson HR, Gavina H, Refsgaard JC (2004). Application of the coupled MIKE SHE/MIKE 11 modelling system to a lowland wet grassland in Southeast England. J Hydrol., 293, 151–179.

105. Thompson, J.R.; Crawley, A.; Kingston, D.G. (2017**).** Future river flows and flood extent in the Upper Niger and Inner Niger Delta: GCM-related uncertainty using the CMIP5 ensemble. *Hydrol. Sci. J.*, *62*, 2239–2265.

106. Thomsen, P.F., Kielgast, J., Iversen, L.L., Wiuf, C., Rasmussen, M., Gilbert, M.T.P., Orlando, L. and Willerslev, E. (2012). Monitoring endangered freshwater biodiversity using environmental DNA, Molecular Ecology, 21, 2565–2573.

107. Udmale, P.; Ichikawa, Y.; Manandhar, S.; Ishidaira, H.; Kiem, A.S. (2014). Farmers' perception of drought impacts, local adaptation and administrative mitigation measures in Maharashtra State, India. Int. J. Disaster Risk Reduct., 10, 250–269.

108. Van Huijgevoort, M.H.; Van Loon, A.F.; Hanel, M.; Haddeland, I.; Horvát, O.; Koutroulis, A.;Machlica, A.; Weedon, G.; Fendeková, M.; Tsanis, I.; et al. (2011). Simulation of Low Flows and Drought Events in WATCH Test Basins: Impact of Different Climate Forcing Datasets; Technical Report No. 26, European Commission Sixth Framework Programme.

109. Van Loon, A.F.; Van Huijgevoort, M.H.J.; Van Lanen, H.A.J. (2012). Evaluation of drought propagation in an ensemble mean of large-scale hydrological models. Hydrol. Earth Syst. Sci. Discuss., 9, 8375–8424.

110. Vázquez, R.F., Feyen, L., Feyen, J. and Refsgaard, J.C. (2002). Effect of grid size on effective parameters and model performance of the MIKE-SHE code, Hydrological Processes, 16, 355–372.

111. V'azquez RF, Feyen J (2003). Effect of potential evapotranspiration estimates on effective parameters and performance of the MIKE SHE-code applied to a medium-size catchment. J Hydrol 270:309–327.

112. V'azquez RF, Feyen J (2007). Assessment of the effects of DEM gridding on the predictions of basin runoff using MIKE SHE and a modelling resolution of 600 m. J Hydrol 334:73–87.

113. Velázquez, J.A., Schmid, J., Ricard, S., Muerth, M.J., Gauvin St-Denis, B., Minville, M., Chaumont, D., Caya, D., Ludwig, R. and Turcotte, R. (2013). An ensemble approach to assess hydrological models' contribution to uncertainties in the analysis of climate change impact on water resources, Hydrology and Earth System Sciences, 17, 565–578.

114. Vicente-Serrano, S.M.; Zabalza-Martínez, J.; Borràs, G.; López-Moreno, J.I.; Pla, E.; Pascual, D.; Savé, R.; Biel, C.; Funes, I.; Azorin-Molina, C.; et al. (2017). Extreme hydrological events and the influence of reservoirs in a highly regulated river basin of northeastern Spain. J. Hydrol. Reg. Stud., 12, 13–32.

115. Vieux, B.E. (2004). Distributed Hydrologic Modeling Using GIS, Dordrecht: Kluwer Academic.

116. Wada, Y.; van Beek, L.P.H.; Wanders, N.; Bierkens, M.F.P. (2013). Human water consumption intensifies hydrological drought worldwide. Environ. Res. Lett., 8, 034036.

117. Wetterhall, F.; Pappenberger, F.; Alfieri, L.; Cloke, H.L.; Thielen-del Pozo, J.; Balabanova, S.; Daˇnhelka, J.; Vogelbacher, A.; Salamon, P.; Carrasco, I.; et al. (2013). HESS Opinions "Forecaster priorities for Improving probabilistic flood forecasts. Hydrol. Earth Syst. Sci., 17, 4389–4399.

118. Wijesekara, G.N., Gupta, A., Valeo, C., Hasbani, J.G., Qiao, Y., Delaney, P. and Marceau, D.J. (2012). Assessing the impact of future land-use changes on hydrological processes in the Elbow River watershed in southern Alberta, Canada, Journal of Hydrology, 412-413, 220–232.

119. Wijesekara, G.N., Farjad, B., Gupta, A., Qiao, Y., Delaney, P. and Marceau, D.J. (2014). A comprehensive land-use/hydrological modeling system for scenario simulations in the Elbow River watershed, Alberta, Canada, Environmental management, 53, 357–381.

120. Winchell, M., Srinivasan, R., Di Luzio, M. and Arnold, J. (2013). ArcSWAT Interface for SWAT2012: User's Guide, Temple, Texas: Blackland Research & Extension Center Texas AgriLife Research; Grassland, Soil and Water Research Laboratory USDA Agricultural Research Service.

121. Xevi E, Christiaens K, Espino A, Sewnandan W, Mallants D,Sorensen H, Feyen J (1997). Calibration, validation and sensitivity analysis of the MIKE-SHE model using the Neuenkirchen catchment as case study. Water Resour Manag 11:219–239.

122. Zhang Z, Wang S, Sun G, McNulty S, Zhang H, Li J, Klaghofer E, Strauss P (2008). Evaluation of the MIKE SHE model for application in the Loess Plateau, China. JAWRA 44(5):1108–1120.

STUDY TEAM

DIRECTOR : Dr. J. V. Tyagi

COORDINATOR : Dr. A. K. Lohani, Scientist 'G'

INVESTIGATING TEAM - NIH

Dr. Sharad K. Jain	:	Ex-Director
Dr. Sanjay K. Jain	:	Scientist 'G'
Dr. T. Thomas	:	Scientist 'E' & PI
Dr. Manish Nema	:	Scientist 'D'
Dr. P. K. Mishra	:	Scientist 'C'
Er. P.K. Agarwal	:	Scientist 'B'

INVESTIGATING TEAM - UKCEH

Prof. Alan Jenkins	:	Director of Science
Dr. Gwyn Rees	:	Science Area Head, WR
Prof. Harry Dixon	:	Group Leader, WRS
Ms. Helen Hougton Carr	:	Senior Hydrologist & Project Manager
Mr. Nathan Rickards	:	Hydrologic Modeller
Ms. Alexandria Kaelin	:	Hydrologist
Ms. Robyn Horan	:	Hydrologist

INVESTIGATING TEAM - UCL

Prof. Julian R. Thompson	:	Professor
Dr. Amanda J. Robinson	:	Research Scholar